THESIS

A THEORETICAL AND EXPERIMENTAL INVESTIGATION INTO THE IR-VUV ION DIP SPECTROSCOPY OF AMINO ACIDS AND ANALOGUE SYSTEMS

Submitted by

Keven James Clawson

Chemistry Department

In partial fulfillment of the requirements

For the Degree of Master of Science

Colorado State University

Fort Collins, Colorado

Fall 2010

COLORADO STATE UNIVERSITY

February 22, 2010

WE HEREBY RECOMMEND THAT THE THESIS PREPARED UNDER OUR SUPERVISION BY KEVEN CLAWSON ENTITLED A THEORETICAL AND EXPERIMENTAL INVESTIGATION INTO THE IR-VUV ION DIP SPECTROSCOPY OF AMINO ACIDS AND ANALOGUE SYSTEMS BE ACCEPTED AS FULFILLING IN PART REQUIREMENTS FOR THE DEGREE OF MASTER OF SCIENCE.

Committee on Graduate work

Randy Bartels

Ellen Fisher

Advisor: Elliot Bernstein

Department Chair: Ellen Fisher

ABSTRACT OF THESIS

A THEORETICAL AND EXPERIMENTAL INVESTIGATION INTO THE IR-VUV ION DIP SPECTROSCOPY OF AMINO ACIDS AND ANALOGUE SYSTEMS

Amino acids are among the fundamental building blocks of life, and as such have been, and continue to be, of much interest for study. While gas phase spectroscopic studies can be very useful in obtaining information about molecular species (in this case various naturally occurring amino acids), the use of computational and theoretical methods can aid these studies in providing a more complete understanding of the properties and behaviors of these species. Here presented are the results of IR-VUV ion dip spectroscopy, coupled with a high-level theoretical examination of the spectroscopic results, including MP2 and CASSCF calculaions.

In IR-VUV ion dip spectroscopy, the isolated neutral molecules are ionized by a single photon of 10.5 eV energy 118 nm. If the neutral ground state amino acids are exposed to IR radiation prior to ionization, an IR spectrum can be determined by observation of the ion intensity of the different fragment mass channels. Species specifically studied include numerous naturally occurring aliphatic and aromatic amino acid species, and amino acid analogue species.

In the case of the aliphatic amino acids, conformer specific decomposition pathways are observed spectroscopically, and further elucidated both through the study of

amino acid analogue species and through high level multiconfigurational CASSCF calculations. It is shown that upon ionization, the localized character of the charge, coupled with the geometry of the neutral parent molecule, directs the decomposition reaction of the molecule. In simple, small aliphatic amino acid and analogue species, these factors are unique to the conformation of the molecule, leading to conformer specific decomposition chemistry. In the amino acid species, the localized charge tends to occur either on one of the available moieties (carboxylic acid, amine, etc.), or on the carbon-carbon bond, depending on the conformer.

The IR-VUV ion dip spectra obtained from the aromatic amino acid species, however, clearly demonstrate different photodecomposition behavior in the aromatic species when compared to the simple, smaller aliphatic species. The conformer specific chemistry which was observed in the smaller molecules was not evident in the aromatic species. This is likely due to the aromatic moiety containing the lowest energy, localized ion state for the molecule which does not lead to ion fragmentation. Thus, the conformer specific decomposition chemistry observed in the non-aromatic species is no longer observed in those species which contain an aromatic moiety.

Keven James Clawson
Chemistry Department
Colorado State University
Fort Collins, CO 80523
Fall 2010

ACKNOWLEDGEMENTS

I would like to thank my advisor, Dr. Elliot Bernstein, for the advice, help, support, aid, and immense amount of patience which he has afforded me over the years. It is not an exaggeration to say that nothing I accomplished in graduate school would have been possible without him. In both scholarly and personal aspects, his council has been freely given and appreciatively received.

All work reported in this thesis has been informed by Dr. Bernstein's knowledgeable advice and suggestions. Any time I was having a difficult time understanding my results, or deciding on where to take my research next, Dr. Bernstein was always available to talk me through whatever difficulty I was having, and always (of course) provide valuable insight along the way.

Beyond his scholarly advice, very few people have ever gone to bat from me like Dr. Bernstein has (repeatedly!), and he will always have my sincere gratitude. So, once again: Thank you Dr. Bernstein.

TABLE OF CONTENTS

Introduction

Often the chemistry of large, complicated systems—such as the chemistry of life—is best understood by first observing the chemistry and behavior of its smaller, more basic components. Once these smaller systems are well understood, one can then observe the interactions and behaviors of these smaller component systems within the larger, more complicated macroscopic system. Amino acids are among the fundamental building blocks of life, and as such have been, and continue to be, of much interest for study.[1–4] The placing of these isolated amino acids into the gas phase allows for the least perturbed study of these basic building blocks of life—free from external biological and environmental effects—and thus the clearest descriptions of their intrinsic behaviors and properties can be obtained.

While gas phase spectroscopic studies can be very useful in obtaining information about molecular species (in this case various naturally occurring amino acids), the use of computational and theoretical methods can aid these studies in providing a more complete understanding of the properties and behaviors of these species. Naturally occurring amino acids, especially those containing aromatic moieties, contain several low-lying, closely separated electronic excited states in both their neutral and cationic states. These various electronic excited states can generate different uni-molecular chemistries,[5–6] which may not necessarily be evident by simply observing spectroscopic results, but can become well understood with the aid of theoretical calculations.

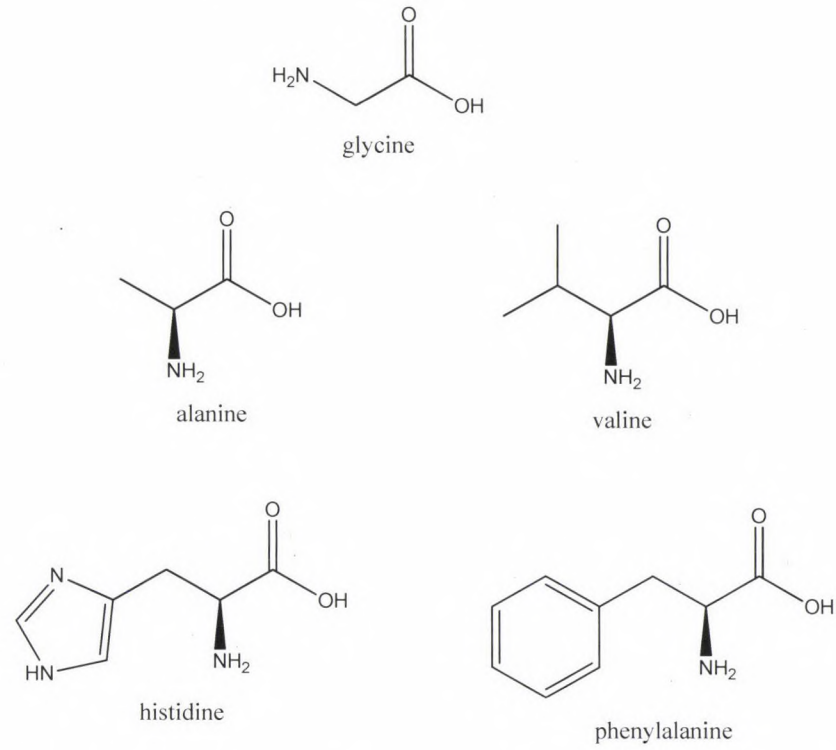

Figure i.1: *Five amino acid species studied within this thesis. Glycine, alanine and valine are aliphatic amino acids (alanine and valine contain a hydrocarbon side chain), and histidine and phenylalanine are referred to as aromatic amino acids, due to the presence of an aromatic moiety.*

Thus, in our own studies, we have combined spectroscopic and theoretical results into a coherent picture of the behavior of several naturally occurring amino acids: glycine, alanine, valine, histidine, phenylalanine, and tyrosine. My own role within this process was the theoretical investigation of these amino acid species, informed by spectroscopic results that were obtained both prior to my involvement in the project and during the course of my involvement as well.

Because larger biologically active molecules such as peptides and proteins consist of smaller building blocks of amino acids and sugars, and the structures of proteins and carbohydrates arise from inter- and intra-molecular interactions within these smaller building blocks, the conformational landscape of amino acids and sugars is of particular interest.[7–11] Understanding how secondary interactions, such as intra-molecular hydrogen

bonding or van der Waals interactions, affect these smaller biological building blocks generates insight into the structure, chemistry, properties, and dynamics of their polymer biologically active systems.

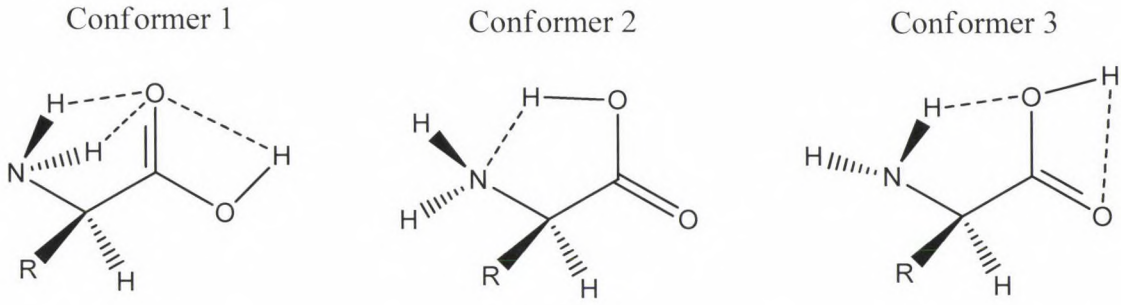

Figure i.2: *The three general lowest energy conformations of amino acids. The R group shown here represents the amino acid side chain, which can be H or a hydrocarbon chain (aliphatic amino acids), or an aromatic functional group (aromatic amino acids).*

The first spectroscopic studies of amino acids for which results and theory seemed to collide were conducted in 1978 by Suenram and Lovas.[12] They report the results of millimeter wave spectroscopy of gas phase glycine and conclude that the conformer referred to in this paper as Conformer 2 (Figure i.2) was the overwhelmingly most abundant apparent conformer of glycine in the gas phase. These results did not agree with the then available theoretical results[13, 14] (which predicted Conformer 1 be the lowest-energy conformer, and thus most abundant), so further study was warranted. In subsequent studies, Suenram and Lovas concluded that both Conformer 1 and 2 were actually present, but, due to Conformer 2's much larger dipole moment, it produced a more intense signal than Conformer 1.[15]

Since those earlier studies, many other spectroscopic studies have been conducted on glycine and many other amino acid species with the goal of elucidating their conformational landscapes.[16–18] In the early nineties, millimeter wave studies were

performed on glycine and alanine, and new conformers were identified.[19, 20] Since then, Alonso and others have taken rotational spectra of most naturally occurring amino acids in the gas phase, and conformers have been identified based upon these studies.[17–22]

Lately, from the early 2000s, the infrared spectra of a number of amino acids have been taken, both in gas cell and in matrix isolation experiments.[23–25] Both methods involve the heating of solid amino acid samples, resulting in a population distribution associated with a heated sample. Thus, the results obtained through these later studies are not fully comparable to results that would be obtained from a sample cooled in a cold molecular beam. Different cooling methods would potentially generate different population distributions among the low energy conformer structures.

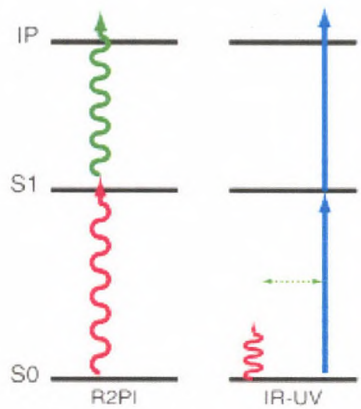

Figure i.3: *Schematic representations of R2PI and IR-UV hole burning spectroscopy techniques. Adapted from de Vries and Hobza (2007)[26].*

In the mid 80s, Levy utilized a technique for obtaining the electronic spectra of gas phase biologically active molecules—resonant two photon ionization (R2PI) spectroscopy—in which he was able to observe spectral contributions from unique conformers.[27] From there, Lee was able to develop an IR–UV hole burning spectroscopy.[28] In this particular technique, ionization is achieved through two resonant photons, and state populations are altered through the use of a scanning IR laser. The

resulting change in mass spectral signal intensity is observed, providing a spectrum for the species (Figure i.3, i.4). These techniques have allowed further spectroscopic study of many biologically active species, and have proven to be useful in understanding their chemical behavior.[26, 29–31]

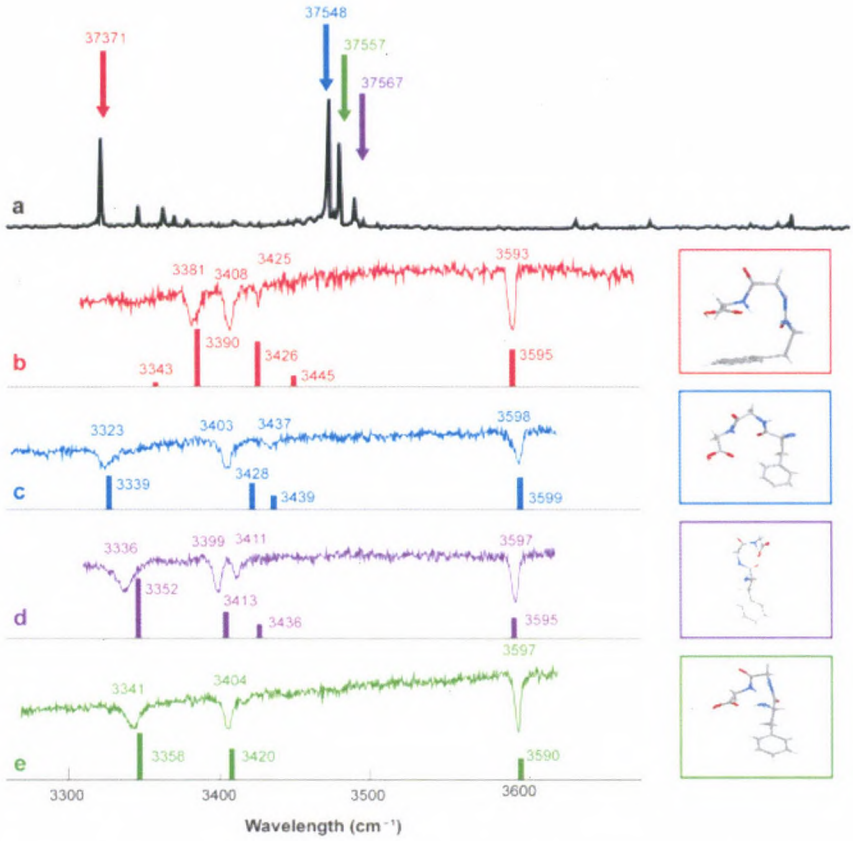

Figure i.4: *Optimized minimum energy structures for phenylalanine-glycine-glycine (Phe-Gly-Gly) (right-hand column) (b–e). Computed frequencies as stick spectra and infrared-ultraviolet spectral hole burning (IR-UV SHB) spectra, recorded with the probe laser at the wavelengths shown by the arrows in corresponding colors in the REMPI spectrum (a). Adapted from de Vries and Hobza*[26].

This type of ion-dip spectroscopy has proven to be very useful, providing vibrational spectra of cold gas phase species, but is limited to species containing an aromatic moiety. The two photon ionization is tuned to a specific vibronic transition localized on the aromatic moiety within the species. Thus, only three naturally occurring amino acids are available for study through this method. Aromatic moiety containing

derivatives of other amino acids have been studied, as have a number of other bioactive molecules, including nucleotides, sugars, and small peptides. Nevertheless, a technique to access *all* bioactive molecules, including those without the intermediate, resonant π state has only recently been developed.[11]

Another complication in ion-dip spectroscopy is the tendency of smaller, aliphatic amino acids to fragment upon ionization. Although larger, aromatic containing molecules are often stable with a localized charge, and thus permit parent ion signal observation, non-aromatic amino acids tend to fragment completely upon ionization, and thus a parent ion signal cannot be observed or monitored. This fragmentation typically occurs because the low lying ion electronic states arise from the removal of neutral backbone ($-CH(NH_2)COOH$) non bonded electrons, on N and/or O atoms in this instance.

Bernstein and Hu in 2007 reported obtaining IR–VUV single photon ion dip spectra of several aliphatic amino acids by monitoring the ion signal intensity of fragment ions.[11] No parent ion signals were observed. It becomes increasingly clear that fully understanding the chemistries and behaviors of amino acids and other biologically active molecules will require an understanding of their neutral ground state (S_0) and ion state (D_0) forms, including various electronic excited states (D_i) of the ion.

Amino acids—being some of the simpler bioactive systems—have been of much theoretical interest, as well. Glycine, for example, has been studied theoretically for many years, with *ab initio* calculations going back as far as 1977 in a paper by Vishveshwara and Pople, in which the lowest energy conformers of glycine were predicted, with Conformer 1 (Figure i.1) predicted to be lower in energy than Conformer 2.[14] (The results

of these calculations were among those that contributed to the early millimeter wave controversy regarding glycine.)

Immediately following these initial studies, further study of glycine was conducted,[32, 33] along with studies of alanine, another small and simple amino acid.[34, 35] As computing resources have increased in capability, further studies have been conducted throughout the years. In the late 90s and early 00s, as new experimental results became available, a renewed interest in the theoretical study of amino acids appeared.[34–38] Usually, analyses of these experimental results were aided by the use of computational methods to predict minimum energy structures, frequencies, etc. The methods used in these calculational studies have varied, but density functional methods (e.g., B3LYP) or higher level *ab initio* methods (e.g., second-order Møller-Plesset perturbation theory, MP2) have been the most common.

In addition to the reported calculations that accompany experimental results, a number of purely theoretical studies have been conducted on glycine in particular, and on other smaller amino acids.[35, 36] Hobza, for example, in recent years has reported studies evaluating computational methods for neutral amino acid structure and energy, basis set benchmarks using the MP2 method on glycine,[37] and extensive CASSCF (Complete Active Space Self-Consistent Field) studies of neutral and ionized glycine.[38]

While most of these reported results are certainly useful in studying ground state neutral species, they are limited in their ability to predict ion state chemistries, especially in systems such as amino acids in which there are several low-lying, closely separated excited ion states. It is clear that the fragmentation of amino acids occurs in the ion state. Thus, in order to better understand the fragmentation behavior of amino acid species, one

must understand the ion state chemistry of amino acids: a multi-configurational (e.g., CASSCF) approach must be utilized for systems with nearly degenerate states. To date, glycine and alanine have been reported at this level,[38, 39] but there are still many unanswered questions about the generalized ion behavior of amino acids and biologically active molecules. Much further study—theoretical and experimental— is needed.

A combination of spectroscopy and theory needs to be employed in order to gain a full understanding of the chemistries associated with many molecules, especially those involved in bioactive systems (like amino acids) or other similar systems in which conformational flexibility plays a large role. Prior to our efforts and reports, the only systems that have been available for coupled, cold IR spectroscopy and theoretical study have been those with either a naturally occurring aromatic moiety or an artificially attached one. While these studies have been useful, they are limited in scope, and do not allow us to obtain a fuller picture of the behavior and interactions of *all* bioactive small building block molecules.

References

1. Junk, G. and Svec, H. *Journal of the American Chemical Society*, **1963**, *85*, 839.
2. Pan, Y.; Zhang, L.; Zhang,T.; Guo, H.; Hong, X.; Sheng, L. and Qi, F. *Physical Chemistry Chemical Physics*, **2009**, *11*, 1189.
3. Weinkauf, R., Schermann, J. P., de Vries, M. S. and Kleinermanns, K. *European Physics Journal D*, **2002**, *20*, 309.
4. Robertson, E. G. and Simons, J. P. *Physical Chemistry Chemical Physics*, **2001**, *3*, 1.
5. Coutinho, L.H.; Homem, M. G. P.; Cavasso-Filho, R. L.; Marinho, R. R. T.; Lago, A. F.; de Souza, G. G. B. and Naves de Brito, A. *Brazilian Journal of Physics*, **2005**, *35*, 940.
6. Garavelli, M. *Theoretical Chemistry Accounts*, **2006**, *116*, 87.
7. Jockusch, R. A.; Kroemer, R. T.; Talbot, F. O.; Snoek, L. C.; Çarçabal, P.; Simons, J. P.; Havenith, M.; Bakker, J. M.; Compagnon, I.; Meijer, G. and von Helden, G. *Journal of the American Chemical Society*, **2004**, *126*, 5709.
8. Çarçabal, P.; Jockusch, R. A.; Hünig, I.; Snoek, L. C.; Kroemer, R. T.;. Davis, B. G.; Gamblin, D. P.; Compagnon, I.; Oomens, J. and Simons, J. P. *Journal of the American Chemical Society*, **2005**, *127*, 11414.
9. Ebata, T.; Hashimoto, T.; Ito, T.; Inokuchi, Y.; Altunsu, F.; Brutschy, B. and Tarakeshwar, P. *Physical Chemistry Chemical Physics*, **2006**, *8*, 4783.
10. Stearns, J. A.; Mercier, S.; Seaiby, C.; Guidi, M.; Boyarkin, O. V. and Rizzo, T. R. *Journal of the American Chemical Society*, **2007**, *129*, 11814.
11. Hu, Y. and Bernstein, E. R. *Journal of Chemical Physiscs* **2008**, *128*, 164311.
12. Suenram, R. D. and Lovas, F. J. *Journal of Molecular Spectroscopy* **1978**, *72*, 372.
13. Oegerle, W. R and Sabin, J. R. *Journal of Molecular Structure*, **1973**, *15*, 131.
14. Vishveshwara, S. and Pople, J. A. *Journal of the American Chemical Society*, **1977**, *99*, 2422.
15. Suenram, R. D. and Lovas, F. J. *Journal of the American Chemical Society* **1980**, *102*, 7180.
16. Philips, L. A.; Webb, S. P.; Martinez, S. J.; Fleming, G. R. and Levy, D. H. *Journal of the American Chemical Society*, **1988**, *110*, 1352.
17. Godfrey, P. D. and Brown, R. D. *Journal of the American Chemical Society*, **1995**,*117*, 2019.
18. Cocinero, E. J.; Lesarri, A.; Grabow, J.; López, J. C. and Alonso, J. L. *ChemPhysChem* **2007**, *8*, 599.
19. Godfrey, P. D.; Firth, S; Hatherley, L. D.; Brown, R. D. and Pierlot, A. P. *Journal of the American Chemical Society*, **1993**,*115*, 9687.
20. Lesarri, A.; Mata, S.; López, J. C. and Alonso, J. L. *Review of Scientific Instruments*, **2003**, *74*, 4799.
21. Lesarri, A.; Cocinero, E. J.; López, J. C. and Alonso, J. L. *Angewandte Chemie International Edition*, **2004**, *43*, 605.
22. Lesarri, A.; Sánchez, R.; Cocinero, E. J.; López, J. C. and Alonso, J. L.; *Journal of the American Chemical Society*, **2005**, *127*, 12952.

23. Linder, R.; Nispel, M.; Häber, T. and Kleinermanns, K. *Chemical Physics Letters,* **2005,** 409, 260.
24. Stepanian, S. G.; Reva, I. D.;. Radchenko, E. D.; Rosado, M. T. S.; Duarte, M. L. T. S.; Fausto, R. and Adamowicz, L. *Journal of Physical Chemistry A,* **1998**, 102, 1041.
25. Stepanian, S. G.; Reva, I. D.;. Radchenko, E. D. and Adamowicz, L. *Journal of Physical Chemistry A,* **2001**, 105, 10664.
26. de Vries, M. S. and Hobza, P. *Annual Reviews in Physical Chemistry*, **2007**. *58*, 585.
27. Rizzo, T. R.; Park, Y. D.; Peteanu, L. A. and Levy, D. H. *Journal of Chemical Physics*, **1986**, *84*, 2534.
28. Page, R. H.; Shen, Y. R. and Lee, Y. T. *Journal of Chemical Physics*, **1988**, *88*, 4621.
29. Robertson, E. G. and Simons, J. P. *Physical Chemistry Chemical Physics*, **2001**, *3*, 1.
30. Simons, J. P.; Jockusch, R. A.; Çarçabal, P.; Hünig, I.; Kroemer, R. T.; Macleod, N. A. and Snoek, L. *International Reviews in Physical Chemistry*, **2005,** *24*, 489.
31. Lee, K. T.; Sung, J.; Lee, K. J.; Park, Y. D.; and Kim, S. K. *Angewandte Chemie International Edition,* **2002**, *41*, 4114.
32. Jensen, J. H. and Gordon, M. S. *Journal of the American Chemical Society,* **1991**, *113*, 7917.
33. Császár, A. G. *Journal of Molecular Structure*, **1995**, *346*, 141.
34. Siam, K.; Klimkowski, V. J.; Ewbank, J. D.; Van Alsenoy, C. and Schafer, L. *Journal of Molecular Structure (Theochem),* **1984**, *110*, 171.
35. Császár, A. G. *Journal of Physical Chemistry* **1996**, *100*, 3541.
36. Falzon, C. T. and Wang, F. *Journal of Chemical Physics*, **2005**, *123*, 214307.
37. Jurečka, P.; Šponer, J.; Černý, J. and Hobza, P. *Physical Chemistry Chemical Physics*, **2006**, *8*, 1985.
38. Muchová, E.; Slavíček, P.; Sobolewski, A. L. and Hobza, P. *Journal of Physical Chemistry A*, **2007**, *111*, 5259.
39. Zhang, L.; Pan, Y.; Guo, H.; Zhang, T.; Sheng, L.; Qi, F.; Lo, P.; and Lau, K. *Journal of Physical Chemistry A*, **2009**, *113*, 5838.

Chapter 1: A Theoretical and Experimental Investigation Into the IR-VUV Ion Dip Spectroscopy of Aliphatic Amino Acid Species

The work reported in this chapter was conducted by me in conjunction with Drs. Joong-Won Shin and Atanu Bhattacharya. The original spectroscopic data were obtained by Dr. Shin and me. The theoretical results, while largely my own work, were aided by Dr. Bhattacharya.

1.1 Introduction

The simplest amino acids are glycine, and small side chain containing aliphatic amino acids, such as alanine, valine, etc. These simplest amino acids are the most computationally efficient biologically active molecules to study (due to their smaller size and relative lack of complexity), and thus are the species that have undergone the most extensive theoretical study.[1–15]

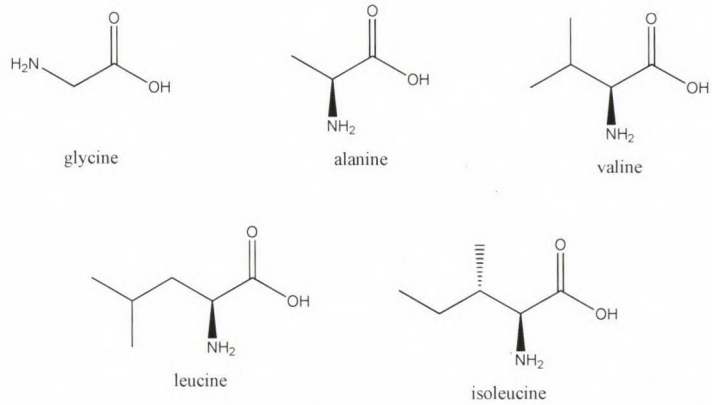

Figure 1.1: *The aliphatic amino acid species. All contain a simple hydrocarbon side chain. For the purposes of this study, the term "aliphatic amino acids" may not necessarily refer to glycine, which has a generally symmetric structure.*

This simplicity prompted the use of these small amino acids for the initial IR–VUV studies,[16,17] and for in-depth calculational studies.[18,19] The three most stable conformers for these species are, in order, Conformer 1, Conformer 2, and Conformer 3 (Figure 1.2), with Conformers 1 and 2 being very close in energy and thus the most abundant in a cold sample.[3,4,20,21] These reported structures were used in assigning the IR–VUV spectra, and were also used as the basis for our computational studies.

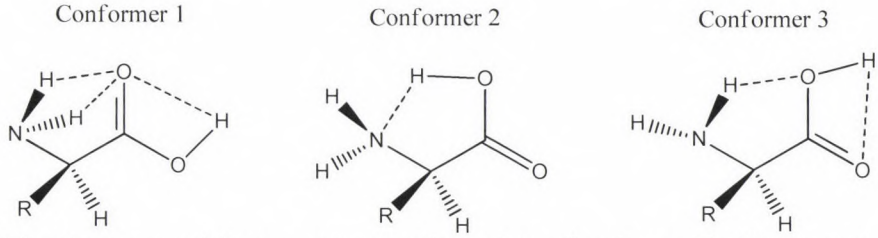

Figure 1.2: *The three general lowest energy conformations of amino acids. The R group shown here represents the amino acid side chain, which in this study can be H (glycine), CH_3 (alanine), or $CH(CH_3)_2$ (Valine).*

One concern when dealing with aliphatic amino acids is the role that the side chain R group plays in influencing the overall geometry of the species. Ideally, a smaller model species, such as alanine, would be used to predict the behavior of other aliphatic side chain containing species. While some studies have been conducted to survey the effect of the side chain on the overall geometry of aliphatic amino acid species,[22–24] few definite conclusions have been made regarding whether alanine could function as an appropriate model for other aliphatic amino acids.

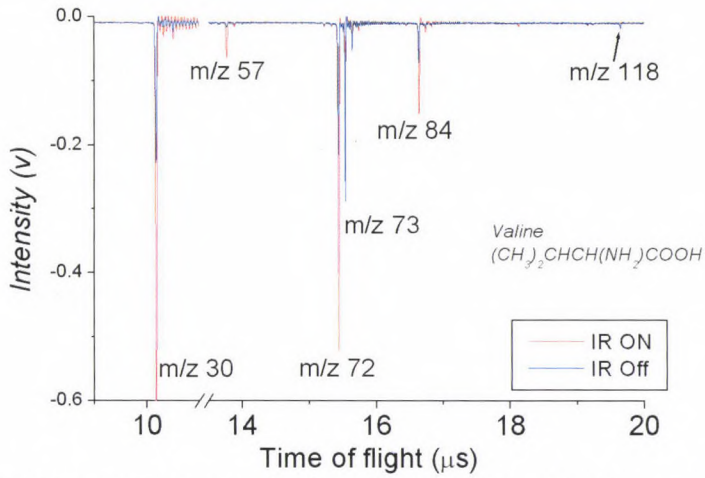

Figure 1.3a: The mass spectrum of valine after ionization with 118 nm radiation only (blue) and after 118 nm + IR radiation (red). All major mass channels are either enhanced or depleted with the addition of the IR radiation. Adapted from Hu and Bernstein.[16]

Here presented are the results of all studies of aliphatic amino acids, including a summary of IR-VUV ion dip spectroscopy that was previously published by Hu and Bernstein[16] (Figure 1.3), as well as more recent work which we have done. The new work includes some study of alanine, and high-level theoretical studies which explore the observed chemistry of aliphatic amino acids upon ionization using 118 nm radiation. The earlier conclusions pertaining to conformer dependent chemistry are verified, and conformer dependent chemical decomposition pathways are further elucidated.

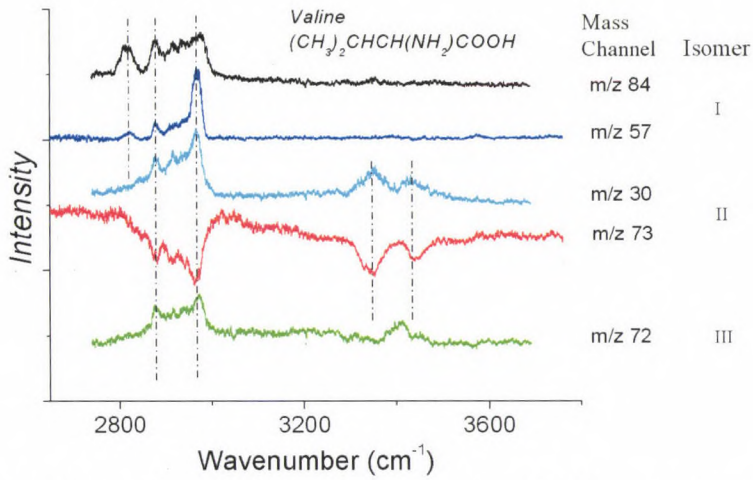

Figure 1.3b: The resultant spectra obtained through monitoring mass channels as the IR frequency is scanned. Modulations in the signal intensity provide a vibrational spectrum of the species, in this case valine. Mass channels are grouped to reflect the neutral parent which best correlates to the observed spectrum. Adapted from Hu and Bernstein.[16]

1.2 Methods and Materials:

Single photon ionization IR–VUV ion dip spectroscopy

The experimental apparatus used to record time of flight, mass and IR spectra in combination with a VUV single photonionization source is shown in Figure 1.4, and is described elsewhere.[16] Commercial samples of amino acids (Aldrich) are used without further purification. The solid sample is placed close to the valve body (Parker General Valve series 9) and is heated to increase its vapor pressure. The entire nozzle body is heated to the sample temperature, which is typically 150–200 °C. This provides an adequate stream of target molecules, with sufficiently low temperature to ensure that the thermally fragile low volatility amino acids remain undissociated in the gas phase.

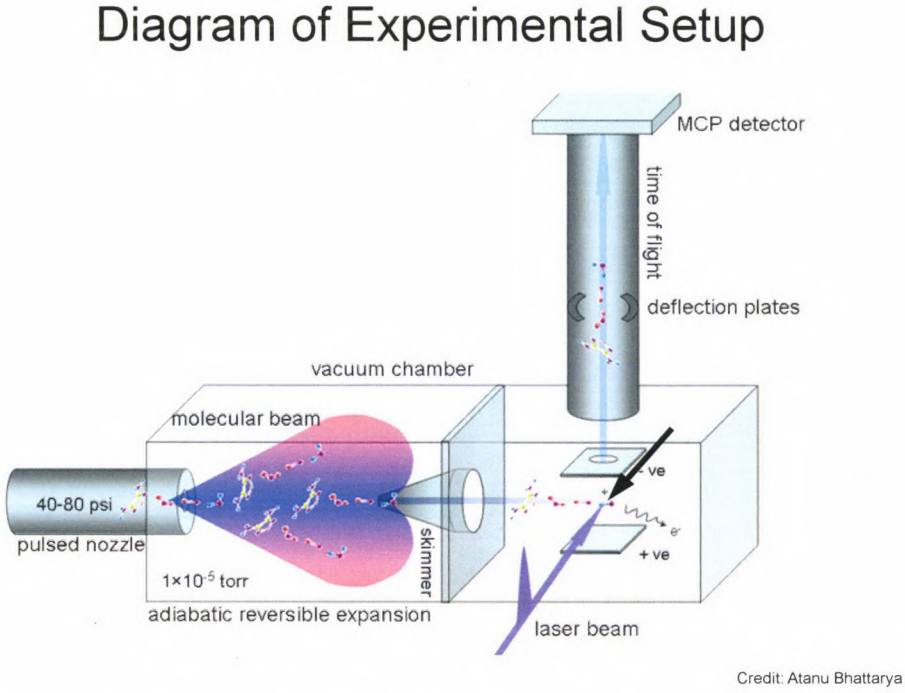

Figure 1.4: *A schematic representation of the experimental apparatus.*

The gaseous amino acid molecules are seeded into a neon/helium gas mixture (70%/30%, total pressure of 2 atm) and the gaseous mixture is expanded into a high vacuum chamber by the pulsed supersonic nozzle with a pulse width of typically 150 μs duration. After passing through a skimmer, the molecular beam interacts with pulsed VUV and IR laser beams in the ionization region of a time of flight mass spectrometer, TOFMS, in which VUV laser generated ions are detected.

The 118 nm radiation is the ninth harmonic of the fundamental output of a Nd^{+3}/YAG laser at 1.064 μm. 355 nm radiation (third harmonic) is focused into a cell with Xe/Ar at a ratio of 1:10 at ~200 Torr total pressure. A MgF_2 lens focuses the 118 nm light in the ionization region of the TOFMS and disperses the remaining 355 nm light.

An IR laser beam, which counterpropagates with respect to the 118 nm laser beam, is focused at the VUV/molecular beam intersection point by a 40 cm focal length lens to access neutral ground state species. Tunable IR radiation is obtained from an optical parametric oscillator, OPO (Laser Vision), pumped by an injection seeded Nd^{+3}:YAG laser (Spectra Physics GCR-3). A type II KDP (KH_2PO_4) doubling crystal is integrated into the OPO to convert the Nd^{+3}:YAG laser fundamental output to 532 nm. Two interchangeable sets of nonlinear crystals ($KTiOAsO_4$, KTA) in the system are used to generate a difference frequency between the output of the first oscillator (712 nm to 2.13 μm) and a portion of the 1064 nm pump beam to provide wavelength coverage from 2.5 to 4.0 μm. The output beam consists of both signal and idler wavelengths from the down conversion of the 532 nm pump. The OPO output energy between 2500 and 4200 cm^{-1} is 3–5 mJ/pulse with a bandwidth of 2–3 cm^{-1}.

The IR absorption spectra are measured by the use of IR plus VUV nonresonant ionization and fragmentation detection spectroscopy. As the IR laser is scanned to excite cooled molecules to higher vibrational modes of their ground electronic state prior to the introduction of VUV light, the fragment ion mass channel intensity is monitored. The vibrational spectrum of the neutral isomeric molecules is thereby obtained, as the fragmentation pattern depends on the total energy in the amino acid cation and on the conformational structure of the amino acid. Both positive and negative intensity changes in the fragment mass channels can be observed as a function of IR absorption, as the various channels for fragmentation become more or less accessible depending on the total energy in the amino acid parent ion.

Computational Details and Procedures

All calculations, unless specified otherwise, were performed using the Gaussian03 software package. All calculations were performed on a local cluster, or on NCSA machines (Mercury, Cobalt, Abe) using a Teragrid account. In general, the initial molecular geometry was taken from a model built in a 3D modeling package, such as Chem3D. The model was then minimized by MM2 molecular mechanics through a GAMESS interface. This geometry was minimized using UHF/6-311++G(d,p) to provide an initial geometry for the desired calculation. Atoms were labeled as shown in Figure 1.5.

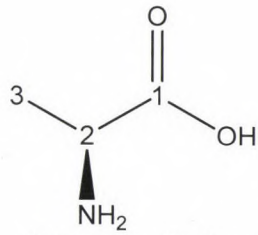

Figure 1.5: *A stick figure representation of alanine, with the carbons numbered as they are used in this chapter. C_1 is the carboxylic acid carbon. C_2 is the carbon attached to the amine group on the amino acid. C_3 is the first (and, in the case of alanine, only) carbon on the R-group side chain.*

Alanine and valine were chosen as representative aliphatic amino acids. Valine was investigated since it had already been investigated through IR-VUV ion dip spectroscopy, and alanine because it is the simplest aliphatic amino acid. According to computational work performed by Hobza,[25] Alonso,[20, 21] and others,[26-29] the three general conformers represented in Figure 1.2 are the three lowest energy, and therefore most abundant, conformers of neutral aliphatic amino acids. Further work by Alonso investigated the energetic landscape of valine within these general conformers, and the secondary structures which arise due to the additional orientations of the aliphatic side chain.[20,21] The lowest energy conformers of valine are represented as 1a, 2a, and 3b

(Figure 1.6). Thus, these three lowest energy configurations of these lowest energy conformers were selected for study.

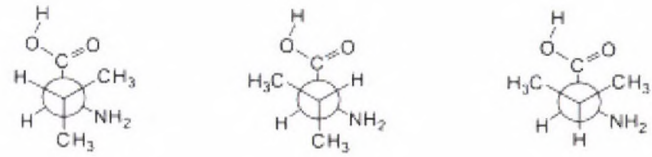

Figure 1.6: *The secondary structure that can arise from orientation of the side chain in some aliphatic amino acids. In our current study, we used the (a) structure for Conformers I and II, and the (b) configuration for Conformer III. Adapted from Alonso.*[20]

To establish an appropriate method for initial investigations, the B3LYP and second order Møller-Plesset perturbation theory (MP2) methods were compared, using the 6-311++G(d,p) basis set for both methods. The ground electronic states of neutral and ionized glycine were compared. Based upon the results of these investigations, the MP2 method was selected. According to work done by Hobza on glycine and similar molecules,[30] the most efficient basis with minimal error when utilizing the MP2 method and dealing with similar systems is the aug-cc-pVTZ Dunning basis set. This did not always prove to be economical, but efforts were made to utilize the largest Dunning-type basis set that available resources permitted.

In performing these large basis set optimizations, a series of MP2 level optimizations were performed, each with a serially larger basis set. Initial MP2 optimizations were performed at the MP2/6-311++G(d,p) level. The minimized geometry from the smaller basis set was then used as the initial geometry for the next larger basis set optimization, e.g., 6-311++G(d,p)→ aug-cc-pVDZ→ cc-pVTZ→ aug-cc-pVTZ.

It quickly became apparent that a full understanding of the chemistry of these aliphatic amino acid systems would require an investigation into their ion state chemistry.

Some rudimentary potential energy surfaces (PESs) were calculated at the MP2 level. While single configuration state function methods are useful for initial ion state calculations, they are limited in scope, and do not consider essential interactions between nearly degenerate excited state configurations. Consequently, a multiconfigurational approach is required. Thus, the CASSCF (Complete Active Space Self Consistent Field) method was employed to study the PESs of several amino acid species, including alanine, valine, histidine, and phenylalanine.

The general method for the CASSCF calculations is as described by Robb.[31–33] Optimized geometries from large basis set MP2 calculations were re-optimized at the RHF/STO-3G level in order to obtain the initial CAS orbitals. From there, an active space was chosen to best represent the chemistry being studied, and a single point CASSCF/STO-3G calculation was run. In this case, the desired active space represented the weak interactions of the amino acid functional groups and the bonding interactions of the chemistry being observed. According to Robb, 6-31G* is usually a sufficiently large basis set to obtain acceptable results when performing CAS calculations. In order to project the basis set up to the desired level, a single point CASSCF/3-21G was run, followed by an optimization at CASSCF/4-31G, then a single point CASSCF/6-31G*, and finally an optimization at CASSCF/6-31G*.

The largest active space that could be efficiently used in the CASSCF calculations using the available resources consisted of ten orbitals. The active space selected for the CASSCF calculations consisted of two non-bonding orbitals on each carboxylic oxygen, one amine non-bonding orbital, three carboxylic acid pi orbitals, and a bonding and nonbonding sigma orbital. The particular sigma orbitals depended on which chemical

bond PES was being calculated. Thus, a total of 16 (or 15, in the case of ions) electrons were placed into ten orbitals to perform CASSCF(16,10) calculations. A sample active space is shown in Figure 1.7.

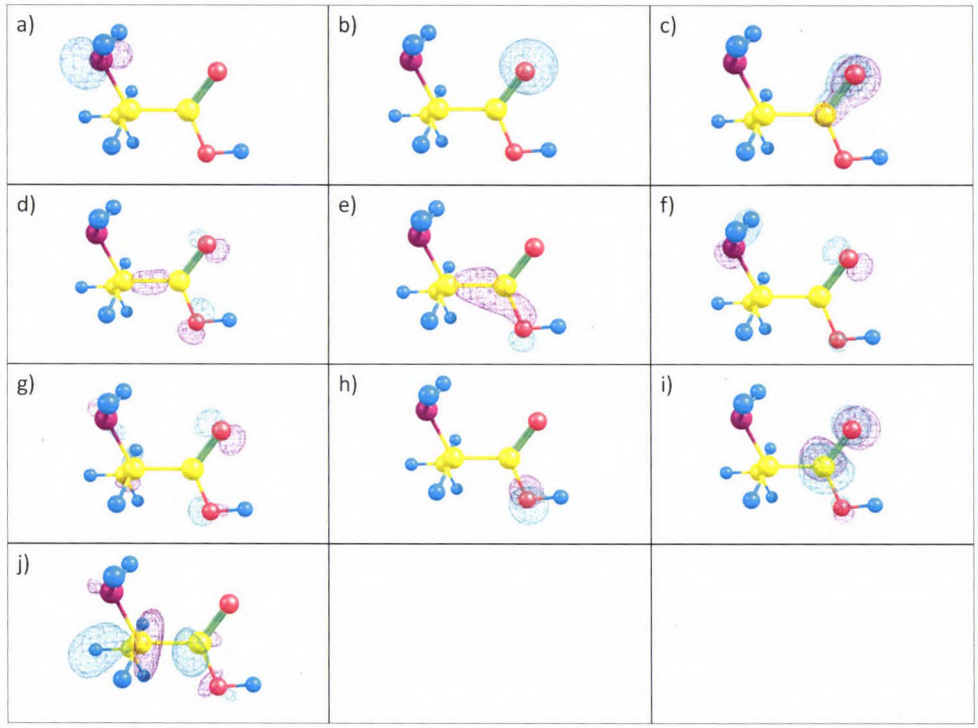

Figure 1.7: *A sample alanine active space, in this case for Conformer 1, employed in the ion calculation. The chosen active space consists of 10 orbitals: two bonding(c, h) and one anti-bonding(i) carboxylic π orbitals, one bonding(e) and one anti-bonding(j) C–C σ bond, and one non-bonding orbital located on the N(a), and four on the carboxylic Os(b,d,f,g).*

1.3 Results and Discussion

The resultant mass spectra from the single photon ionization (SPI) IR–VUV ion dip spectroscopy for glycine and valine, as reported by Hu and Bernstein[11], are shown in Figure 1.3a, and the IR spectra obtained from glycine and valine are presented in Figure

1.3b. Since the publication of the initial paper, further study on additional amino acid species utilizing the same method was attempted. In the case of alanine, a fragment mass spectrum was obtained, and is shown in Figure 1.8.

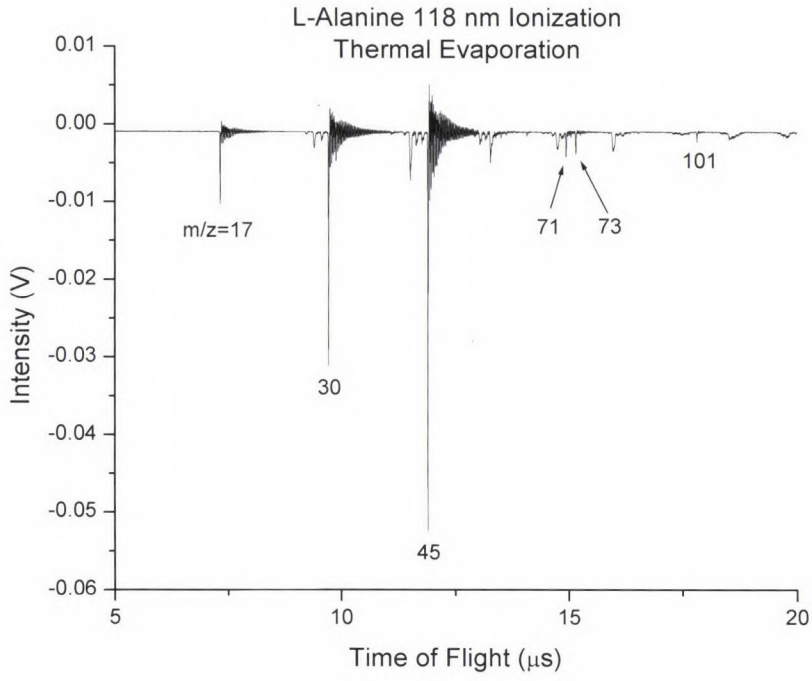

Figure 1.8: *Mass spectrum of alanine, obtained through single photon 118 nm ionization.*

The fragmentation pattern for all aliphatic amino acids seems to be that Conformer 1 and Conformer 3 both undergo a C_1–C_2 bond break (Figure 1.5), whereas Conformer 1 also undergoes some mechanism which creates the loss of either an OOH or an NH_2OH group (Figure 1.9). Conformer 2 undergoes a proton transfer from the carboxylic OH to the amine nitrogen, followed by the loss of CO_2. Conformer 2 also can lose its side chain group following the loss of CO_2—this channel is enhanced when additional energy from the IR laser is introduced into the system (Figure 1.3b). In the case of glycine, Conformer 2 likely undergoes the loss of its side chain group (a single

hydrogen), but IR energy does little to enhance this channel, and thus it is difficult to verify this through spectroscopic means.

The fragment mass spectrum obtained from alanine seems consistent with the mass spectra obtained from other aliphatic amino acid species, such as valine (Figure 1.3a). The observed mass channels of 30 ($CHNH_3$) and 45 (CH_3CHNH_3) amu correspond to similar Conformer 2 decomposition chemistries in other aliphatic species, thus it is likely that the signal observed was indeed the result of non-decomposed sample. The 71 and 73 amu mass channels correspond to the loss of water and methane from alanine, respectively.

Thermal evaporation of aliphatic amino acid samples can generate a gas-phase sample which can be studied. It is possible that with more sensitive equipment the same method of ion generation and IR–VUV ion dip spectroscopy could be used to study additional species. It is also likely that placing the sample into the gas phase through other methods, such as laser ablation, could result in a greater concentration of sample in the gas phase and thus produce a greater signal intensity.

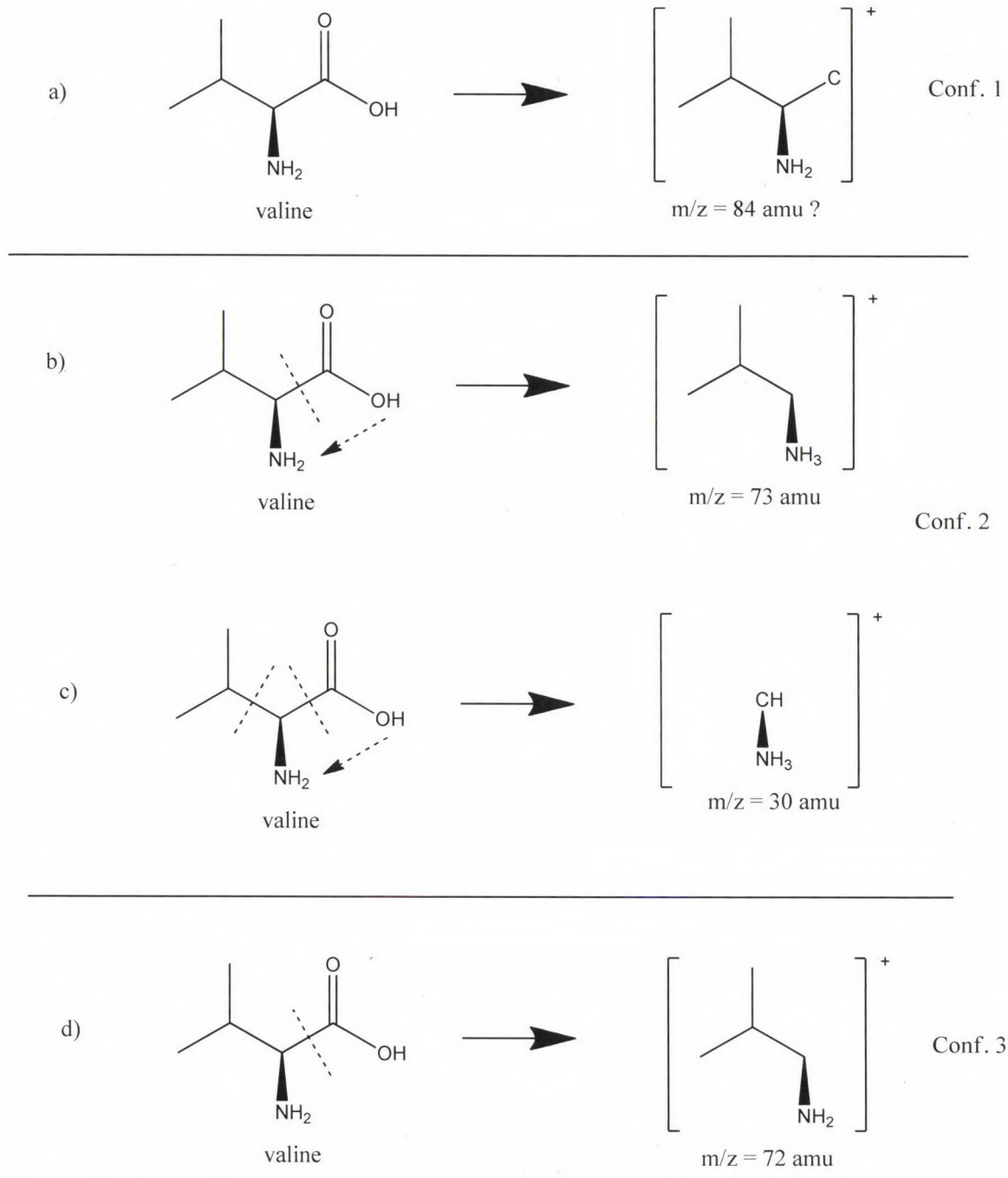

Figure 1.9: *Proposed fragmentations and fragments based on the valine IR-VUV ion dip spectra. (Note: (d), while labeled as Conformer 3, is likely a mix of Conformers 1 & 3). The ? represents uncertainty about the exact structure.*

Proof of method has been shown, and the method of SPI IR–UV ion dip spectroscopy opens up a new realm of spectroscopic study. Whereas previous

spectroscopic methods of studying bioactive molecules were only able to focus on species containing an aromatic moiety, now a much broader realm of biologically active molecules (amino acids, saccharides, etc.) is available for study in a molecular beam. A comprehensive picture of biologically active species can now be addressed. A pattern for the conformer-specific fragmentation of simple aliphatic amino acids is already beginning to emerge.

Similar, conformer-dependent fragmentation patterns are observed in all three species. Conformer 1 gives rise to fragments corresponding to the loss of either OOH or NH_2OH in both glycine and valine. Fragments arising from Conformer 2 and corresponding to the loss of CO_2, and the loss of CO_2 with the R group side chain are seen in glycine, alanine, and valine. Conformers 1 and 3 can give rise to fragments corresponding to the loss of COOH, as is seen in glycine and valine. No parent ion is observed via single photon VUV ionization in any of the species. Further details are provided in Table 1.1, and in Figure 1.9.

Table 1.1: *A comparison of the observed mass fragments (in amu) produced by 118 nm single photon ionization of glycine, alanine, and valine.*

	Conformer 1		*Conformer 2*		*Conformer 1/3*
	Loss of 33*	Loss R + 17**	Loss of CO_2	Loss R + CO_2	Loss of COOH
Glycine	33	--	31	30	30
Alanine	--	--	45	30	--
Valine	84	57	73	30	72

* mass fragment of 33 can be assigned as either OOH or NH_2OH
** mass fragment of 17 can be either OH or NH_3

In the spectra obtained from valine (Figure 1.3b), mass channels 73 and 30 both exhibit features corresponding to Conformer 2. It is interesting to note that mass channel 73 amu exhibits a negative change upon the absorption of IR radiation by the neutral

parent, while mass channel 30 amu exhibits a positive change. These channels correspond to the loss of CO_2, and the loss of CO_2 with the R-group side chain, respectively. Thus, it is likely that the loss of the R-group side chain is a secondary process to the initial loss of CO_2, and that the additional energy provided by the IR radiation encourages this secondary fragmentation.

Overall, the spectroscopic results show that aliphatic amino acids exhibit a clear conformer dependence when fragmenting upon single-photon ionization. Based on the similar results of glycine, valine, and alanine, the conformation specific fragmentations shown in Table 1.1 can be assumed to be the general fragmentation patterns all aliphatic amino acids will exhibit.

B3LYP vs MP2

The results of B3LYP and MP2 calculations for neutral and ionized glycine are summarized in Table 1.2, and their respective geometries are represented in Figure 1.9. When dealing with neutral structures, the B3LYP calculations resulted in generally more symmetric structures than the MP2 calculations. When compared to calculations performed with larger basis sets (aug-cc-pVDZ or better) or more advanced methods (CASSCF, or the CCSD(T) results reported by Hobza[14]), the more symmetric structures proved to be more compatible with the results of these higher level calculations.

When addressing ion structures, however, the B3LYP results proved to be less accurate when compared to higher level calculational results than those generated by MP2. The emphasis on symmetry which seems to occur within the B3LYP method resulted in highly inaccurate bond angles. Furthermore, B3LYP overly elongated the C_1–

C_2 bond in all three conformers studied, a feature which was especially inaccurate in Conformer 2.

Table 1.2: *A comparison of the B3LYP and MP2 results of glycine. Neutral species are listed as relative to the ground state neutral minimum energy of Conformer 1 (the lowest-energy conformer.) Vertical and adiabatic ion energies are listed as relative to the neutral minimum of the conformer. All energies are reported in eV.*

	B3LYP/6-311++G(d,p)				*MP2/6-311++G(d,p)*			
	Neutral	Vertical	Adiab.	Diff.	Neutral	Vertical	Adiab.	Diff.
Conf. 1	0	9.75	9.08	0.67	0	10.03	9.12	0.91
Conf. 2	0.02	9.82	9.31	0.51	0.02	10.17	9.59	0.58
Conf. 3	0.07	9.40	8.87	0.53	0.06	9.91	9.20	0.71

The MP2 method was superior when predicting the adiabatic ion structure of conformer 2. While B3LYP predicted a highly inaccurate structure (Figure 1.10), the MP2 method predicted the hydrogen transfer mechanism which was consistent with the experimental results. Although this pathway would later be explored in greater detail and at higher levels, this early result proved to be very useful in guiding further study. (It should be noted here that, while the MP2 method was superior to B3LYP, and useful for initial calculations, it was not the overall appropriate method for dealing with ion species.)

a)

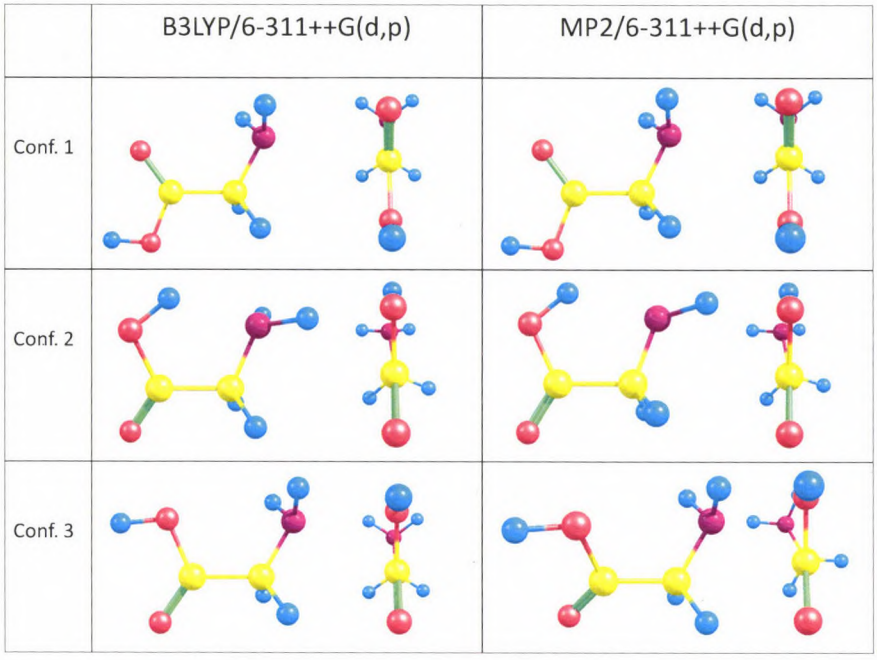

b)

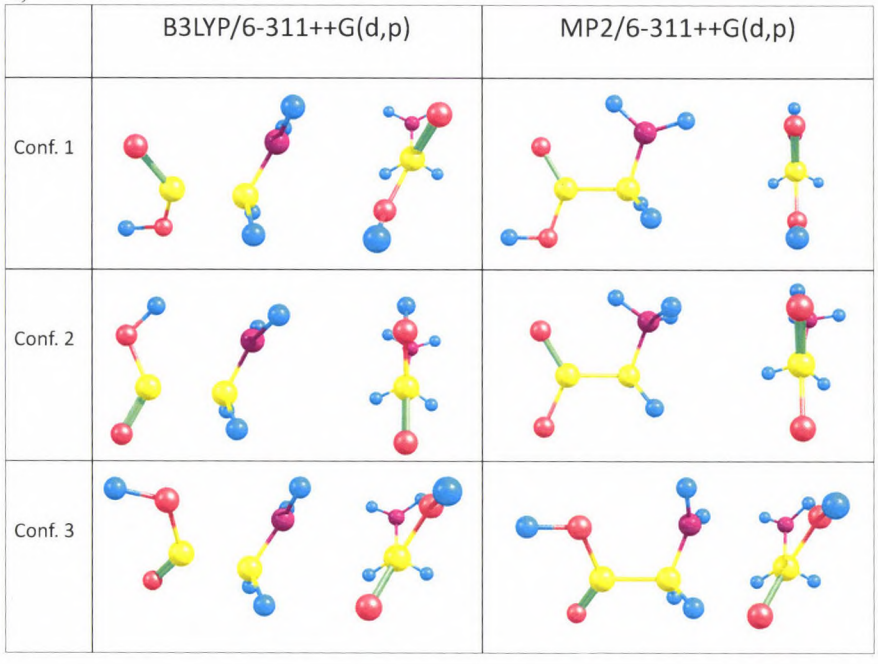

Figure 1.10: *The minimized geometries of neutral (a) and ionized (b) glycine, calculated at the B3LYP/6-311++G(d,p) and MP2/6-311++G(d,p) levels.*

MP2 vs CASSCF

The results of MP2 and CASSCF calculations are seen in Tables 1.3 and 1.4 and in Figure 1.11. While the MP2 calculations were performed with a much larger basis set than the CASSCF calculations, some general observations can be made.

Table 1.2: *Alanine Vertical and Adiabatic Ionization Energies (eV above S_0) calculated at the MP2/cc-pVTZ and CASSCF(15,10)/6-31G* levels of theory.*

	Conformer 1		*Conformer 2*		*Conformer 3*	
	MP2	CASSCF	MP2	CASSCF	MP2	CASSCF
Vertical*	10.02	8.71	9.99	8.88	9.93	8.52
Adiabatic	9.01	7.63	9.51**	8.19**	9.13	7.74
Difference	1.01	1.08	0.48	0.69	0.80	0.78

*Reported Value (all conformers): 8.88 eV.[30]
**This is actually what is referred to elsewhere as Conformer 2a

One particularly noticeable difference in results between the MP2 and CASSCF calculations is the difference in the adiabatic ion structure for Conformer 2. According to the MP2 results, a hydrogen transfer from the carboxylic OH to the amine N of the amino acid occurs in a barrier-less reaction that results in a structure referred here as Conformer 2a (Figure 1.12). The CASSCF results, however, predict an adiabatic ion structure that has not yet undergone this hydrogen transfer. As will be discussed later in the results section, a small barrier is predicted (~0.2 eV) between the adiabatic ion and a transition to Conformer 2a. In either case, the predicted vertical ionization energy of 8.8 eV is

sufficient to easily overcome any existing barrier, ultimately resulting in the energetically favored Conformer 2a geometry.

Table 1.3: *Alanine Electronic State Ion Energies (eV above S_0) [CASSCF(15,10)/6-31G(d)].*

	Conformer 1	*Conformer 2*	*Conformer 3*
D_0	8.7072111	8.8773705	8.5208031
D_1	10.5073794	9.9547218	10.4963229
D_2	11.1120957	11.0989089	11.7032526

Beyond differences in geometry, the CASSCF results for vertical ionization energies are closer to the reported values than are the MP2 results, despite the use of a smaller basis set. According to published benchmarks by Hobza, basis sets even larger than the ones utilized within this study are necessary to obtain proper ionization energies in MP2 calculations.[31] These results corroborate Hobza's conclusions.

The relative energy differences between vertical ionization energies and adiabatic ion energies, however, were the same within the margin of error for both methods. With regard to the ground state ion energy, the MP2 method, with a sufficiently large basis set, can be used to obtain acceptable relative adiabatic and vertical ionization energies. However, CASSCF, with its smaller necessary basis set, is much more cost effective in obtaining these results. Additionally, the single-reference nature of MP2 provides further limitations which the CASSCF method can overcome (exploration of excited states, etc.). These issues are discussed elsewhere by Robb[32–34] and Garavelli.[6]

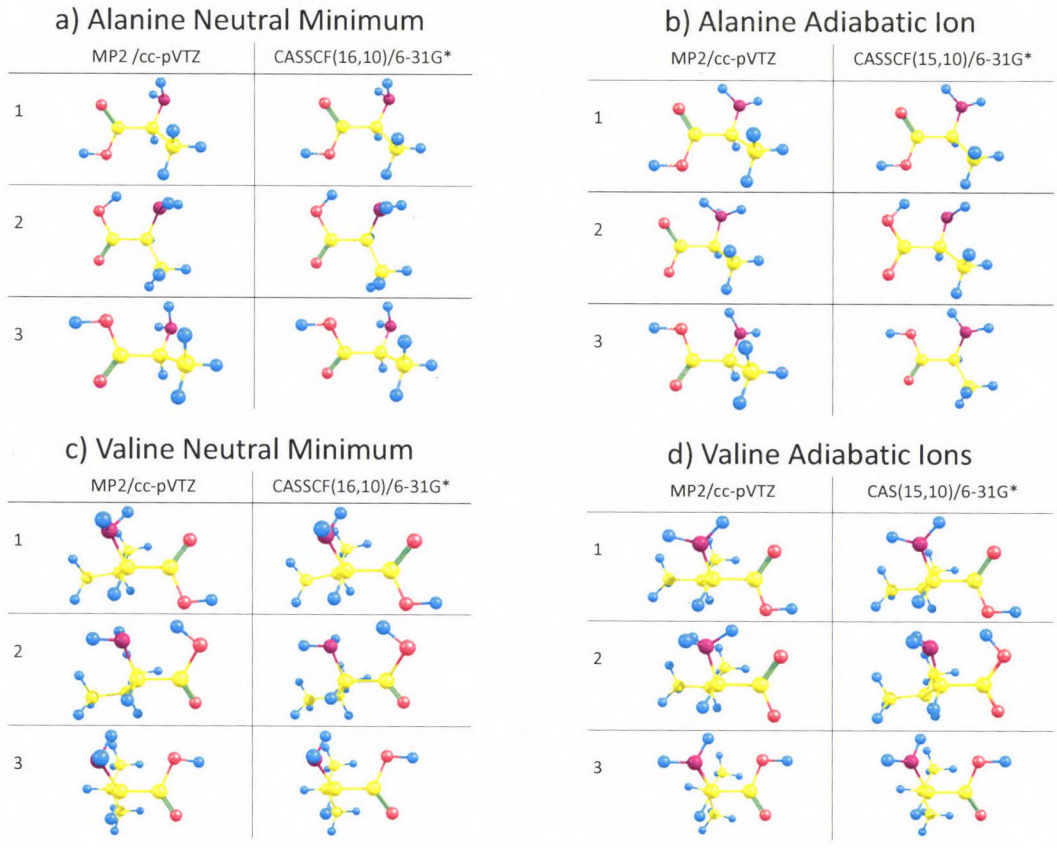

Figure 1.11: *The neutral ground state and ground adiabatic ion geometries of alanine (a, b) and valine (c, d), calculated at the MP2/cc-pVTZ and CASSCF(16/10)/6-31G* levels.*

From a calculational perspective, alanine does seem to be a reasonable model for the more complicated aliphatic amino acids. The side chain does interact with the other amino acid functional groups (amine, carboxylic acid), and when comparing alanine and valine, the side chain seems to interact in similar ways based on calculated geometries. Barrier heights are similar to within a few tenths of an eV for these two molecules, and predicted reaction pathways are similar. The biggest difference is that the larger side chain on valine seems to have a lower dissociation barrier than the smaller side chain on alanine (larger radicals tend to be more stable than smaller ones), although these are still similar to within a few tenths of an eV.

CASSCF in detail

Utilizing CASSCF(16,10)/6-31G* or CASSCF(15,10)/6-31G* (for neutral and ionized species, respectively), the full range of conformer potential energy surfaces can be explored.

Conformer 1

Spectroscopic evidence from glycine and valine suggests that Conformer 1 in the aliphatic species undergoes a C_1–C_2 bond dissociation upon photoionization (see Figure 1.5 for numbering), causing the loss of COOH. (Figure 1.9, Table 1.1). In alanine, the barrier height between the adiabatic ion (7.6 eV) and the transition state for a simple C_1-C_2 bond dissociation (8.6 eV) is around 1.0 eV, and the transition state energy is around 0.1 eV below the calculated vertical ionization energy of 8.7 eV. In valine, the adiabatic ion and transition state are calculated to be 7.5 and 7.9 eV, respectively. Thus, the assignments based on spectroscopic observations are clearly possible and likely.

Additionally, spectroscopic evidence suggests that Conformer 1 generally loses either an OOH or a NH_2OH group (Table 1.1, Figure 1.9). It is still not entirely clear what the mechanism is, or even whether it is an OOH or an NH_2OH group which is lost. The pathways investigated in this study included the breaking of a C-O bond (Figure 1.12c), and the breaking of the C_2-C_3 bond (Figure 1.12b). In neither case did the investigated pathway seem to be a likely reaction pathway for the observed chemistry.

a)

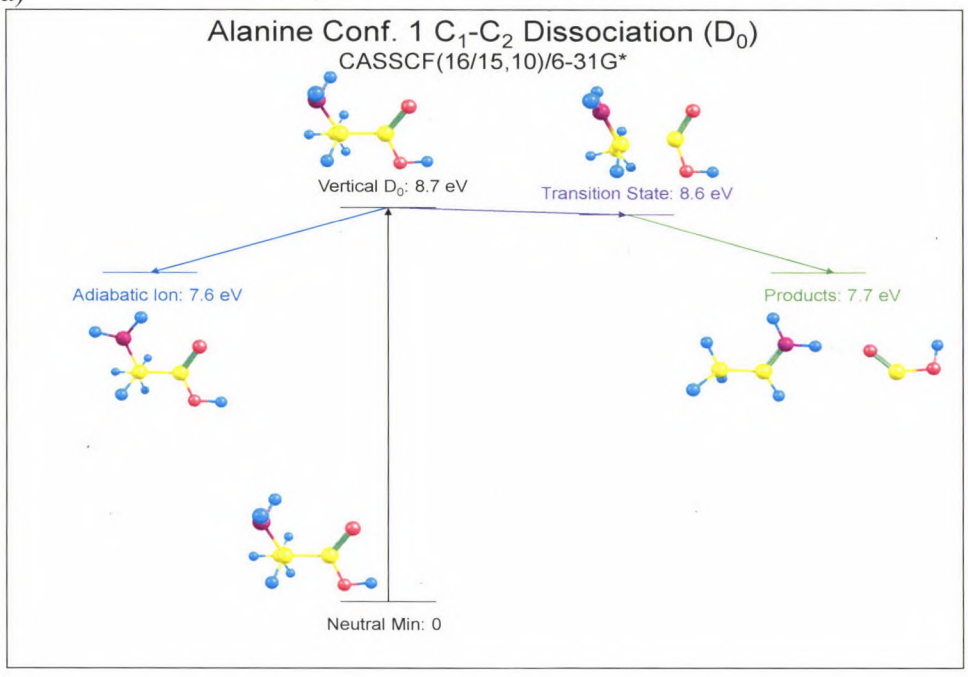
Alanine Conf. 1 C_1-C_2 Dissociation (D_0)
CASSCF(16/15,10)/6-31G*
Vertical D_0: 8.7 eV
Transition State: 8.6 eV
Adiabatic Ion: 7.6 eV
Products: 7.7 eV
Neutral Min: 0

b)

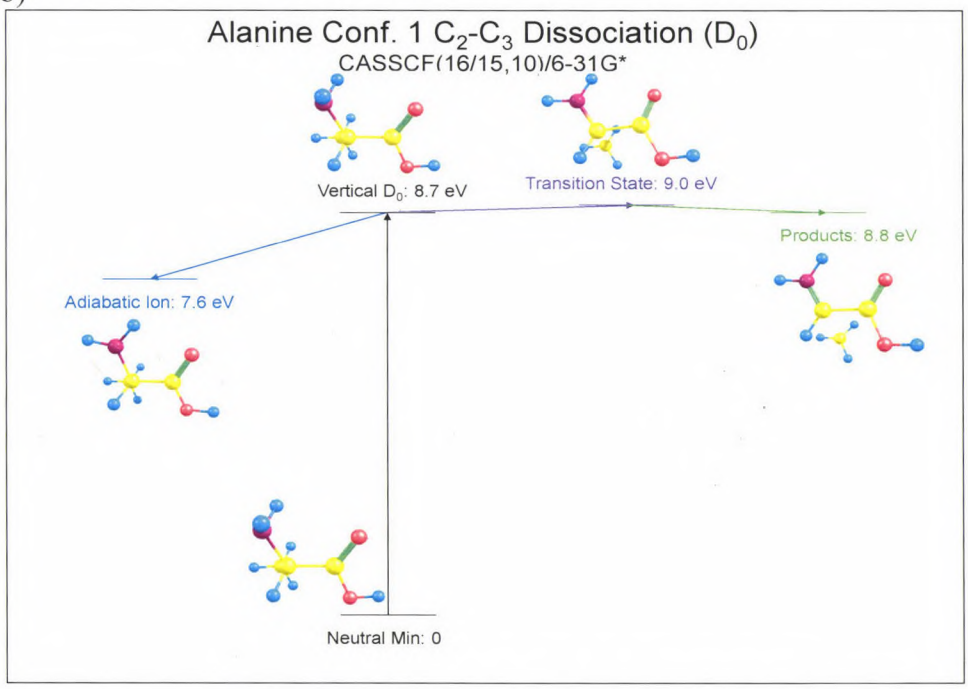
Alanine Conf. 1 C_2-C_3 Dissociation (D_0)
CASSCF(16/15,10)/6-31G*
Vertical D_0: 8.7 eV
Transition State: 9.0 eV
Products: 8.8 eV
Adiabatic Ion: 7.6 eV
Neutral Min: 0

c)

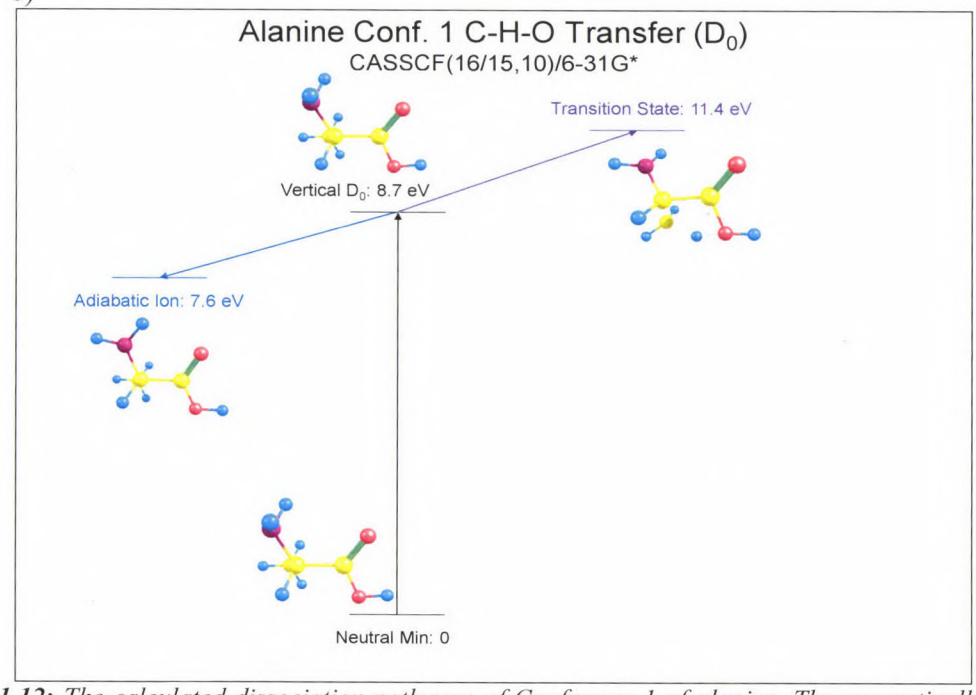

Figure 1.12: *The calculated dissociation pathways of Conformer 1 of alanine. The energetically favored pathway is seen in (a), the dissociation of the C_1-C_2 bond. Other pathways are seen in (b) and (c).*

In a couple of instances, the reaction chemistry of electronically excited ion states was investigated. It was found that, as the structure approached transition state geometry, the excited state ion relaxed back down into the ground electronic ion state (D_0) via a conical intersection. (This is discussed in greater detail in Chapter 2.) Thus, in all conformers, it was assumed that specific excited electronic ion states did not produce unique chemistry.

Conformer 2

Spectroscopic evidence indicates that Conformer 2 generally undergoes two main reaction pathways: 1) the loss of CO_2, and 2) the loss of CO_2 with the additional loss of the R-group side chain. In both cases, the CO_2 elimination was assumed to be the result of a hydrogen transfer from the carboxylic OH to the amine N (Figure 1.9), and the

calculational results verify these preliminary judgements (Figure 1.13). The barrier heights of a C_1-C_2 and of a C_2-C_3 dissociation, and the barrier height of a carboxylic OH to amine N proton transfer were all calculated for alanine and valine. While the barrier heights for a C_1-C_2 bond dissociation and for a hydrogen transfer are initially similar (Figure 1.12a, 1.12c), the ultimate products resulting from the hydrogen transfer / loss of CO_2 pathway are clearly more energetically favorable (7.5 eV for the products of a C_1-C_2 bond dissociation vs. 5.8 eV for the products of a hydrogen transfer followed by the loss of CO_2). Additionally, as we will show in Chapter 2, the charge location upon ionization in Conformer 2 further favors the hydrogen transfer pathway.

Upon hydrogen transfer, the loss of CO_2 by means of a C_1-C_2 bond break is clearly favored over the immediate loss of the aliphatic side chain by mean of a C_2-C_3 bond break, in both alanine and valine (Figure 1.13). After the loss of CO_2 has occurred, the remaining barrier toward the loss of the aliphatic side chain group is 1.6 eV in alanine and 1.1 eV in valine. In both cases, this is possible, but the additional energy provided by the absorption of IR radiation by the neutral parent clearly increases the likelihood of this mechanism taking place (Figures 1.3b, 1.9, 1.13).

a)

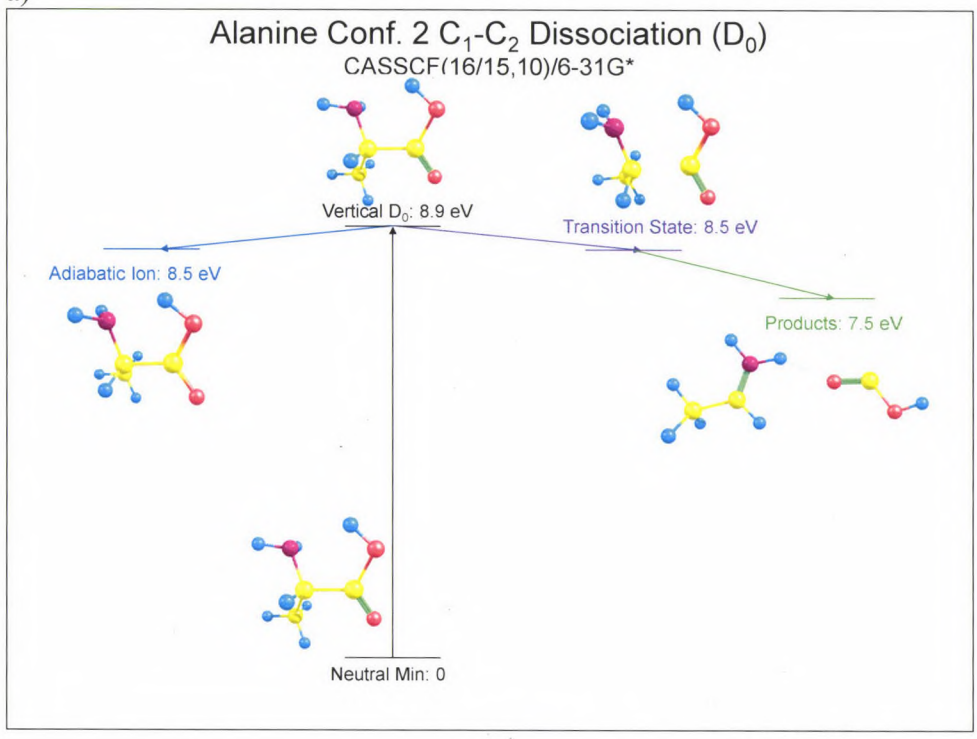
Alanine Conf. 2 C_1-C_2 Dissociation (D_0)
CASSCF(16/15,10)/6-31G*
Vertical D_0: 8.9 eV
Transition State: 8.5 eV
Adiabatic Ion: 8.5 eV
Products: 7.5 eV
Neutral Min: 0

b)

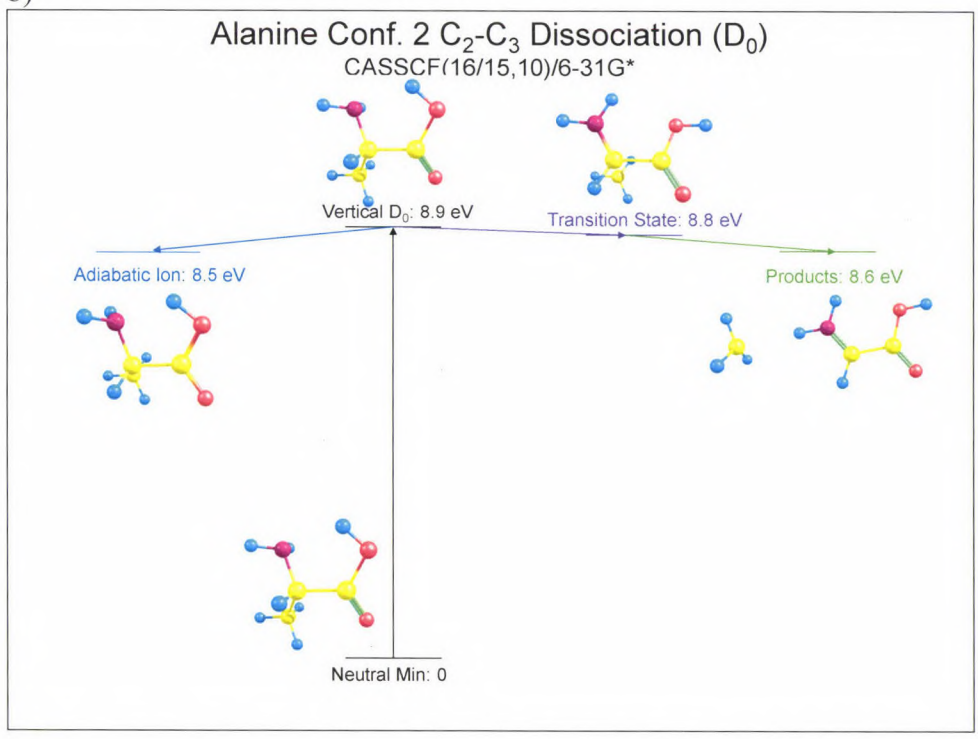
Alanine Conf. 2 C_2-C_3 Dissociation (D_0)
CASSCF(16/15,10)/6-31G*
Vertical D_0: 8.9 eV
Transition State: 8.8 eV
Adiabatic Ion: 8.5 eV
Products: 8.6 eV
Neutral Min: 0

c)

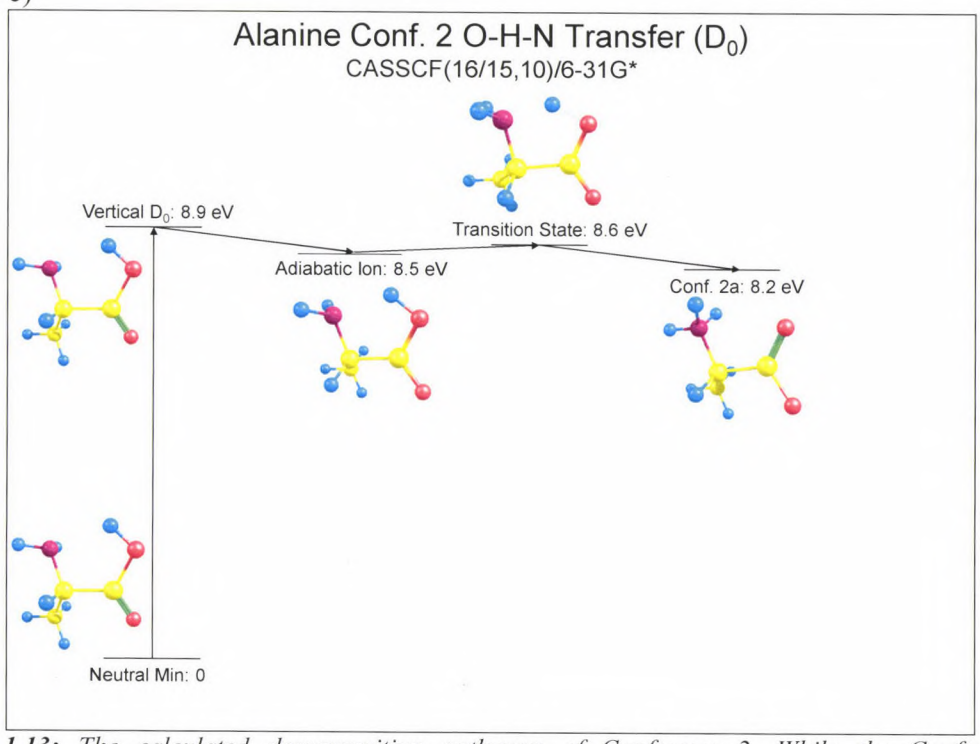

Figure 1.13: *The calculated decomposition pathways of Conformer 2. While the Conformer 2a intermediate may not be the initially energetically favored pathway, the secondary CO_2 elimination pathways following this transfer result in energetically favored products.*

Conformer 3

Conformer 3, due to its higher energy, is likely present in relatively small quantities in our experiments, and so its contribution is likely quite small. Spectroscopically, the only pathway that was suggested for Conformer 3, and thus the only pathway that was explored, was the breaking of the C_1-C_2 bond (Figure 1.14). For both alanine and valine, this pathway is shown to be even more likely than in Conformer 1 (Figure 1.12a). The barrier height is typically around 0.2 eV below the calculated vertical ionization energy.

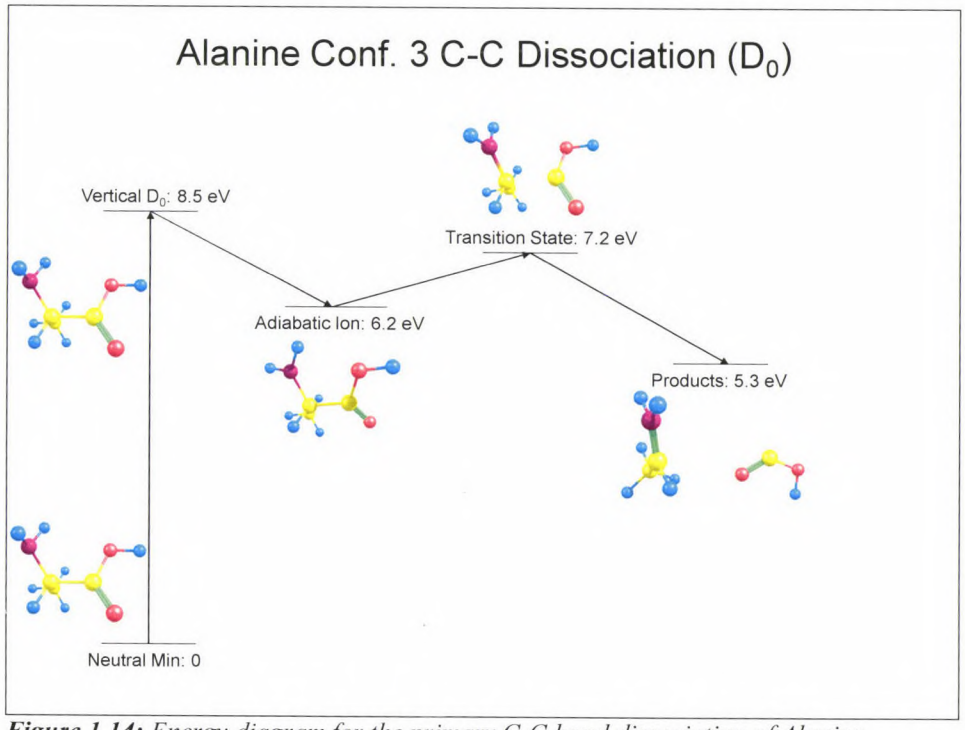

Figure 1.14: *Energy diagram for the primary C-C bond dissociation of Alanine.*

The spectroscopically observed fragmentations of aliphatic amino acids in general are fully consistent with the calculated PESs of the alanine and valine, along with the generalizations we can make based upon our theoretical results. Spectroscopically, we never see a fragment corresponding to the simple loss of an R-group side chain, and in no conformer is the immediate loss of the R-group side chain calculated to be energetically favored For Conformers 1 and 3, the loss of COOH is calculated to be possible and favored, which is corroborated by the observed fragments of 30 amu in glycine and of 72 in valine. For Conformer 2, a proton transfer followed by (or simultaneous with) the loss of CO_2 is clearly favored, and can lead to a stable product fragment. This is seen in the mass fragments of 31 amu in glycine, 45 amu in alanine, and 73 amu in valine. Upon losing CO_2, Conformer 2 can additionally lose its side chain R-group (mass fragment 30

is observed in all three species). The spectra obtained for valine (Figure 1.3) makes clear that this process occurs after the initial loss of CO_2, and that this additional loss of the R-group side chain is enhanced when additional energy in the form of IR radiation is introduced into the neutral molecule. This enhancement is also consistent with the calculations.

1.4 Conclusions

Photoionized aliphatic amino acids undergo conformer specific chemistry. The unique spectra obtained from different fragment mass channels clearly indicate this type of behavior, which is also predicted by calculations. The fragments observed in the various single photon ionization IR–VUV experiments coincide with predicted decomposition pathways, and the spectra obtained in the various fragment channels indicate that the predicted parent conformers give rise to the fragment.

Alanine, being the smallest aliphatic amino acid, appears to be a good model for most aliphatic amino acids. The smaller system is more computationally efficient, and similar enough to valine in its results that it can be considered a reasonable model. Among the aliphatic amino acids that contain simple hydrocarbons as a side chain, the side chain does appear to interact to some degree with the other functional groups, but in similar ways for all species. In any case, considering both spectroscopic and calculational studies, the photochemistry of aliphatic amino acids can be well understood.

Further theoretical exploration into additional conformers is possible, especially if these conformers are observed in solvated conditions, or within peptide structures. The

most likely direction for future study of simple aliphatic amino acids though, based upon a systematic micro to macro approach, is to observe what changes in behavior are observed upon the formation of simple dipeptides, such as Gly–Gly, Gly–Ala, or Ala-Ala. Exploration of other amino acids is clearly an important direction to pursue, as well.

1.5 References

1. Junk, G. and Svec, H. *Journal of the American Chemical Society*, **1963**, *85*, 839.
2. Weinkauf, R., Schermann, J. P., de Vries, M. S. and Kleinermanns, K. *European Physics Journal D*, **2002**, *20*, 309.
3. Robertson, E. G. and Simons, J. P. *Physical Chemistry Chemical Physics*, **2001**, *3*, 1.
4. Vishveshwara, S. and Pople, J. A. *Journal of the American Chemical Society*, **1977**, *99*, 2422.
5. de Vries, M. S.; and Hobza, P. *Annual Reviews in Physical Chemistry*, **2007**. *58*, 585.
6. Császár, A. G. *Journal of Molecular Structure*, **1995**, *346*, 141.
7. Siam, K.; Klimkowski, V. J.; Ewbank, J. D.; Van Alsenoy, C. and Schafer, L. *Journal of Molecular Structure (Theochem)*, **1984**, *110*, 171.
8. Császár, A. G. *Journal of Physical Chemistry* **1996**, *100*, 3541.
9. Zheng, Y.; Neville, J. J. and Brion, C. E. *Science*, **1995**, *270*, 786.
10. Sellers, H-L. and Schäfer, L. *Chemical Physics Letters*, **1979**, *63*, 609.
11. Rodríguez-Santiago, L.; Sodupe, M; Oliva, A. and Bertran, J. *Journal of Physical Chemistry A*, **2000**, *104*, 1256.
12. Papp, P.; Urban, J.; Matejčík, Š.; Stano, M. and Ingolfsson, O. *The Journal of Chemical Physics*, **2006**, *125*, 204301.
13. Császár, A. G. and Perczel, A. *Progress in Biophysics & Molecular Biology* **1999**, 71, 243.
14. Černý, J. and Hobza, P. *Physical Chemistry Chemical Physics*, **2007**, *9*, 5291.
15. Dehareng, D. and Dive, G. *International Journal of Molecular Science*, **2004**, *5*, 301.
16. Hu, Y. and Bernstein, E. R. *Journal of Chemical Physiscs* **2008**, *128*, 164311.
17. Hu, Y. and Bernstein, E. R.; *Journal of Physical Chemistry A*, **2009**, *113*, 8454.
18. Muchová, E.; Slavíček, P.; Sobolewski, A. L. and Hobza, P. *Journal of Physical Chemistry A*, **2007**, *111*, 5259.
19. Zhang, L.; Pan, Y.; Guo, H.; Zhang, T.; Sheng, L.; Qi, F.; Lo, P. and Lau, K. *Journal of Physical Chemistry A*, **2009**, *113*, 5838.
20. Lesarri, A.; Cocinero, E. J.; López, J. C. and Alonso, J. L. *Angewandte Chemie International Edition*, **2004**, *43*, 605.
21. Blanco, S.; Lesarri, A.; López, J. C. and Alonso, J. L. *Journal of the American Chemical Society*, **2004**, *126*, 11675.
22. Sanz, M. E.; Lesarri, A.; Peña, M. I.; Vaquero, V.; Cortijo, V.; López, J. C. and Alonso, J. L. *Journal of the American Chemical Society*, **2006**, *128*, 3812.
23. Sanz, M. E.; Cortijo, V.; Caminati, W.; López, J. C. and Alonso, J. L. *Chemistry European Journal* **2006**, *12*, 2564.
24. Cocinero, E. J.; Lesarri, A.; Grabow, J.; López, J. C. and Alonso, J. L. *ChemPhysChem* **2007**, *8*, 599.
25. Bludský, O.; Chocholoušová, J.; Vacek, J.; Huisken, F. and Hobza, P. *Journal of Chemical Physics*, **2000**, *113*, 4629.
26. Pan, Y.; Zhang, L.; Zhang, T.; Guo, H.; Hong, X.; Sheng, L. and Qi, F. *Physical Chemistry Chemical Physics*, **2009**, *11*, 1189.

27. Kamariotis, A.; Boyarkin, O. V.; Mercier, S. R.; Beck, R. D.; Bush, M. F.; Williams, E. R. and Rizzo, T. R. *Journal of the American Chemical Society,* **2006**, *128*, 905.
28. Oegerle, W. R. and Sabin, J. R. *Journal of Molecular Structure*, **1973**, *15*, 131.
29. Godfrey, P. D. and Brown, R. D. *Journal of the American Chemical Society*, **1995**,*117*, 2019.
30. Klasinc, L. *Journal of Electron Spectroscopy and Related Phenomena*, **1976**, *8*, 161.
31. Jurečka, P.; Šponer, J.; Černý, J. and Hobza, P. *Physical Chemistry Chemical Physics*, **2006**, *8*, 1985.
32. Robb, M. http://www.ch.ic.ac.uk/robb/casscf.php
33. Bearpark, M. J.; Ogliaro, F.; Vreven, T.; Boggio-Pasqua, M.; Frisch, M. J.; Larkin, S. M.; Morrison, M. and Robb, M. A. *Journal of Photochemistry and Photobiology A: Chemistry,* **2007**,*190* 207.
34. Smith, B. R.; Bearpark, M. J.; Robb, M. A. Bernardi, F. and Olivucci, M. *Chemical Physics Letters,* **1995**, *242*, 27.

Chapter 2: Conformation Specific and Charge Directed Reactivity of Radical Cation Intermediates of α-substituted (Amino, Hydroxy, and Keto) Bioactive Carboxylic Acids

The work reported in this chapter was performed by Dr. Atanu Bhattacharya, Dr. Joong-Won Shin, and me. Dr. Bhattacharya is responsible for the original spectroscopic data and much computational analysis. I contributed to the computational results for glycine and valine. Dr. Shin provided vibrational analysis.

2.1 Introduction

Radical cation intermediates of α-substituted carboxylic acid based biological building blocks, such as amino acids, peptides and proteins, lactic acid, and pyruvic acid, have major roles in biochemistry and medicinal chemistry,[1] and are responsible for the development of a wide range of human physiological disorders.[2,3] In the past few years, the properties of different bioactive carboxylic acid derived radicals have attracted considerable attention, both from experimental[4-10] and theoretical points of view.[11-22]

The location of the charge and hydrogen bonding in a radical cation is of great importance for its reactivity and stability.[23] One of the most important aspects of the reaction dynamics of radical cation intermediates of peptides involves an extremely rapid (subfemtosecond) transfer of charge[24] and alteration of their reactivity due to variation of local sites for ionization.[23] Recent theoretical studies have predicted that charge migration in radical cations of glycine, following the removal of an electron from three different

orbitals, strongly depends on specific orientations of the atoms in the molecule (conformations).[25] Such charge migration can lead to distinct reaction dynamics for different glycine conformers;[26] however, this prediction has not yet been experimentally confirmed.

The flexibility of three dimensional structures of α-substituted bioactive carboxylic acids permits great conformational diversity. Different conformers can interconvert *via* hindered rotations about single bonds, giving rise to conformational isomerism. The behavior of these ionized conformers can be governed by their initial detailed molecular structures. Therefore, a detailed characterization of conformation specific reactivity of radical cation intermediates of α-substituted bioactive carboxylic acids would be invaluable for understanding the phenomenon of oxidative stress at a molecular level. A few studies of conformer selective dynamics of isolated radical cation intermediates of α-substituted bioactive carboxylic acids have recently appeared in the literature.[26,27]

For unambiguous tracking of a conformation specific biochemical reaction and its dynamics, isolation, identification, and fragmentation behavior of conformations are essential prerequisites. We carry out such an analysis using a supersonic jet expansion to obtain an internal temperature low enough to suppress interconversion between different conformers of lactic acid (α-hydroxy acid), pyruvic acid (α-keto acid), and glycine and valine (α-amino acids). Once the conformers are trapped in different local minima of their ground state potential energy surfaces, conformation specific fragmentation patterns for radical cation intermediates are proven by observing different infrared (IR) spectra (corresponding to different conformers) obtained at different fragment mass spectrometry

signals generated through the ionization process. The experimental studies are accompanied by highly correlated *ab initio* calculations at the MP2 and CASSCF levels of theory. The conformation specific differences in reactivity are explained by conformation mediated localization of the positive charge (or hole) on the radical cations formed through single photon vacuum ultraviolet (10.5 eV) ionization.

2.2 Experimental Methods

The experimental setup used to record time-of-flight mass spectra and IR-VUV ionization spectra has been previously described in detail.[28] Lactic acid and pyruvic acid are placed behind a pulsed valve body (Parker General Valve series 9) and are heated to about 50°C to increase their vapor pressure. The gaseous molecules are brought into the molecular beam by a neon/helium gas mixture (69%/31%) at 30 psig backing pressure. After passing through a skimmer, the molecular beam interacts with pulsed VUV and IR laser beams in the ionization region of a time of flight mass spectrometer.

The IR laser beam, which precedes by 50 ns and counterpropagates with respect to the 118 nm laser beam, is focused at the VUV/molecular beam interaction point by a 60 cm focal length lens to probe neutral ground state species. The 118 nm radiation is the ninth harmonic of the fundamental output of a Nd:YAG laser at 1064 nm. 355 nm radiation (third harmonic) of the Nd:YAG laser is focused into a cell filled with Xe/Ar at a ratio of 1:10 at 200 Torr total pressure. An MgF_2 lens focuses the 118 nm light in the ionization region of the time of flight mass spectrometer (TOFMS) and disperses the remaining 355 nm light. The tunable IR laser output generated by an OPO/OPA system

(Laser Vision), pumped by 532 nm radiation from another Nd:YAG laser, has an energy of 3-5 mJ/pulse and a bandwidth of ~2 cm^{-1} in the 2800-3800 cm^{-1} range.

2.3 Theoretical Methods

For rigorous descriptions of the PES of radical cationic bioactive carboxylic acids, highly correlated multiconfigurational methods are necessary.[29] These multiconfigurational methodologies are particularly important for calculating surfaces with "near degeneracy effects" caused by presence of conical intersections between the many low lying valance ion states. Ground electronic surface topology is often found[29] to be altered by proximity of an upper excited electronic state surface along a particular reaction coordinate near a conical intersection, which can only be calculated through multiconfigurational methods. Monoconfigurational methods such as HF or MP2 often overestimate or underestimate the energy barrier to a transition state on the ground electronic surface of the radical ion near conical intersections. Illustrations of such a consideration are found recently for many organic compounds[30] and for Conformer I of lactic acid and Conformer II of glycine and valine. Therefore, in the present work, exploration of cationic PESs is performed using the CASSCF level of theory. Furthermore, a number of configurations are expected to contribute to a particular electronic state of the radical cations. In fact, for glycine the $n\sigma_O$ and $n\pi_O$ configurations have equal weight (0.5) near the $(D_1/D_0)_{CI}$ on the ground cationic PES. The use of multiconfigurational methodology to explore PESs of the radical cationic lactic acid, glycine, valine, and pyruvic acid is thereby mandatory. To calculate dynamic correlation,

more expensive CASMP2 or CCSD(T) can be used; however, dynamical correlation energy is not always a contributing factor to the total energy. In particular, CASMP2 results do not improve the energetics significantly for the radical cation intermediates studied here. Thus the less expensive CASSCF level of theory with a 6-31G(d) basis set is used in the present study. Improving the basis set does not significantly improve the energetics at the CASSCF level of theory as long as a balanced active space is employed.[31]

All geometry optimizations relevant to the ion state decomposition of lactic acid, pyruvic acid, glycine, and valine are carried out at the CASSCF/6-31G(d) and MP2/aug-cc-pVDZ levels of theory using the Gaussian 03[32] and MOLPRO[33] programs. To explore the ion state PESs, the active space comprises 9 electrons distributed in 8 orbitals, denoted as CASSCF(9,8). The orbitals used in the active space of lactic acid, pyruvic acid, glycine, and valine are illustrated in Figure 2.S1 in the supporting information. We determine the lowest VIE explicitly calculating the energy difference between neutral and cation at the Franck-Condon geometry employing the MP2/aug-cc-pVDZ level of theory. Critical points (minima and transition states) are characterized by analytical frequency calculations. Minimum energy paths are calculated using an intrinsic reaction coordinate (IRC) algorithm implemented in the Gaussian 03 program suite. Conical intersection searches are performed using the algorithm implemented in Gaussian 03.

2.4 Experimental Results

Lactic acid

Lactic acid has three internal rotation axes that can give rise to a number of conformational isomers. It also has a chiral carbon which leads to the existence of enantiomers. As IR-VUV photoionization spectroscopy is not sensitive to molecular chirality effects, identification of different enantiomers of lactic acid is not possible using this spectroscopic technique; however, this technique can identify different conformers of lactic acid present in the molecular beam.

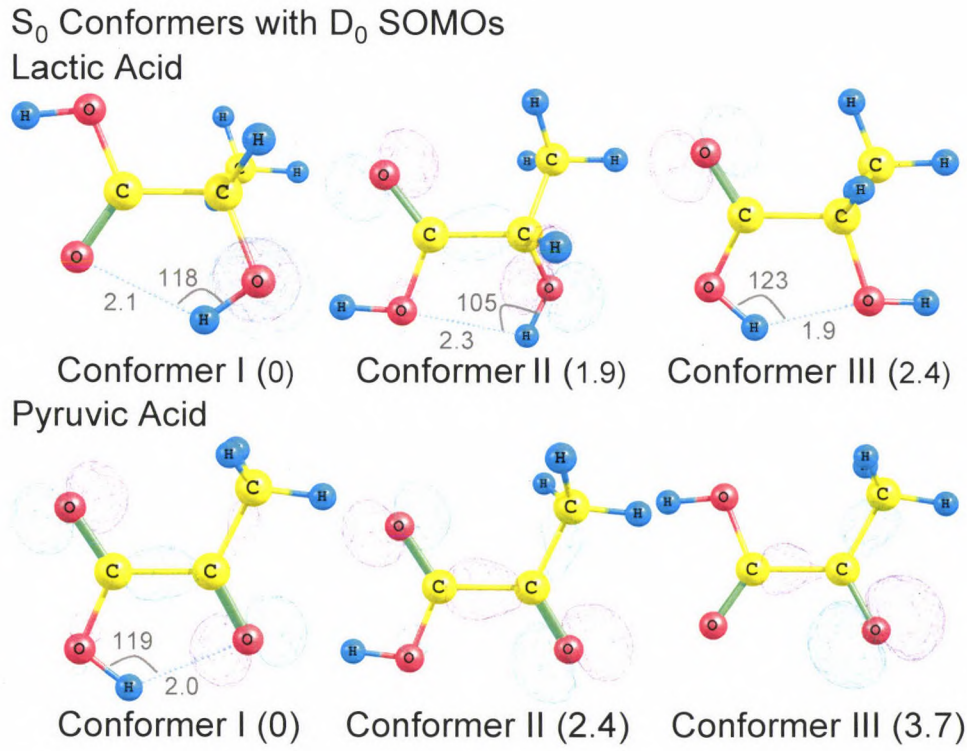

Figure 2.1: *The three lowest energy conformers of ground state (S_0) neutral lactic acid and pyruvic acid with calculated (MP2/aug-cc-pVDZ) relative energies (in kcal/mol), showing their bond distances and bond angles. The density plots for the SOMO (singly occupied molecular orbital) of lactic acid and pyruvic acid at the FC (Franck-Condon) point on the cationic D_0 surface calculated at the CASSCF(9,8)/6-31G(d) level of theory are also shown. The two colors for these orbitals indicate the plus and minus phases of the wavefunctions.*

The three lowest energy conformers of neutral lactic acid with calculated (MP2/aug-cc-pVDZ) relative energies (in kcal/mol) are depicted in Figure 2.1. These results are in agreement with previous theoretical calculations,[34] and the available microwave[35] and FTIR[36] spectroscopy data. The conformers differ mainly by different types of intramolecular hydrogen bonding linkages: O-H····O=C (Conformer I), O-H····O(H)CO (Conformer II), and C(O)O-H····O-H (Conformer III). Conformer I in Figure 2.1 represents the lowest energy conformer. The remaining possible conformers, which are not shown in the figure, are estimated to have a total population of less than 0.1% at 298 K,[36] and therefore have been considered of no interest for our present molecular beam study.

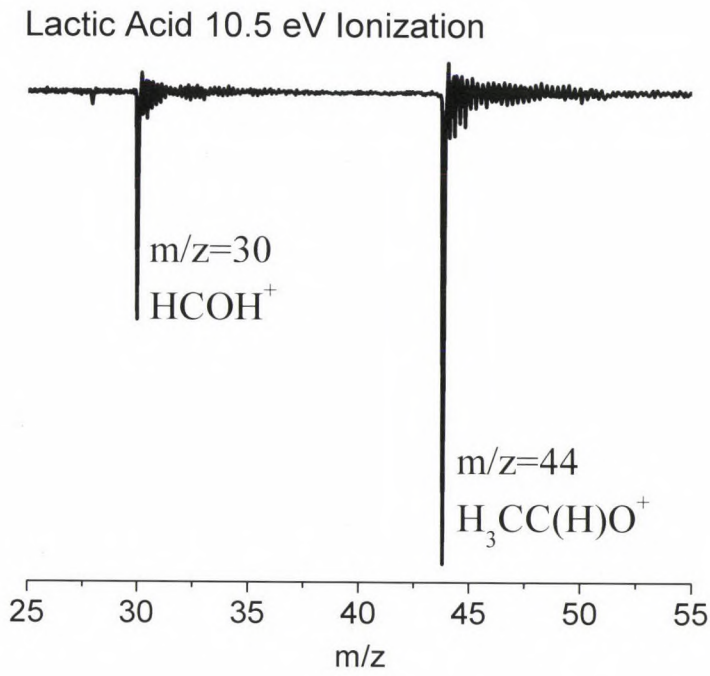

Figure 2.2: *Time of flight mass spectrum for lactic acid ionized at 10.5 eV.*

Figure 2.2 shows the TOF mass spectrum of lactic acid obtained through single photon ionization at 10.5 eV. The ion signals at m/z=44 and 30 amu correspond to $H_3CC(H)CO^+$ and $HCOH^+$ fragments, respectively. The absence of a parent ion signal indicates that lactic acid undergoes complete molecular fragmentation following single photon vertical ionization at 10.5 eV. The more intense fragment ion signal at m/z=44 amu in the mass spectrum can be assigned to a product resulting from the intramolecular hydrogen transfer from the α-OH to the COOH group followed by the breaking of the C_α-$C_{carboxylic}$ bond from either Conformer I or II. This fragment ion signal cannot be generated from Conformer III because the hydrogen bond is formed by the carboxylic acid OH group H atom bonding to the α-OH group. The ion signal at m/z=30 amu can be attributed to a product formed upon direct C_α-$C_{carboxylic}$ bond dissociation followed by the elimination of the CH_3 radical from all three lowest energy conformers of lactic acid. Therefore, with the diversity of different possible fragmentation pathways for each conformer, the TOFMS alone does not enable us to identify unambiguously the fragmentation patterns of the radial cation intermediates of lactic acid in a conformation specific way. IR-VUV photoionization spectroscopy can, however, aid in such analysis.

The infrared spectra of lactic acid, recorded by monitoring the fragment signals at m/z=44 and 30 amu obtained through IR-VUV spectroscopy, are presented in Figure 2.3. Enhancement of the ion signal intensity is observed at both fragment mass channels when the IR radiation is absorbed by a characteristic normal mode of vibration for a specific conformer of lactic acid. Several calculated (MP2/aug-cc-pVDZ) scaled (0.96) harmonic vibrational frequencies are also displayed in Figure 2.3 below the experimental spectra, with their corresponding conformers. The IR spectra obtained at fragment mass channels

of m/z=44 and 30 amu are in good agreement with the scaled (0.96) harmonic calculated IR frequencies of conformers I and II, respectively.

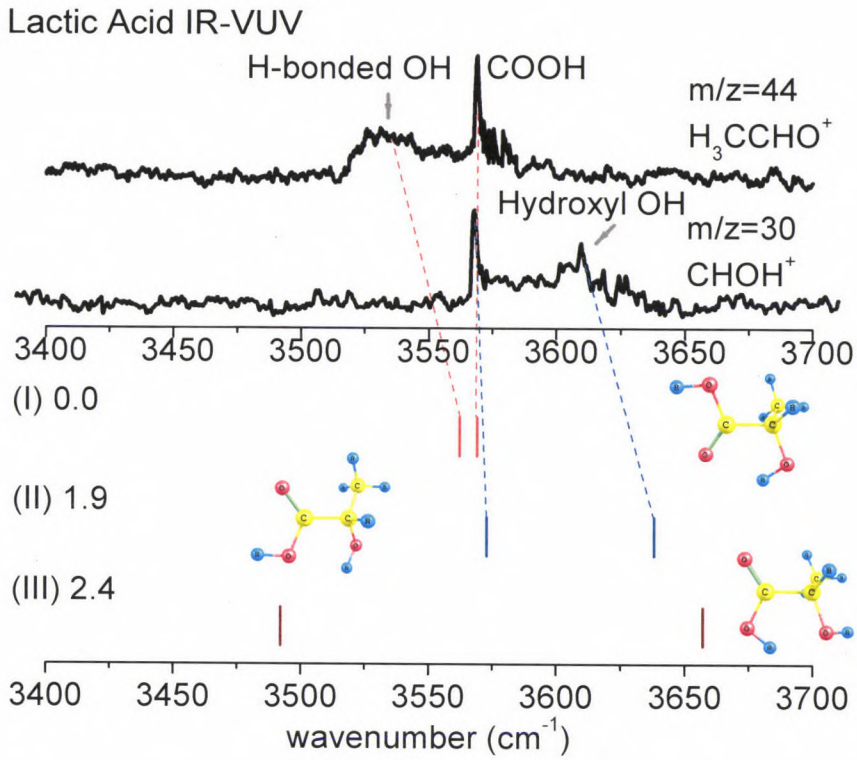

Figure 2.3: *IR-VUV spectra of lactic acid recorded monitoring fragment signals at m/z=44 and 30 amu in the region of free or hydrogen bonded OH stretching modes. Colored vertical bars represents calculated (MP2/aug-cc-pVDZ), scaled (0.96), harmonic frequencies for the different conformers of lactic acid. For Conformer I, the left vertical bar indicates the hydrogen bonded OH stretch. For Conformer II, the right vertical bar indicates hydrogen bonded OH stretch.*

A qualitative assignment of the IR spectra can be generated by considering the OH vibrational mode energy in light of its involvement with hydrogen bonding. Hydrogen bonding in the molecular system is responsible for the red shift (100-300 cm^{-1} depending on the strength of H-bond) in the ν_{OH} stretch vibrational frequency compared to the free (non hydrogen bonded) OH stretching mode.[37] Additionally, absorption of an

OH stretching mode associated with a hydrogen bonded OH moiety is also often broadened due to complex anharmonic coupling mechanisms involving normal modes associated with the O-H····O hydrogen bond forming atoms and other overtone and combination modes.[38]

The above considerations are clearly pertinent for the spectra in Figure 2.3. Sharp peaks corresponding to the free carboxylic acid OH stretch (near 3569 cm^{-1}) are observed in both spectra. A broad feature appears to the red of the free carboxylic acid OH stretch in the IR spectrum obtained at fragment mass channel m/z=44 amu; this feature can be assigned as a relatively strongly hydrogen bonded hydroxyl OH stretch. A sharp feature appears to the blue of the free carboxylic acid OH stretch in the IR spectrum recorded at fragment mass channel m/z=30 amu; this feature can be attributed to a relatively free non hydrogen bonded hydroxyl OH stretch. The relative positions of the hydroxyl OH stretching mode (either hydrogen bonded or free) in the two spectra provide qualitative information about the relative strength of O-H····O intramolecular interaction for conformers I and II. The larger red shift of the hydroxyl OH oscillator of Conformer I confirms that this conformer possesses a stronger O-H····O hydrogen bond interaction. Absence of a strongly red shifted hydroxyl OH oscillator in Conformer II corroborates a weak interaction between the α-hydroxy OH and COOH groups. The mismatch between experimental and theoretical results for hydrogen bonded or free hydroxyl OH frequencies in the spectra presumably arises due to strong anharmonic coupling and coupling between the harmonic frequency mode and low frequency combination modes, which are not considered in the calculation at the MP2/aug-cc-pVDZ level of theory. The qualitative observation of a red shift of more than 130 cm^{-1} associated with the hydrogen

bonding effect for Conformer I is, however, well reproduced in the calculation. Therefore, the relative positions of hydroxyl OH stretching mode (either hydrogen bonded or free) in the two spectra provide clear information about the relative strength of O-H$\cdots$O intramolecular interaction for conformers I and II.

Furthermore, since a free hydroxyl OH vibration is observed at 3610 cm^{-1} by monitoring the fragment signal at m/z=30 amu, one can conclude that Conformer I has no significant contribution to the ion signal at m/z=30 amu. No hydrogen bonded carboxylic acid OH stretch frequency is observed in either of these spectra; thus Conformer III does not contribute to either the fragment signal at m/z=44 or 30 amu.

Pyruvic acid

Figure 2.1 depicts the three lowest energy conformers of neutral pyruvic acid with their calculated (MP2/aug-cc-pVDZ) relative energies (in kcal/mol). The conformers differ by the type of hydrogen bonding, and relative orientation of the α-keto group with respect to the COOH group. Conformer I is the lowest energy conformer, which is in agreement with the literature.[39,40] The TOF mass spectrum of pyruvic acid obtained using single photon ionization at 10.5 eV is depicted in Figure 2.4. The spectrum contains a parent ion signal at m/z=88 amu and one fragment signal, corresponding to H_3CCO^+, at m/z=43 amu. The fragment ion signal at m/z=43 amu can be attributed to a product resulting from direct C_α-$C_{carboxylic}$ bond dissociation from all three low energy conformers. Further identification of the different conformers contributing to the direct C_α-$C_{carboxylic}$ bond dissociation channel is performed using IR-VUV photoionization spectroscopy.

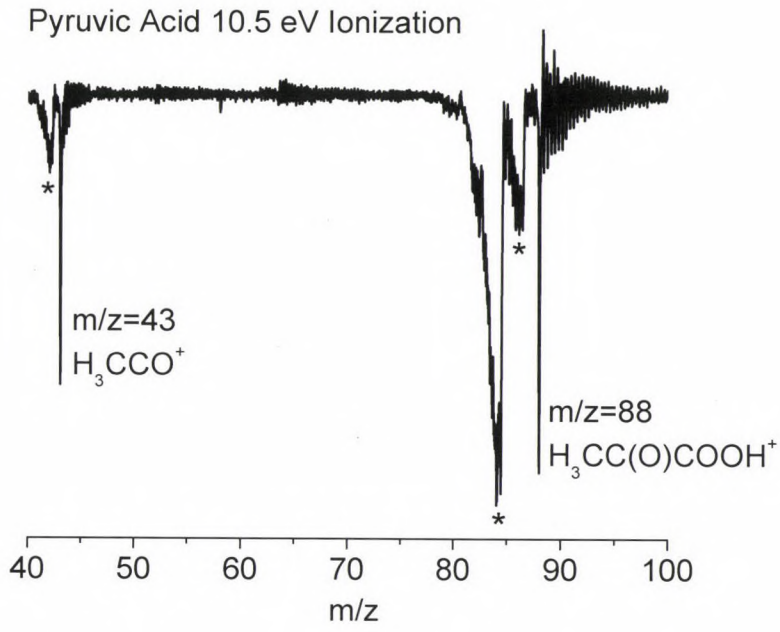

Figure 2.4: *Time of flight mass spectrum for pyruvic acid ionized at 10.5 eV. The ion signals denoted by * are due to diffusion pump oil which was present in the vacuum chamber.*

The infrared spectrum, obtained by monitoring the pyruvic acid parent ion signal at m/z=88 amu, is given in Figure 2.5. No vibrational features are observed in the m/z=43 amu mass channel. An enhancement in ion signal intensity is observed at the mass channel m/z=88 amu (parent ion signal) IR radiation is absorbed by a specific normal mode of vibration for a particular conformer of pyruvic acid. Enhancement of the parent ion signal intensity in the presence of IR radiation arises due to the enhancement in ionization cross section of the parent molecule from its vibrationally excited states. The IR spectrum in Figure 2.5 comprises two features resulting from the two different environments of the carboxylic acid OH bond: one is associated with the free OH stretch (3582 cm^{-1}) and other is associated with the hydrogen bonded carboxylic acid OH stretch (3460 cm^{-1}). The sharp feature in the spectrum at 3582 cm^{-1} exhibits an excellent fit with

the calculated IR frequency of the free carboxylic acid OH stretch for conformers II and III, which is also in good agreement with recent FTIR measurements.[40]

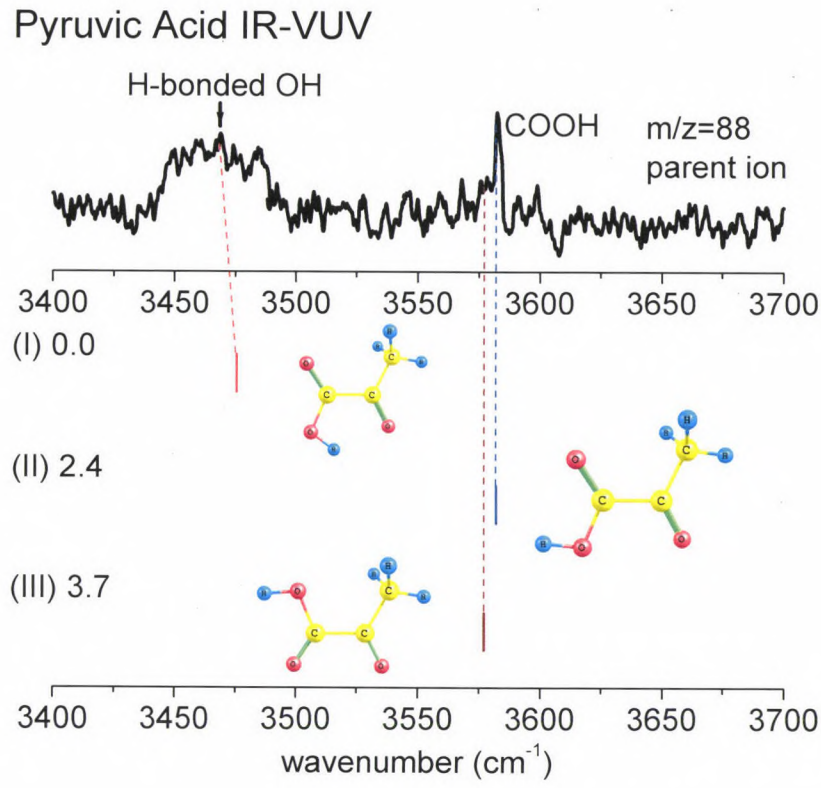

Figure 2.5: *IR-VUV spectra of pyruvic acid recorded monitoring the parent ion signal at m/z=88 amu in the region of free or hydrogen bonded OH stretching modes. Colored vertical bars represents calculated (MP2/aug-cc-pVDZ), scaled (0.96), harmonic frequencies for the different conformers of pyruvic acid.*

The broad feature to the red of the free OH stretch in the spectrum can be ascribed to a hydrogen bonded carboxylic OH stretch, which is qualitatively consistent with the calculated vibrational frequency of hydrogen bonded carboxylic acid OH stretch for Conformer I. The free carboxylic acid OH stretch observed at 3582 cm^{-1} is also in agreement with the calculated vibrational frequency for the Conformer III; however, this conformer is estimated to have a total population less than 0.2% at 300 K using a Boltzmann population distribution, and therefore, has been considered to contribute little

to the present study. We can, thus, conclude that both conformers I and II are present in the molecular beam. The only fragment signal observed following single photon ionization of pyruvic acid at 10.5 eV corresponds to H_3CCO^+, at m/z=43 amu; in principle, it can be generated from both of these two conformers. The fragmentation mechanism will be further explored using theoretical calculations.

Glycine and Valine

To probe conformation specificity for the reactivity of radical cationic glycine and valine we reillustrate here the results for these two molecules that were previously experimentally examined by our group.[41] We here reexamine some of those results to assess conformation specificity for the reactivity of radical cationic glycine and valine.

Three lowest energy conformers of neutral glycine and valine, which differ again mainly by different types of intramolecular hydrogen bonding linkages, are illustrated in Figure 2.6. Single photon ionization of glycine at 10.5 eV reveals two intense fragment signals at m/z=30 and 31 amu along with weaker fragment signals at m/z=42 and 43 amu.[41] The fragment signal at m/z=30 amu ($H_2CNH_2^+$) can be attributed to a product formed upon direct C_α-$C_{carboxylic}$ bond dissociation from all three conformers of glycine. The fragment signal at m/z=31 amu ($H_2CNH_3^+$) can be assigned to a product formed upon hydrogen transfer from the COOH to the α-NH_2 group followed by C_α-$C_{carboxylic}$ bond dissociation. No IR spectrum could be recorded monitoring the fragment signal at m/z=31 amu; however, in our original previous study,[41] an IR spectrum is obtained monitoring the fragment signal at m/z=30 amu, which is reproduced in Figure 2.7. The IR spectrum reveals three distinct features that arise from free symmetric (3360 cm^{-1}) and

asymmetric (3440 cm^{-1}) NH_2 stretches and a free carboxylic acid OH stretch (3587cm^{-1}). This assignment is consistent with the calculated scaled harmonic vibrational frequencies for conformers I and III of glycine. No hydrogen bonded carboxylic acid OH stretch is observed in the IR spectrum obtained at the ion signal of m/z=30 amu, which indicates that the fragment $H_2CNH_2^+$ is not generated from Conformer II through C_α-$C_{carboxylic}$ bond dissociation. Only conformers I and III, instead, follow the C_α-$C_{carboxylic}$ bond dissociation pathway.

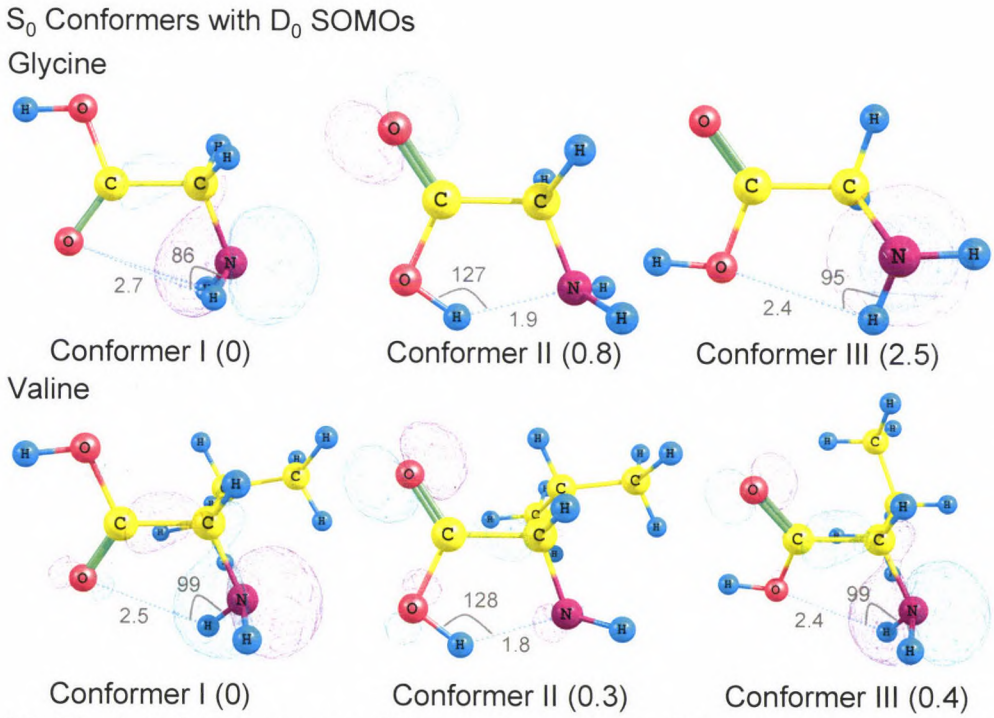

Figure 2.6: *The three lowest energy conformers of ground state (S_0) neutral glycine and valine with calculated (MP2/aug-cc-pVDZ) relative energies (in kcal/mol), showing their bond distances and bond angles. The density plots for the SOMO (singly occupied molecular orbital) of glycine and valine at the FC (Franck-Condon) point on the cationic D_0 surface calculated at the CASSCF(9,8)/6-31G(d) level of theory are also shown. The two colors for these orbitals indicate the plus and minus phases of the wavefunctions.*

The fragment signal at m/z=31 amu ($H_2CNH_3^+$) is unique with regard to the possible fragmentation mechanism of the glycine radical cation because it can only be generated from Conformer II through a hydrogen transfer from the COOH group to the α-NH_2 group followed by C_α-$C_{carboxylic}$ bond dissociation. Thus, one can conclude that the fragment $CH_2NH_3^+$ results from Conformer II: this assignment is experimentally demonstrated[41] using an equivalent fragment signal of valine obtained at m/z=73 amu ($((CH_3)_2C(H)C(H)NH_3^+$).

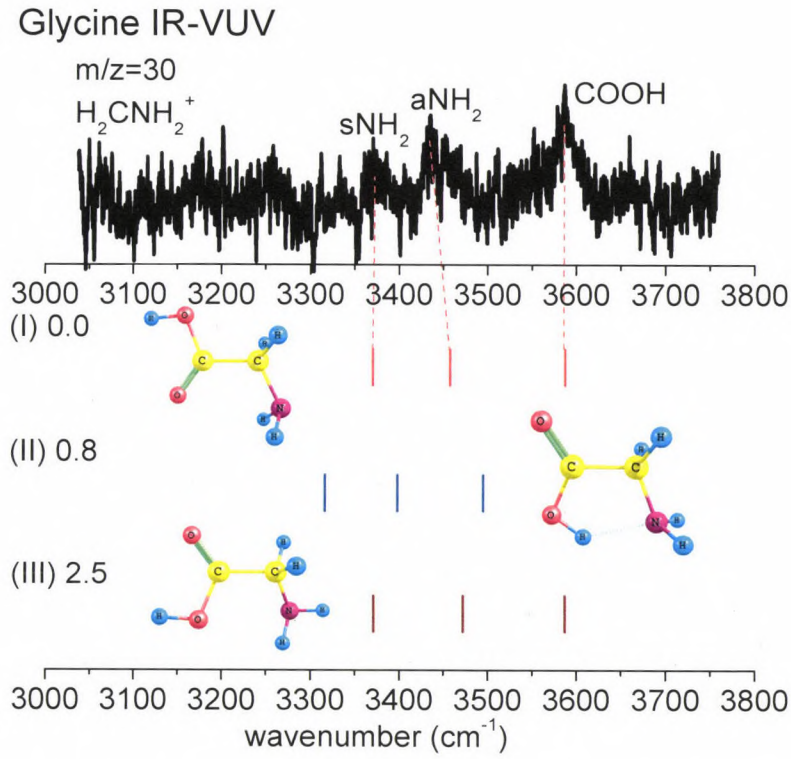

Figure 2.7: *IR-VUV spectra of glycine recorded monitoring the fragment ion signal at m/z=30 amu in the region of free or hydrogen bonded OH stretching mode and NH_2 stretching mode. Colored vertical bars represents calculated (MP2/aug-cc-pVDZ), scaled (0.96), harmonic frequencies for the different conformers of glycine. The IR spectrum is reproduced from Ref. 41.*

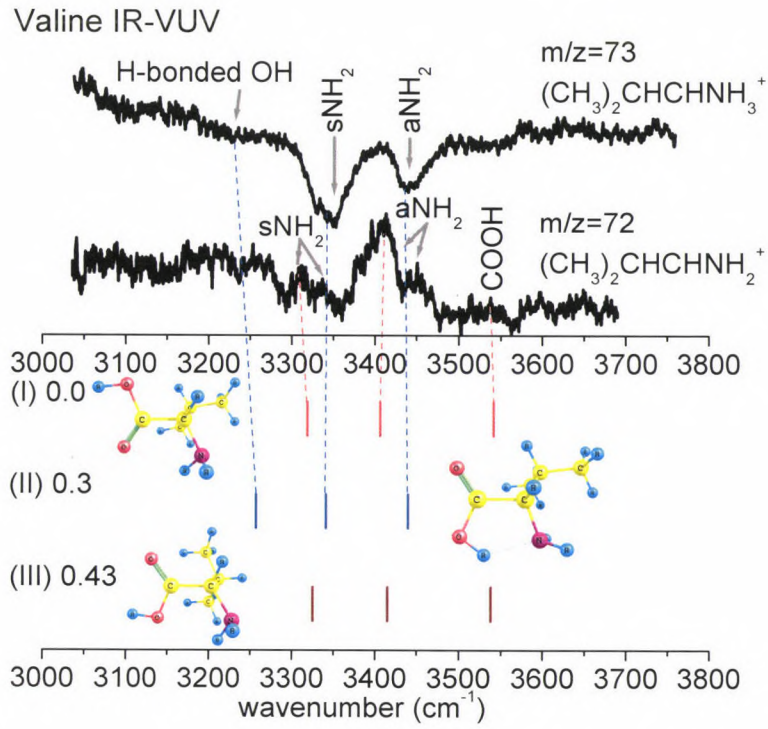

Figure 2.8: *IR-VUV spectra of valine recorded monitoring the fragment signal at m/z=72 and 73 amu in the region of OH and NH_2 stretching modes. Colored vertical bars represents calculated (MP2/aug-cc-pVDZ), scaled (0.96), harmonic frequencies for different conformers of valine. The IR spectra are reproduced from Ref. 41.*

Single photon ionization of valine at 10.5 eV exhibits fragment signals at m/z=30, 72, and 73 amu.[41] The fragment signal at m/z=73 amu can be related to a product formed upon a hydrogen transfer from COOH to the α-NH_2 group followed by C_α-$C_{carboxylic}$ bond dissociation. The IR spectrum (Figure 2.8) obtained at this fragment mass channel (negative) reveals a broad feature below 3300 cm^{-1}, corresponding to a hydrogen bonded carboxylic acid OH, and two distinguishable bands, which arise from free symmetric (3346 cm^{-1}) and asymmetric (3436 cm^{-1}) NH_2 stretches. This assignment is also in agreement with the calculated scaled harmonic vibrational frequencies for Conformer II of valine. The noticeable broadening of each feature associated with symmetric and asymmetric NH_2 stretching modes in the spectrum possibly arises from almost free

rotation of the isopropyl group along the C_α-C_β bond in valine, which renders two additional conformers each retaining the hydrogen bonded network in the α-amino carboxylic acid moiety or retaining possible interactions between the NH_2 and OH moieties. The source of negative signals at mass channel m/z=73 amu has been previously discussed.[41]

The fragment signal at 72 amu can be related to the direct C_α-$C_{carboxylic}$ bond dissociation pathway for all three conformers of valine. The IR spectrum (Figure 2.8) obtained by monitoring this fragment signal shows one hydrogen bonded NH stretch (3309 cm^{-1}) and one free NH stretch (3409 cm^{-1}); the position of each feature is clearly different from that obtained at the fragment mass channel m/z=73 amu. The IR spectrum obtained monitoring the fragment signal at m/z=72 amu is also in agreement with the calculated scaled vibrational frequencies for Conformer I. In addition, each spectral feature obtained monitoring the fragment signal at m/z=72 amu is associated with a weak shoulder, the position of which is slightly blue to the more intense feature. The shoulder peaks are in good agreement with the calculated scaled vibrational frequencies of free and hydrogen bonded NH stretches for Conformer III. As mentioned above with regard to the line widths of the NH stretch modes observed in Figure 2.8, the isopropyl group conformations may also be a reason that the carboxyl OH transition near 3575 cm^{-1} is both weak and broad for conformers I and III.

Thus, conformers I and II of both radical cationic glycine and valine dissociate through two distinctly different decomposition pathways. Conformer I undergoes direct C_α-$C_{carboxylic}$ bond dissociation, whereas Conformer II undergoes hydrogen transfer followed by C_α-$C_{carboxylic}$ bond dissociation. Thus radical cationic reactivity of glycine

and valine, which are α-amino aliphatic carboxylic acids, is shown to be conformation specific. Conformer III for glycine and valine follows a direct C_α-$C_{carboxylic}$ bond dissociation pathway.

2.5 Theoretical Results

Specific knowledge of the molecular ion state produced upon sudden removal of an electron from a molecule is essential to determine the likely fragmentation mechanisms of the nascent radical cation. Here, we determine relevant molecular ion states produced by vertical ionization at 10.5 eV from comparison between the computed (at MP2/aug-cc-pVDZ) VIE and the experimental ionization energy (10.5 eV), coupled with available photoelectron spectroscopy data[42] (Table 2.T1 in Supporting Information). These analyses indicate that ionization of lactic acid, pyruvic acid, glycine, and valine at 10.5 eV efficiently populates only the ground doublet molecular (radical cation) ion state (D_0).

In the one electron model (Koopmans' theorem),[43] removal of an electron from a neutral molecule creates a hole in the molecular electronic distribution, that resides at the singly occupied molecular orbital (SOMO) of the nascent radical cation. The SOMO, therefore, represents the electronic character of the nascent molecular cation, which specifies the potential energy landscape for the cation. The hole densities for the SOMO of the three different conformers of lactic acid and pyruvic acid at the Franck-Condon point on the D_0 surface, computed at the CASSCF(9,8)/6-31G(d) level of theory, are shown in Figure 2.1. The two colors indicate the plus and minus phases of

wavefunctions. For Conformer I of lactic acid, the SOMO is entirely localized on the α-hydroxy O atom (np_O) of the molecular ion, which is notably perpendicular to the C_α-$C_{carboxylic}$ σ bond. For Conformer II, the SOMO is delocalized over the nonbonding orbitals of the α-hydroxy O (np_O), carbonyl O ($n\sigma_O$), and the C_α-$C_{carboxylic}$ σ bond. Furthermore, the np_O of the α-hydroxyl O atom in Conformer II is almost parallel to the C_α-$C_{carboxylic}$ bond. For Conformer III of lactic acid, on the other hand, the SOMO is entirely localized on the carbonyl O atom ($n\sigma_O$). Therefore, the localization sites of the hole in the nascent, Franck-Condon, vertical radical cation of lactic acid on the D_0 surface are clearly conformation specific.

For both conformers I and II of pyruvic acid, the SOMO is delocalized over the non bonding orbitals of the α-carbonyl O atom, the carboxylic acid carbonyl O atom, and the C_α-$C_{carboxylic}$ σ bond with predominant contribution from the α-carbonyl O atom. For Conformer III, the SOMO is localized primarily on the α-carbonyl O atom of the radical cation. Additionally, the np_O of the α-carbonyl oxygen atom is parallel to the C_α-$C_{carboxylic}$ bond for all three conformers of pyruvic acid. Therefore, contrary to the lactic acid conformers, localization site of the hole in the nascent radical cation of pyruvic acid on the D_0 surface is not entirely conformer dependent.

The density for the SOMO of the different vertical ion conformers of glycine and valine on their D_0 ion surface computed at the CASSCF(9,8)/6-31G(d) level of theory are shown in Figure 2.6. For conformers I and III of glycine and valine, the SOMO is located on the α-amine N (np_N) of the molecular Franck-Condon ion. For glycine, the np_N in Conformer I is parallel to the C_α-$C_{carboxylic}$ bond and in Conformer III, it is perpendicular to the C_α-$C_{carboxylic}$ bond. Both conformers I and III of valine, however, have an np_N

parallel to the C_{α}-$C_{carboxylic}$ bond. In contrast, the SOMO for Conformer II of glycine and valine, is primarily localized on the carbonyl O atom of the molecular ion. These assignments for the SOMO of α-amino carboxylic acids are in good agreement with what has been recently suggested by Powis, *et al* for a structurally similar alanine radical cation.[44] Therefore, the localization site for the hole of Conformer I and II of glycine and valine in D_0 state is clearly conformation specific.

Following sudden removal of an electron from a molecule, the nascent radical cation is typically not formed in its equilibrium geometry. On the femtosecond time scale, the Franck-Condon ion will evolve to the adiabatic ion while lowering its electronic energy through structural rearrangement. The excess energy (E_{VIE}-E_{AIE}) due to vertical-to-adiabatic evolution is stored in the vibration of the bonds of the molecular ion under isolated conditions; this vibrational energy can often cause the dissociation of the radical cation. In some cases, following vertical to adiabatic evolution of the ion, hydrogen transfer provides additional excess energy (E_{VIE}-E_{AIE}+$\Delta H_{reaction}$) to surmount the energy barrier for molecular dissociation.[41] If a molecule absorbs a photon of 10.5 eV and dissociates to products, the total ΔH_{rxn} has be less than 10.5 eV in order to form products following the law of conservation of energy. The total ΔH_{rxn} can be computed using thermochemical calculations. Thermochemical calculations alone are not, however, sufficient for the exploration of fragmentation pathways of radical cation intermediates of bioactive carboxylic acids because a unimolecular fragmentation reaction is likely to occur through the lowest activation barrier, not necessarily for the reaction that is most exothermic. As a result, the energy barrier to the transition state to form a certain product becomes an important consideration. In general, a lower barrier for a reaction renders a

unimolecular fragmentation reaction faster; moreover, a lower activation barrier channel is more likely to dominate if an equilibrium is not established prior to the reaction.

The product distributions observed through mass spectrometry following single photon VUV (10.5 eV) ionization of α-substituted bioactive aliphatic carboxylic acids indicate that the initial step in the decomposition of their radical cation intermediates involves two common mechanisms: (1) a hydrogen transfer (either from the carboxylic acid group to the α-substituent or *vice versa*); and (2) direct C_{α}-$C_{carboxylic}$ bond dissociation. Therefore, we consider below the theoretical exploration of these two channels of decomposition in order to judge which of them is energetically or dynamically more favorable for a particular conformer.

The potential energy diagrams along the two reaction pathways (hydrogen transfer and COOH elimination) for different conformers of radical cationic lactic acid, pyruvic acid, glycine, and valine on the D_0 surfaces, obtained at the CASSCF(9,8)/6-31G(d) level of theory, are shown in Figures 2.9-2.10, 2.12-2.13, respectively. The hydrogen transfer pathway is indicated by adding a suffix 'a,' and C_{α}-$C_{carboxylic}$ bond dissociation pathway is referred including a suffix 'b' in the aforementioned figures.

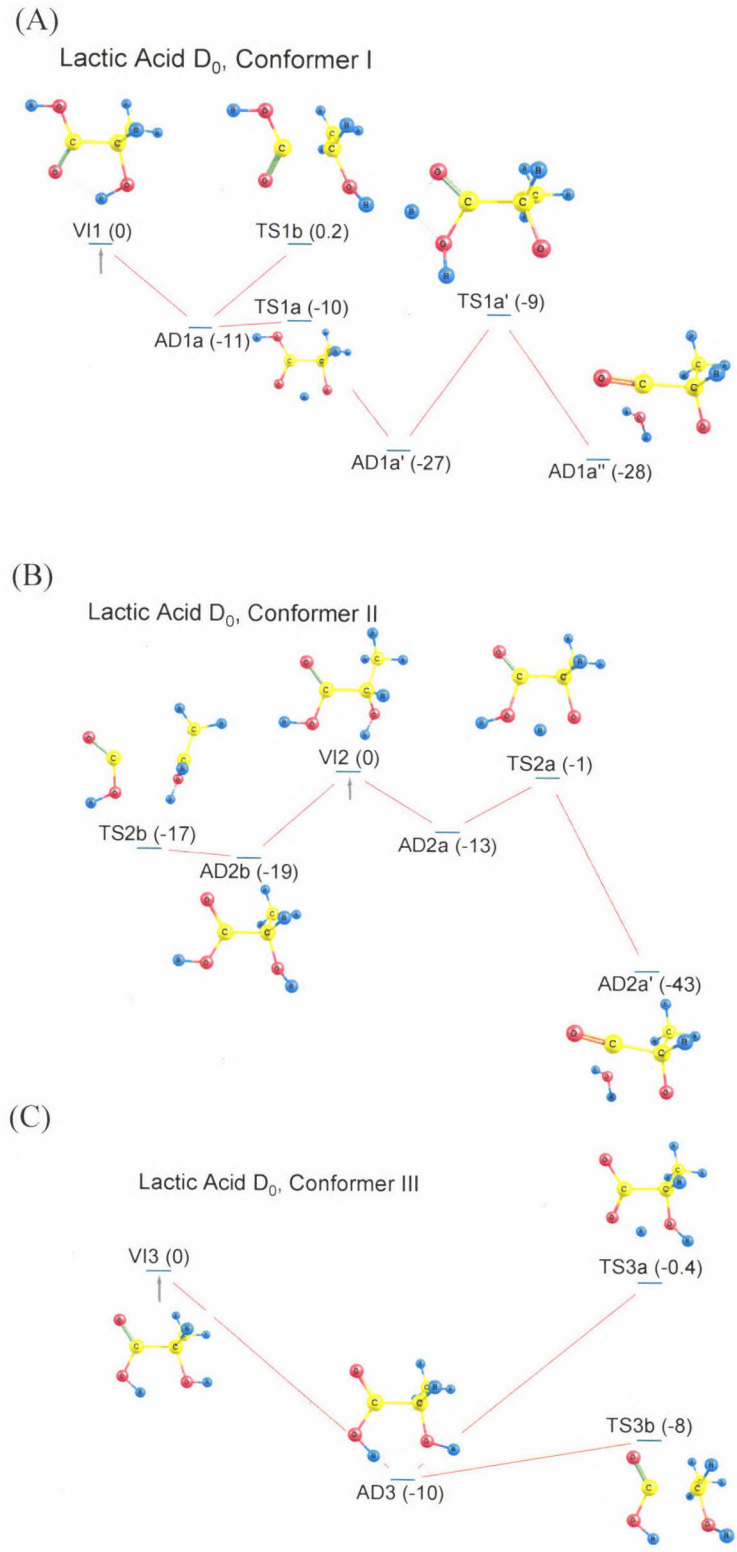

Figure 2.9: *Potential energy diagram for lactic acid on its D_0 ion surface calculated at the CASSCF(9,8)/6-31G(d) level of theory. Two decomposition pathways are shown: a) hydrogen transfer, and b) direct C_α-$C_{carboxylic}$ bond dissociation. Relative energies are in kcal/mol. Vertical arrows show the accessed FC point for the ion.*

The potential energy diagram of lactic acid on its D_0 ion surface (Figure 2.9) reveals that the direct C_α-$C_{carboxylic}$ bond dissociation pathway is the minimum energy pathway (associated with the lowest activation barrier) for conformers II and III. Therefore, these two conformers will lead to a predominately kinetically controlled product at low temperature through this dissociation channel. The C_α-$C_{carboxylic}$ bond dissociation pathway possesses, however, different exothermicities for these two conformers (-17 kcal/mol for Conformer II and -8 kcal/mol for Conformer III). The hydrogen transfer pathway (from α-OH to COOH), on the other hand, is computed to be the minimum energy pathway for Conformer I of lactic acid.

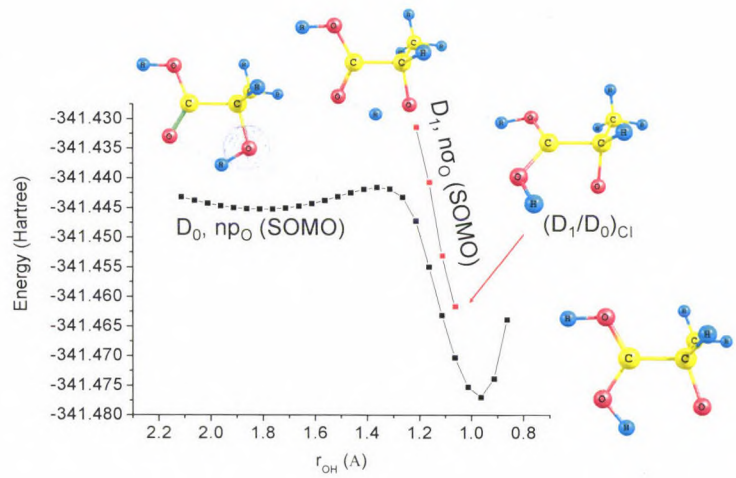

Figure 2.10: *Hydrogen transfer pathways for Conformer I with location of the $(D_1/D_0)_{CI}$ conical intersection computed at CASSCF(9,8)/6-31G(d) level of theory.*

At the CASSCF level, a $(D_1/D_0)_{CI}$ conical intersection for lactic acid is localized in the hydrogen transfer reaction coordinate, as illustrated in Figure 2.10. The adiabatic energy gap between D_1 and D_0 surface in the conical intersection is calculated to be 400 cm^{-1}, indicating a strong nonadiabatic coupling between D_1 and D_0 surfaces. As

mentioned previously, ground electronic surface topology is found to be affected by the proximity of the upper excited electronic surface near the conical intersection.[45] Clearly, these results provide further justification for utilizing a multiconfigurational method such as CASSCF in order to fully explore such effects.

Furthermore, a hydrogen transfer reaction is considered to be the minimum energy pathway for Conformer I of lactic acid, regardless of which doublet electronic state is accessed through the 10.5 eV radiation. The conical intersection located at the reaction coordinate ensures that similar chemistry will occur on both the D_0 and D_1 surfaces.

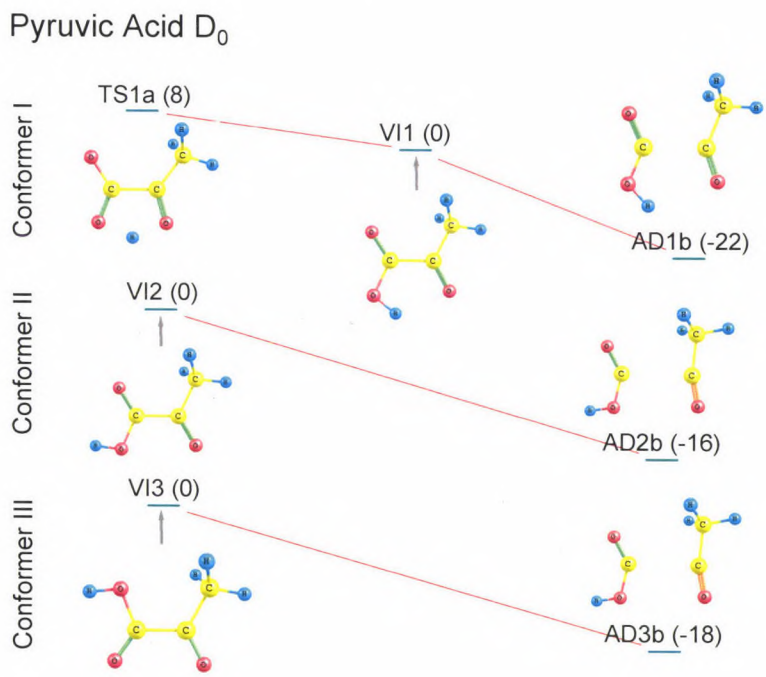

Figure 2.11. *Potential energy diagram for pyruvic acid on its D_0 ion surface calculated at the CASSCF(9,8)/6-31G(d) level of theory. Two decomposition pathways are shown: a) hydrogen transfer, and b) direct C_α-$C_{carboxylic}$ bond dissociation. Relative energies are in kcal/mol. Vertical arrows show the accessed FC point for the ion.*

The potential energy diagram of pyruvic acid on its D_0 ion surface (Figure 2.11) indicates that the C_α-$C_{carboxylic}$ bond dissociation is the minimum energy pathway for all three conformers of pyruvic acid. A zero activation barrier exists in this reaction coordinate for all three conformers. The computed activation barrier from the FC point on the D_0 surface of pyruvic acid shows hydrogen transfer from COOH to the α-keto substituent, on the other hand, as a highly endothermic process (by 8 kcal/mol). Therefore, hydrogen transfer for this cation should not (and does not) occur for Conformer I.

The potential energy diagram for glycine on its D_0 surface (Figure 2.12) shows that a C_α-$C_{carboxylic}$ bond dissociation is the minimum energy pathway for conformers I and III. This reaction coordinate possesses a zero activation energy for Conformer I and an activation energy of 16 kcal/mol for Conformer III. The hydrogen transfer pathway, however, is the minimum energy pathway for Conformer II of glycine. A zero activation energy barrier exists in the C_α-$C_{carboxylic}$ bond dissociation pathway for conformers I and III of valine (Figure 2.13). The hydrogen transfer pathway for valine is calculated to be the minimum energy pathway for Conformer II.

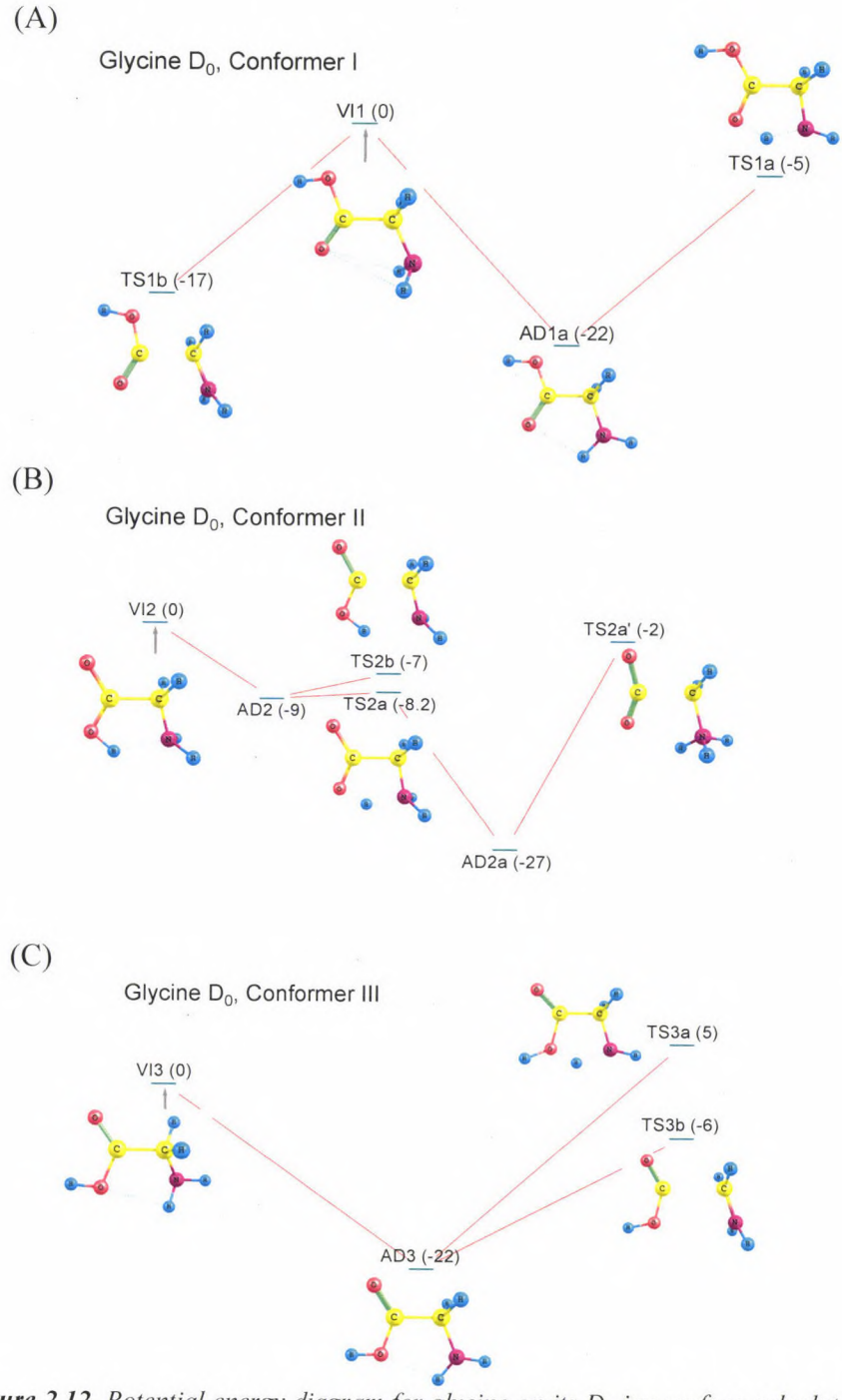

Figure 2.12. *Potential energy diagram for glycine on its D_0 ion surface calculated at the CASSCF(9,8)/6-31G(d) level of theory. Two decomposition pathways are shown: a) hydrogen transfer, and b) direct C_α-$C_{carboxylic}$ bond dissociation. Relative energies are in kcal/mol. Vertical arrows show the accessed FC point for the ion.*

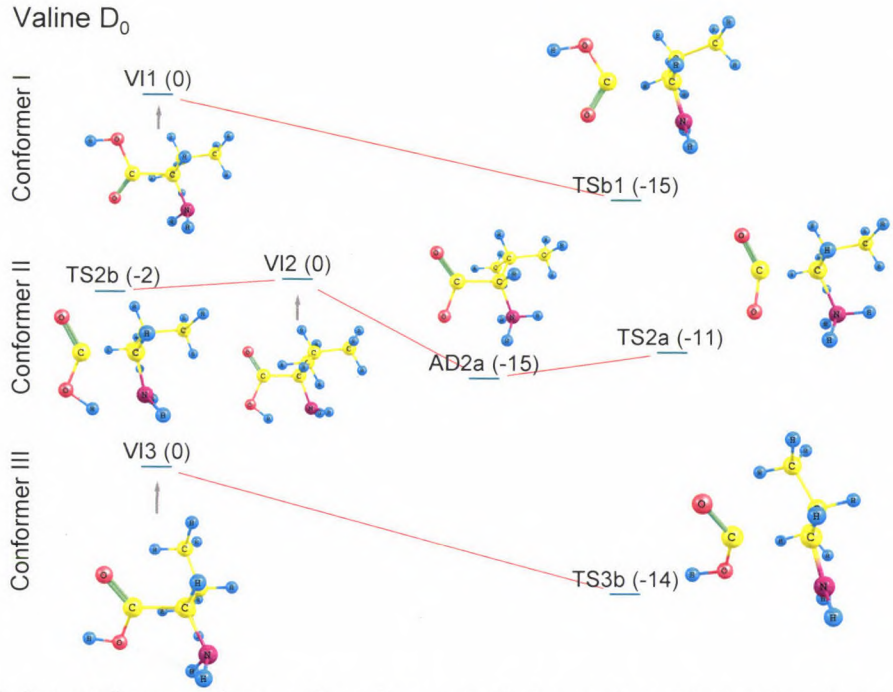

Figure 2.13. *Potential energy diagram for valine on its D_0 ion surface calculated at the CASSCF(9,8)/6-31G(d) level of theory. Two decomposition pathways are shown: a) hydrogen transfer, and b) direct C_α-$C_{carboxylic}$ bond dissociation. Relative energies are in kcal/mol. Vertical arrows show the accessed FC point for the ion.*

To obtain further information on the ground doublet ion surface topology of Conformer II of glycine, we investigate the influence of $(D_1/D_0)_{CI}$ conical intersection on the ground surface. The CASSCF calculations reveal that the upper D_1 electronic surface for the Conformer II is highly nonadiabatically coupled with the D_0 surface along the hydrogen transfer reaction coordinate. A $(D_1/D_0)_{CI}$ conical intersection is localized in the hydrogen transfer reaction coordinate of Conformer II, which is illustrated in Figure 2.14. The adiabatic energy difference between the D_0 and D_1 surfaces near the $(D_1/D_0)_{CI}$ conical intersection is calculated to be 500 cm^{-1}, which suggests strong nonadiabatic coupling between the D_1 and D_0 surfaces. Again, the multiconfigurational approach of CASSCF is justified.

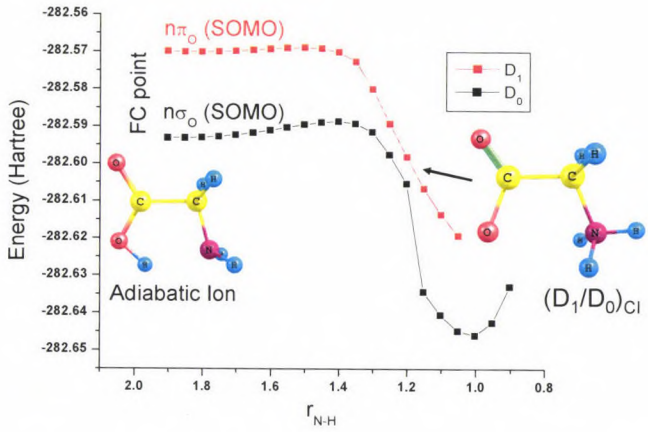

Figure 2.14. *Hydrogen transfer pathway for Conformer II of glycine with localization of* $(D_1/D_0)_{CI}$.

Overall the theoretical results show that initial structures of the bioactive carboxylic acids have significant influence on their subsequent reactivity following ionization. Intramolecular hydrogen bonding can alter the local charge distribution in these radical cation intermediates. Moreover, a relationship between charge, structure, and reactivity emerges from this study. If charge is localized on the carboxylic acid group, a hydrogen transfer is favored from COOH to the α-substituent. If the charge is localized on the α-substituent and the SOMO is parallel to the C_α-$C_{carboxylic}$ bond, a charge transfer occurs to the C_α-$C_{carboxylic}$ bond, facilitating a direct C_α-$C_{carboxylic}$ bond dissociation without any activation energy barrier. These theoretical findings fully corroborate the experimental observations.

2.6 Discussion

A number of observations are crucial for understanding the conformation specific reactivity of radical cation intermediates of α-substituted bioactive carboxylic acids.

Undoubtedly, if the excess energy, obtained through the vertical to adiabatic evolution of the molecular ion, is enough to surmount the activation energy needed to initiate a decomposition reaction, fragmentation of radical cation intermediates takes place. This excess energy may also result in the interconversion between different cation conformations. The interconversion energy for lactic acid, glycine, and valine on their ground cation surface is computed to be within the range of 2-6 kcal/mol, which is much smaller than the available excess energy (ranging from 10 to 20 kcal/mol) stored in the molecular vibrations following vertical ionization. Therefore, identical products could possibly be generated from different conformers through interconversion following ionization, which can diminish conformation specific behavior. This consideration, however, can be ruled out: the significant difference in IR spectra (Figures 2.3 and 2.8 for lactic acid and valine, respectively) recorded by monitoring the fragment signals does not suggest such an interconversion. The IR spectra recorded at different fragment signals are distinctly different for lactic acid and valine,[41] and they do not appear to be the superposition of two or more components. This suggests that VUV photoionization does not induce interconversion of the radical cation intermediates of lactic acid and valine. Instead, different conformers move along different reaction pathways following ionization. Thus, the vertical to adiabatic evolution and subsequent fragmentation are faster than the conformational interconversion. The fragmentation dynamics of the radical cation intermediates of these two bioactive carboxylic acids studied in the present work are, therefore, predicted to be ultrafast so that each molecule retains the memory of its original conformation.

Both the mechanism for radical cation formation (*e.g.*, electron impact or single photon ionization) and the radical cation's position on the ion potential energy surface (*e.g.*, Franck-Condon, adiabatic, *etc.*) can be essential factors for the radical cation relaxation and/or unimolecular reaction. Details of the potential energy surface barriers for conformer interconversion and fragmentation reactions control the initial radical cation behavior: which pathway will dominate depends entirely on which part of the PES is accessed by the molecule following photoionization. This fact is directly evidenced by the present IR-VUV spectroscopic study of lactic acid and by our previous valine study.[41] The vibrational features observed in the pyruvic acid parent mass channel arise from contributions from different conformers present in the molecular beam. No vibrational features are observed in the fragment ion mass channel.

The theoretical results demonstrate that the direct C_α-$C_{carboxylic}$ bond dissociation channel requires a specific conformational orientation such that the SOMO (usually a nonbonding p-orbital) on the α-substituent stays parallel to the C_α-$C_{carboxylic}$ σ bond (see the following structures: TS1b, AD2b, and TS3b of lactic acid in Figure 2.9; TS1b, TS3b of glycine in Figure 2.12; and TS1b, TS3b of valine in Figure 2.13). This suitable geometrical orientation facilitates hole migration from $2p_O$ (SOMO) to the C_α-$C_{carboxylic}$ σ bond. This charge migration (or hole transfer) initiates direct C_α-$C_{carboxylic}$ bond dissociation because the bond that breaks is the one to which the hole is finally localized in the radical cation. Conformers that have the SOMO localized on the α-substituent and parallel to the C_α-$C_{carboxylic}$ bond at the FC point on the cationic surface, can undergo ultrafast (expected to be on attosecond time scale)[46,47] charge migration from the α-substituent to the C_α-$C_{carboxylic}$ bond and can thereby generate direct COOH elimination

products. Such conformers include Conformer II of lactic acid, all three conformers of pyruvic acid, Conformer I of glycine, and conformers I and III of valine. All these conformers require no activation energy for the C_α-$C_{carboxylic}$ bond dissociation reaction pathway from the FC point on the D_0 surface (Figures 2.9-2.10, 2.12-2.13).

Conformers for which the SOMO is localized on the α-substituent and for which a structural rearrangement is required to make the SOMO parallel to the C_α-$C_{carboxylic}$ bond possess a finite activation barrier for the C_α-$C_{carboxylic}$ bond dissociation. This mechanism is exemplified by Conformer I of lactic acid and Conformer III of glycine. Conformers for which the SOMO is localized on the carboxylic acid group undergo hydrogen transfer from the carboxylic acid group to the α-substituent. This mechanism occurs for Conformer III of lactic acid and Conformer II of glycine and valine.

Thus, conformation specific reactivity of radical cation intermediates is solely directed by two specific properties of the molecular ion: 1) the specific localization of the charge; and 2) the initial intramolecular hydrogen bonding structure. The hydrogen bonding structure of these species can favor or hinder charge migration and hydrogen transfer. This conclusion is consistent with the idea of a 'charge directed reactivity' of peptides observed by Weinkauf, *et al.*[23(a)] Their study finds that fragmentation products of peptides, generated by vertical ionization, depend upon specific peptide sequences that can assist or hinder hole migration. Weinkauf, *et al.*[23(b)] later modeled charge propagation within a peptide as arising from a steric requirement for bond alignment along the peptide chain to facilitate hole migration. We also find similar steric requirements for charge transfer to occur from the SOMO on the α-substituent to the C_α-$C_{carboxylic}$ bond for α-substituted carboxylic acids. Thus a 'through bond' mechanism[45] is supported for charge

migration. Knowledge of the relative timescales (barriers) of charge transfer, hydrogen transfer, and structural change is essential in order to obtain further detailed insights on the interplay of these three processes for the reactivity of radical cation intermediates of α-substituted bioactive carboxylic acids.

Radical cationic pyruvic acid shows a special stability with respect to lactic acid, glycine, and valine. A qualitative comparison of TOMFS intensities between the parent ion and fragment ion signals for pyruvic acid indicates that less than 45% of pyruvic acid parent ions dissociate following VUV ionization at 10.5 eV. The extra stability of pyruvic acid radical cation has recently been proposed and related to π-delocalization of the positive charge following enolization of the α-keto form.[12] The enol form of pyruvic acid on the cationic surface is predicted to be exothermically stabilized by more than 20 kcal/mol (CASSCF(9,8)/6-31G(d) result). A similar stabilizing factor is absent for the radical cation intermediates of glycine, valine, or lactic acid.

Thermochemical calculations (Reaction 2.R1 in Supporting Information) for lactic acid predict that the two fragment ions at m/z=30 and 44 amu can be generated on the cation's ground potential energy surfaces, following 10.5 eV vertical photoionization. Photoionization of lactic acid at 10.5 eV does not evidence a fragment at mass channel m/z=45 amu corresoponding to direct $C_{\square}$-$C_{carboxylic}$ bond dissociation, as this fragment can further dissociate to the m/z=30 amu ion. Electron impact (EI) ionization,[48] which generates the m/z=45 amu ion, is not directly relevant to the photoionization results because EI ionization does not necessarily place the created ion at the Franck-Condon point or even on the same potential energy surface as does photoionization.[49]

2.7 Conclusions

In this work, we illustrate the conformation specific and charge directed reactivity of the radical cation intermediates of lactic acid, pyruvic acid, glycine, and valine. The conformation specificity and charge directed reactivity suggested for these systems can be generalized for radical cation intermediate behavior for all bioactive carboxylic acids. Lactic acid, glycine, and valine, when ionized to the lowest vertical ionization region, undergo complete and conformation specific fragmentation. Conformational analysis for each molecule is carried out through IR spectroscopy complemented by theoretical results.

Conformers of these molecules, for which the α-substituent donates a hydrogen bond to the carboxylic acid group, favor either C_α-$C_{carboxylic}$ bond dissociation or hydrogen transfer from the α-substituent to the carboxylic acid group. The hydrogen transfer, however, depends on the activation barrier and the relative orientation of the singly occupied molecular orbital with respect to the C_α-$C_{carboxylic}$ bond. Conformers for which the α-substituent of these molecules accepts a hydrogen bond from the carboxylic acid OH facilitate hydrogen transfer from the carboxylic acid OH to the α-substituent. Pyruvic acid, on the other hand, does not undergo complete dissociation following ionization, resulting in a stable radical cation. We have identified two different conformers of pyruvic acid, both of which undergo, to some extent, C_α-$C_{carboxylic}$ dissociation; however, the reaction pathways associated with C_α-$C_{carboxylic}$ dissociation for the two conformers have different exothermicities. Thus, the reactivity and stability of

radical cationic bioactive carboxylic acids is dependent on the properties of their original conformations.

Ab initio calculations show that the electronic hole (positive charge) in the nascent radical cationic lactic acid, glycine, and valine is primarily localized on the hydroxyl O or amine N atom if the α-substituent donates a hydrogen bond to the carboxylic acid group (conformers I and II of lactic acid, and I and II of glycine and valine). This structure favors either C_{α}-$C_{carboxylic}$ bond dissociation or hydrogen transfer from the α-substituent to the carboxylic acid group. The actual mechanism, however, depends on the relative orientation of the SOMO with respect to the C_{α}-$C_{carboxylic}$ σ-bond and the activation barrier associated with the reaction coordinate. If the α-substituent accepts a hydrogen bond from the carboxylic acid OH group (Conformer III of lactic acid and II of glycine and valine), a stabilization effect due to hydrogen bonding lowers the energy of the lone pair orbitals of the α-substituent. In this case, the hole is localized on the carboxylic acid group, and this structure facilitates hydrogen transfer from carboxylic acid OH to the α-substituent. Thus, different structural orientations of the molecule give rise to different fragmentation patterns in α-hydroxy and α-amino aliphatic bioactive carboxylic acids: the reactivity of these systems is primarily governed by the local charge distribution.

The pyruvic acid radical cation, generated near its lowest vertical ionization region, does not completely undergo fragmentation. Two different conformers (I and II) of pyruvic acid are identified by recording IR spectra monitoring the parent ion signal. Both conformers undergo, to some extent, the C_{α}-$C_{carboxylic}$ bond dissociation; however, theoretical calculations infer that different exothermicities of the reaction associated with

the two conformers may provide different energy distributions for the products (COOH and H_3CCO^+).

To study the role of the local ion environment on conformation specific reactivity and stability of isolated biomolecules further, we have started experiments on simple α-substituted amides, and β-hydroxy/thiol amino acids. All these hitherto unexplored systems are in principle open to IR-VUV photoionization spectroscopic study. Other experiments that would be helpful in further exploring conformation specificity for the reactivity of radical cation intermediates include velocity map imaging experiments to measure different components of translational energy distribution following C_α-$C_{carboxylic}$ bond dissociation from different conformers, and photoelectron spectroscopy to determine the molecular ion states. Also, theoretical exploration of the relative time scales of charge transfer, hydrogen transfer, and structural rearrangement for a particular conformer of bioactive carboxylic acids would be advantageous.

2.8 Acknowledgment

Parts of these studies are supported by grants from the US ARO and NSF.

2.9 References

1. (a) Berlett, B. S.; Stadtman, E. R. *J. Biol. Chem.* **1997**, *272*, 20313-20316. (b) Stadtman, E. R. *Annu. Rev. Biochem.* **1993**, *62*, 797. (c) Davis, M. J.; Truscott, R. J. W. *J. Photochem. Photobiol., B* **2001**, *63*, 114. (d) Bensasson, R. V.; Land, E. J.; Truscott, T. G. *Excited States and Free Radicals in Biology and Medicine*; Oxford University Press: New York, **1983**. (e) Stubbe, J.; van der Donk, W. A. *Chem. Rev.* **1998**, *98*, 705.
2. (a) Varadarajan, S.; Yatin, S.; Kansi, J.; Jahanshahi, F. *Brain Res. Bull.* **1999**, *50*, 133-141. (b) Schoneich, C.; Pogocki, D.; Hug, G. L.; Bobrowski, K. *J. Am. Chem. Soc.* **2003**, *125*, 13700. (c) Yashiro, H.; White, R. C.; Yurkovskaya, A. V.; Forbes, M. D. E. *J. Phys. Chem. A* **2005**, *109*, 5855.
3. Kantorow, M.; Hawse, J. R.; Cowell, T. L.; Benhamed, S.; Pizarro, G. O.; Reddy, V. N.; Heijtmancik, J. F. *Proc. Natl. Acad. Sci. U.S.A.* **2004**, *101*, 9654.
4. (a) Splitter, J. S.; Turecek, F. *Application of Mass Spectrometry to Organic Stereo Chemistry*; Wiley-VCH, Inc.: New York, **1994**. (b) Barlow, C. K.; Moran, D.; Random, L.; McFadyen, W. D.; O'Hair, R. A. J. *J. Phys. Chem. A* **2006**, *110*, 8304.
5. (a) Chis, V.; Brustolon, M.; Morari, C.; Cozar, O.; David, L. *J. Mol. Struct.* **1999**, *482*, 283. (b) Brustolon, M.; Chis, V.; Maniero, A. L.; Brunel, L.C. *J. Phys. Chem. A* **1997**, *101*, 4887.
6. Sanderud, A.; Sagstuen, E. *J. Phys. Chem. B* **1998**, *102*, 9353.
7. Hawkins, C. L.; Davis, M. J. *J. Chem. Soc., Perkin Trans. 2* **1998**, 2617.
8. Hug, G. L.; Fessenden, R. W. *J. Phys. Chem. A* **2000**, *104*, 7021.
9. Bonifacic, M.; Stefanic, I.; Gug, G. L.; Armstrong, D. A.; Asmus, K. –D. *J. Am. Chem. Soc.* **1998**, *120*, 9930.
10. Armstrong, D. A.; Rauk, A. Yu, D. *J. Chem. Soc., Perkin Trans. 2* **1995**, 553.
11. (a) Sutherland, K. N.; Mineau, P. C.; Orlova, G. *J. Phys. Chem. A* **2007**, *111*, 7906-7914. (b) Simon, S.; Sodupe, M.; Bertran, J. *J. Phys. Chem. A* **2002**, *106*, 5697-5702.
12. Raczynska, E. D.; Hallmann, M.; Duczmal, K. *J. Iran. Chem. Res.* **2008**, *1*, 57.
13. Rauk, A. Yu, D. Armstrong, D. A. *J. Am. Chem. Soc.* **1997**, *119*, 208.
14. Yu, D.; Rauk, A.; Armstrong, D. A. *J. Am. Chem. Soc.* **1995**, *117*, 1789.
15. Barone, V.; Adamo, C.; Grand, A. Jolibois, F.; Brunel, Y.; Subra, R. *J. Am. Chem. Soc.* **1995**, *117*, 12618.
16. Barone, V.; Adamo, C.; Grand, A.; Subra, R. *Chem. Phys. Lett.* **1995**, *242*, 351.
17. Rega, N.; Cossi, M.; Barone, V. *J. Am. Chem. Soc.* **1997**, *119*, 12962.
18. Rega, N.; Cossi, M.; Barone, V. *J. Am. Chem. Soc.* **1998**, *120*, 5723.
19. Ban, F.; Gauld, J. W.; Boyd, R. J. *J. Phys. Chem. A* **2000**, *104*, 5080.
20. Ban, F.; Wetmore, S. D.; Boyd, R. J. *J. Phys. Chem. A* **1999**, *103*, 4303.
21. Himo, F. Ericksson, L. A. *J. Chem. Soc., Perkin Trans. 2* **1998**, *305*.
22. Rodriguez-Santiago, L.; Sodupe, M.; Oliva, A.; Bertran, J. *J. Phys. Chem. A* **2000**, *104*, 1256.
23. (a) Weinkauf, R.; Schanen, P.; Yang, D.; Soukara, S.; Schlag, E. W. *J. Phys. Chem.* **1995**, *99*, 11255-11265. (b) Weinkauf, R.; Schanen, P.; Metsala, A.; Schlag, E. W.; Burgle, M.; Kessler, H. *J. Phys. Chem.* **1996**, *100*, 18567. (c) Chu,

I. K.; Rodriquez, C. F.; Lau, T.; Hopkinson, A. C.; Siu, K. W. M.; *J. Phys. Chem. B* **2000**, *104*, 3393. (d) Barlow, C. K.; Wee, S.; McFadyen, W. D.; O'Hair, R. A. J.; *Dalton Trans.* **2004**, *20*, 3199. (e) Turecek, F.; Carpenter, F. H.; Polce, M. J.; Wesdemiotis, C. *J. Am. Chem. Soc.* **1999**, *121*, 7955. (f) Hopkinson, A. C.; Siu, K. W. M. In *Peptide Radical Cations in: Principles of Mass Spectrometry Applied to Biomolecules*; Laskin, J., Liftshitz, C., Eds.; John Wiley and Sons: NJ, **2006**, pp 301-335.

24. (a) Remacle, F.; Levine, R. D. *Proc. Natl. Acad. Sci. U.S.A.* **2006**, *103*, 6793-6798. (b) Remacle, F.; Levine, R. D. *Z. Phys. Chem.* **2007**, *221*, 647.
25. Kuleff, A. I.; Cederbaum, L. S. *Chem. Phys.* **2007**, *338*, 320.
26. Shemesh, D.; Gerber, R. B. *J. Chem. Phys.* **2005**, *122*, 241104.
27. (a) Choi, K. –W.; Ahn, D. –S.; Lee, J. –H.; Kim, S. K. *Chem. Commun.* **2007**, 1041-1043. (b) Zhang, L.; Pan, Y.; Guo, H.; Zhang, T.; Sheng, L.; Qi, F. *J. Phys. Chem. A* **2009**, *113*, 5838.
28. (a) Hu, Y. J.; Fu, H. B.; Bernstein, E. R. *J. Chem. Phys.* **2006**, *125*, 184308. (b) *ibid.* **2006**, *125*, 184308. (c) *ibid.* **2006**, *125*, 154306. (d) *ibid.* **2006**, *124*, 024302. (e) *ibid.* **2006**, *125*, 154305. (f) Shin, J. –W.; Bernstein, E. R. *ibid.* **2009**, *130*, 214306.
29. (a) Garavelli, M. *Theor Chem Acc* **2006** *116*: 87–105. (b) Smith, B. R.; Bearpark, M. J.; Robb, M. A.; Bernardi, F.; Olivucci, M. *Chemical Physics Letters* **1995** *242* 27. (c) Yarkony, D. R.; J. Phys. Chem. A 2001, 105, 6277.
30. (a) Bhattacharya, A.; Guo, Y. Q.; Bernstein, E. R. *J. Phys. Chem. A* **2009**, *113*, 811-823. (b) Soto, J.; Arenas, J. F.; Otero, J. C.; Pelaez, D. *J. Phys. Chem. A*, **2006**, *110*, 8221.
31. (a) Blancafort, L. *J. Am. Chem. Soc.* **2006**, *128*, 210. (b) Muchova, E.; Slvicek, P.; Sobolewski, A. L; Hobza, P. *J. Phys. Chem. A,* **2007**, *111*, 5259.
32. Frisch, M. J.; Trucks, G. W.; Schlegel, H. B.; Scuseria, G. E.; Robb, M. A.; Cheeseman, J. R.; Montgomery, J.; Vreven, J. A. T.; Kudin, K. N.; Burant, J. C.; Millam, J. M.; Iyengar, S. S.; Tomasi, J.; Barone, V.; Mennucci, B.; Cossi, M.; Scalmani, G.; Rega, N.; Petersson, G. A.; Nakatsuji, H.; Hada, M.; Ehara, M.; Toyota, K.; Fukuda, R.; Hasegawa, J.; Ishida, M.; Nakajima, T.; Honda, Y.; Kitao, O.; Nakai, H.; Klene, M.; Li, X.; Knox, J. E.; Hratchian, H. P.; Cross, J. B.; Adamo, C.; Jaramillo, J.; Gomperts, R.; Stratmann, R. E.; Yazyev, O.; Austin, A. J.; Cammi, R.; Pomelli, C.; Ochterski, J. W.; Ayala, P. Y.; Morokuma, K.; Voth, G. A.; Salvador, P.; Dannenberg, J. J.; Zakrzewski, V. G.; Dapprich, S.; Daniels, A. D.; Strain, M. C.; Farkas, O.; Malick, D. K.; Rabuck, A. D.; Raghavachari, K.; Foresman, J. B.; Ortiz, J. V.; Cui, Q.; Baboul, A. G.; Clifford, S.; Cioslowski, J.; Stefanov, B. B.; Liu, G.; Liashenko, A.; Piskorz, P.; Komaromi, I.; Martin, R. L.; Fox, D. J.; Keith, T.; Al-Laham, M. A.; Peng, C. Y.; Nanayakkara, A.; Challacombe, M.; Gill, P. M. W.; Johnson, B.; Chen, W.; Wong, M. W.; Gonzalez, C.; Pople, J. A. *GAUSSIAN 03, (Revision B.04)*, Gaussian, Inc., Pittsburgh, PA, **2003**.
33. Werner, H.-J.; Knowles, P. J. *MOLPRO (Version 2000.1)*, University of Sussex, UK, **1999**.
34. Pecul, M.; Rizzo, A.; Leszczynski, J. *J. Phys. Chem. A*, **2002**, *106*, 11008.
35. van Eijck, B. *J. Mol. Spectrosc.* **1983**, *101*, 113.

36. Borba, A.; Gomez-Zavaglia, A.; Lapinski, L.; Fausto, R. *Phys. Chem. Chem. Phys.* **2004**, *6*, 2101-2108.
37. Pimentel, G. C.; McClellan, A. L. *The Hydrogen Bond*, Freeman, San Francisco, **1960**.
38. (a) Berthomieu, C.; Sandorfy, C. *J. Mol. Spectrosc.* **1965**, *15*, 15. (b) Durocher, G.; Sandrofy, C. *J. Mol. Spectrosc.* **1965**, *15*, 22. (c) Foldes, A.; Sandorfy, C. *J. Mol. Spectrosc.* **1966**, *20*, 262. (d) Nibbering E. T. J.; Elsaesser, T. *Chem. Rev.* **2004**, *104*, 1887. (e) Elsaesser, T.; Huse, N.; Dreyer, J.; Dwyer, J. R.; Heyne, K.; Nibbering, E. T. J. *Chem. Phys.* **2007**, *341*, 175. (f) Kozich, V.; Dreyer, J.; Ashihara, S.; Werncke, W.; Elsaesser, T. *J. Chem. Phys.* **2006**, *125*, 074504.
39. Tarakeswar, P.; Manogaran, S. *J. Mol. Struc.* **1998**, *430*, 51.
40. Plath, K. L.; Takahashi, K.; Skodje, R. T.; Vaida, V. *J. Phys. Chem. A*, **2009**, *113*, 7294.
41. Hu, Y.; Bernstein, E. R. *J. Chem. Phys.* **2008**, *128*, 164311.
42. (a) Debies, T. P.; Rabalais, J. W. *J. Electron Spectrosc. Relat. Phenom.* **1974**, *3*, 315. (b) McGlynn, S. P.; Meeks, J. L. *J. Electron Spectrosc. Relat. Phenom.* **1975**, *6*, 269.
43. Schatz, G. C.; Ratner, M. A. *Quantum Mechanics in Chemistry*, Prentice-Hall, Englewood Cliffs, New Jersey, **1993**.
44. Powis, I.; Rennie, E. E.; Hergenhahn, U.; Kugeler, O.; Bussy-Socrate, R. *J. Phys. Chem. A* **2003**, *107*, 25.
45. Marcus, R. A.; Sutin, N. *Biochim. Biophys. Acta* **1985**, *811*, 265.
46. Dodonova, N. Y. *J. Photochem. Photobiol. B* **1993**, *18*, 111.
47. Cody, G. D.; Boctor, N. Z.; Filley, T. R.; Hazen, R. M.; Scott, J. H.; Sharma, A.; Yoder, Jr., H. S. *Science*, **2000**, *289*, 1337.
48. http://webbook.nist.gov/cgi/cbook.cgi?ID=C50215&Units=SI&Mask=200#Mass-Spec.
49. (a) Hildenbrand, D. L. *Int. J. Mass Spectrom.* **2000**, *197*, 237. (b) *J. Phys. B: At. Mol. Opt. Phys.* **2003**, *36*, 261. (c) *Int. J. Mass Spectrom.* **2004**, *235*, 155.

2.10 Supporting Information

Table 2.T1: *Computed vertical ionization energies (VIEs) at the MP2/aug-cc-pVDZ and CASSCF(9,8)/6-31G(d) levels of theory. A comparison with experimental values is also given. Experimental results are based on photoelectron spectroscopy results.*[1,2]

Compound	Conformation	Calc. VIE (eV) MP2/aug-cc-pVDZ	Calc. ion states CAS(9,8)/6-31G(d)		Expt. VIE (eV)	
			State	Excitation energy (eV)	D_0	D_1
Lactic Acid					-	-
	I	11.00	D_0, np_O	0.0		
			D_1, $n\sigma_O$	1.7		
	II	10.44	D_0, $n\sigma_O$	0.0		
			D_1, $n\pi_O$	1.2		
	III	10.90	D_0, $n\sigma_O$	0.0		
			D_1, $n\pi_O$	1.0		
Pyruvic Acid					10.42	12.31
	I	10.49	D_0, $n\sigma_O$	0.0		
			D_1, $n\sigma_O$	2.0		
	II	10.92	D_0, $n\sigma_O$	0.0		
			D_1, $n\pi_O$	3.2		
	III	11.00	D_0, $n\sigma_O$	0.0		
			D_1, $n\pi_O$			
Glycine					10.00	11.11
	I	10.22	D_0, $n\sigma_N$	0.0		
			D_1,π_{COOH}	4.3		
	II	10.28	D_0, $n\sigma_O$	0.0		
			D_1, π_{COOH}	1.2		
	III	10.12	D_0, np_N	0.0		
			D_1, $n\sigma_O$	4.0		

1. Debies, T. P.; Rabalais, J. W. *J. Electron Spectrosc. Relat. Phenom.* **1974**, *3*, 315.
2. McGlynn, S. P.; Meeks, J. L. *J. Electron Spectrosc. Relat. Phenom.* **1975**, *6*, 269.

Lactic Acid:

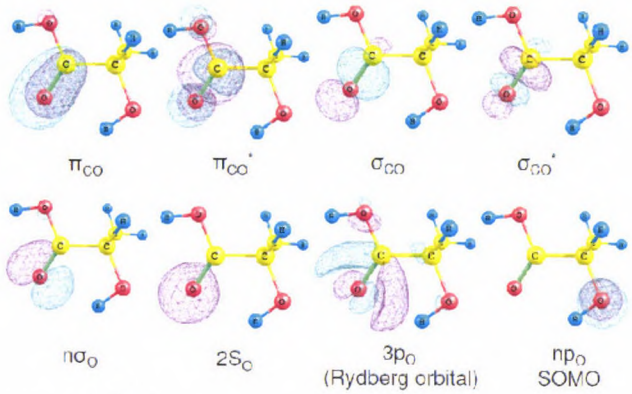

Pyruvic Acid:

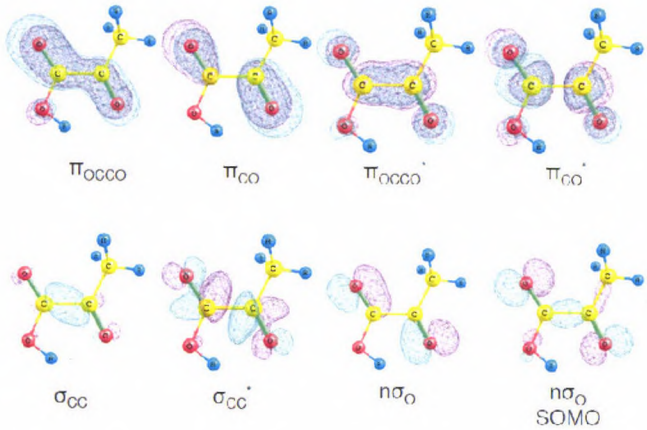

Glycine:

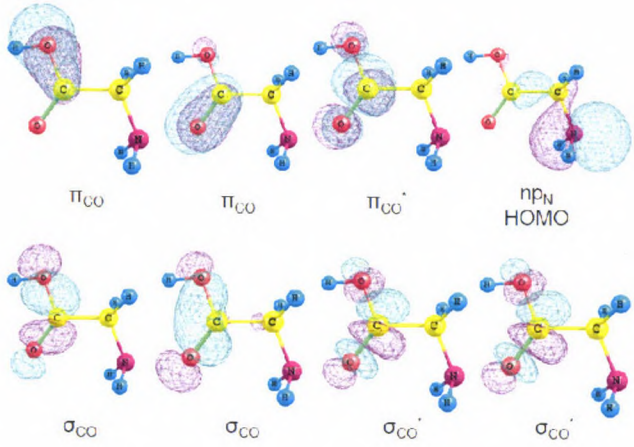

Figure 2.S1: *Natural orbitals used in the active space for CASSCF calculations for radical cationic lactic acid, pyruvic acid, glycine. These orbitals comprise the active space with 9 electrons in 8 orbitals. Only orbitals of the lowest energy conformer of lactic acid, pyruvic acid, and glycine are shown below.*

Reaction 2.R1: *Thermochemical Calculations of Lactic Acid (Data taken from http://www.mdpi.org/ijms/papers/8050407.pdf and (b) Vatani, A.; Mehrpooya, M.; Gharagheizi, F. Int. J. Mol. Sci.* ***2007****, 8, 407.)*

Reaction 1.

$$CH_3CH(OH)COOH \rightarrow CH_3 + COOH + CHOH^+$$

ΔH_f^0 (CHOH) = –227.5 kJ/mol

ΔH_f^0 (COOH) = –587.5 kJ/mol

ΔH_f^0 (CH_3) = –371.5 kJ/mol

ΔH_f^0 (*Lactic Acid*) = –682.96 kJ/mol

$AIP(CHOH) = 8.6\ eV$, calculated at MP2/aug-cc-pVDZ

$$\Delta H_{rxn} = \left[\Delta H_f^0(CH_3) + \Delta H_f^0(CHOH) + AIP(CHOH) + \Delta H_f^0(COOH) - \Delta H_f^0(Lactic\ Acid)\right]$$

$$\Delta H_{rxn} = 0.183\ eV + AIP(CHOH)$$

$$\Delta H_{rxn} = 0.183\ eV + 8.6\ eV = 8.78\ eV$$

Therefore, this reaction is thermodynamically accessible following photoionization of lactic acid at 118 nm (10.5 eV).

Reaction 2.

$$CH_3CH(OH)COOH \rightarrow CH_3CHO^+ + CO + H_2O$$

ΔH_f^0 (CO) = –110.5 kJ/mol

ΔH_f^0 (H_2O) = –285.8 kJ/mol

ΔH_f^0 (CH_3CHO) = –160.2 kJ/mol

$AIP(CH_3CHO) = 8.3\ eV$

$$\Delta H_{rxn} = \left[\Delta H_f^0(CH_3CHO) + AIP(CH_3CHO) + \Delta H_f^0(CO) + \Delta H_f^0(H_2O) - \Delta H_f^0(Lactic\ Acid)\right]$$

$$\Delta H_{rxn} = 0.13\ eV + AIP(CH_3CHO)$$

$$\Delta H_{rxn} = 1.3\ eV + 8.3\ eV = 9.6\ eV$$

Therefore, this reaction is also thermodynamically accessible following photoionization of lactic acid at 118 nm (10.5 eV).

Chapter 3: The IR-VUV Ion Dip Spectroscopy of Naturally Occurring Aromatic Amino Acids

The work performed in this chapter was a joint effort between Dr. Joong-Won Shin and me. All reported spectra were obtained by Dr. Shin, while I contributed all computational data.

3.1 Introduction

Amino acids, being among the most basic building blocks of life, have been of much interest for study. IR absorption spectroscopy can be a useful tool in studying these systems: absorption line widths, intensities, and energies can give direct information about the structure and behaviors they exhibit. IR absorption spectra of gas phase species can be obtained by ion- or fluorescence- dip spectroscopy,[1-4] a technique that has been applied to various systems, such as isolated or paired nucleobases,[5] amino acids with aromatic chromophores (phenylalanine and tryptophan),[6,7] or aromatic substituted sugars.[8] These studies have been performed using IR laser systems that cover the near- to mid-IR region (e.g., 2500 to 7000 cm^{-1}). In this range X-H (X=C,O,N), stretching vibrations can be probed and the results can provide insight into the conformational landscape of these species.

Numerous studies have been conducted on naturally occurring amino acid species through the use of R2PI ion dip spectroscopy. This is accomplished by selecting a specific electronic transition associated with the aromatic moiety to employ two-photon ionization. Conformational assignments have been made based on these spectra.[9-14]

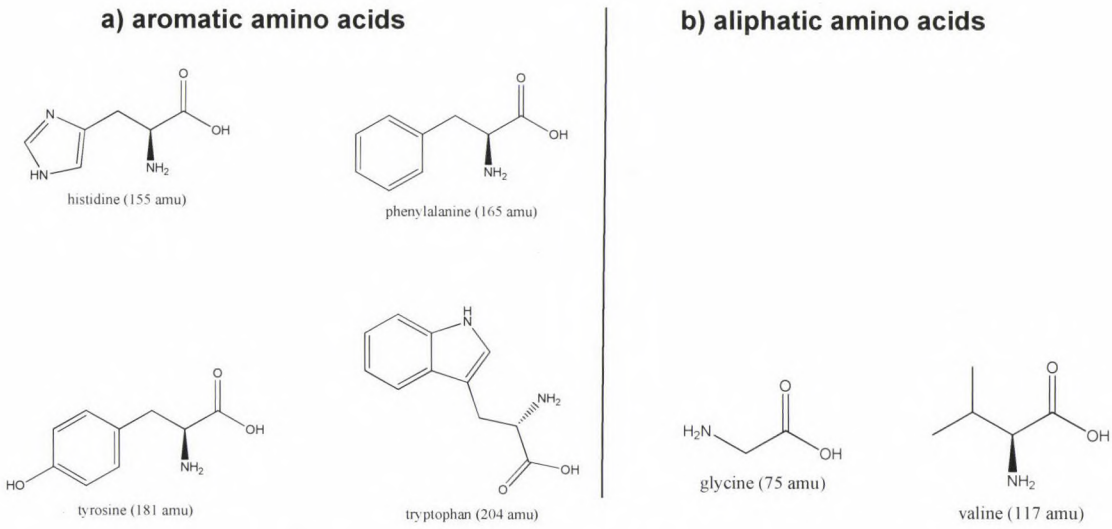

Figure 3.1: *The aromatic amino acids studied in this chapter (a), and representative samples of aliphatic amino acids (b)*

Lately, IR-VUV studies have been performed on gas phase aliphatic amino acid species, and these results further explored through high-level calculations. It is clear that photoionized amino acids undergo conformer specific chemistry.[15, 16] The unique spectra obtained by monitoring different fragment mass channels indicate conformer specific behavior, and this conformer specific behavior has been further corroborated through the use of high level calculations. Neutral parent conformers give rise to unique fragment ions upon single-photon ionization. The side chain of an aliphatic amino acid can interact with the functional groups of the amino acids to alter the neutral ground state geometry, as well as affect the chemistry of the amino acid ions (Chaper 1).

In our present study, the ionization/detection step for IR vibrational absorption is through single photon ionization (SPI) at 10.5 eV (118 nm). This energy is sufficient to ionize a number of amino acids and sugars directly. Thereby, the structure and dynamics of such species can be investigated through analysis of their CH, OH, and NH modes, and vibrational overtones and combinations, in general. These spectroscopic studies are then

aided through the use of high level calculations to assist in, and enable, interpretation of the data.

Here we present the results of SPI IR-VUV ion dip spectroscopy studies performed on a number of aromatic amino acid species. These results are further explored through second order Møller-Plesset perturbation theory (MP2) and Complete Active Space Self Consistent Field (CASSCF) calculations, focused primarily on two representative species: histidine and phenylalanine. The aromatic amino acids behave differently from the aliphatic amino acids, both with respect to spectroscopic results and the theoretical exploration of the neutral and cation chemistry.

3.2 Methods and Materials

IR-VUV Ion Dip Spectra

The experimental apparatus used to record time of flight mass and IR spectra in combination with a VUV single photonionization source is described elsewhere.[15,16] Commercial samples of amino acids (Aldrich) are used without further purification.

The amino acid samples were placed into the gas phase by means of matrix assisted laser desorption. Approximately 0.5 mmol of amino acid was placed into 8 ml of 10% formic acid / methanol. This was then added to 10 ml of a 0.05 mM solution of the dye Rhodamine 6G in methanol. This combined matrix and sample solution was evenly sprayed onto an ablation drum.

The sample was ablated with 532 nm wavelength laser pulse generated from a Nd^{+3}/YAG laser (second harmonic). The gaseous amino acid molecules are seeded into a neon/helium gas mixture (70%/30%, total pressure of 2 atm) and the gaseous mixture is expanded into a high vacuum chamber by a pulsed supersonic nozzle with a pulse width of typically 150 μs duration. After passing through a skimmer, the molecular beam interacts with pulsed VUV and IR laser beams in the ionization region of a time of flight mass spectrometer, TOFMS, in which VUV laser generated ions are detected.

The 118 nm radiation is the ninth harmonic of the fundamental output of a Nd^{+3}/YAG laser at 1.064 μm. 355 nm radiation (third harmonic) is focused into a cell with Xe/Ar at a ratio of 1:10 at ~200 Torr total pressure. A MgF_2 lens focuses the 118 nm light in the ionization region of the TOFMS and disperses the remaining 355 nm light.

An IR laser beam, which counterpropagates with respect to the 118 nm laser beam, is focused at the VUV/molecular beam intersection point by a 40 cm focal length lens to access neutral ground state species. Tunable IR radiation is obtained from an optical parametric oscillator, OPO (Laser Vision), pumped by an injection seeded Nd^{+3}:YAG laser (Spectra Physics GCR-3). A type II KDP (KH_2PO_4) doubling crystal is integrated into the OPO to convert the Nd^{+3}:YAG laser fundamental output to 532 nm. Two interchangeable sets of nonlinear crystals ($KTiOAsO_4$, KTA) in the system are used to generate a difference frequency between the output of the first oscillator (712 nm to 2.13 μm) and a portion of the 1064 nm pump beam to provide wavelength coverage from 2.5 to 4.0 μm. The output beam consists of both signal and idler wavelengths from the down conversion of the 532 nm pump. The OPO output energy between 2500 and 4200 cm^{-1} is 3–5 mJ/pulse with a bandwidth of 2–3 cm^{-1}.

IR absorption spectra are measured by the use of IR plus VUV nonresonant ionization and fragmentation detection spectroscopy. As the IR laser is scanned to excite cooled molecules to higher vibrational modes of their ground electronic state prior to the introduction of VUV light, the fragment ion mass channel intensity is monitored. The vibrational spectrum of the neutral molecular conformers is thereby obtained, as the fragmentation pattern depends on the total energy in the amino acid cation and on the isomeric structure of the neutral parent amino acid molecule. Both positive and negative intensity changes in the fragment mass channels can be observed as a function of IR absorption, as the various channels for fragmentation become more or less accessible depending on the total energy in the amino acid parent ion. No parent ion is detected by VUV ionization.

Computational Details and Methods

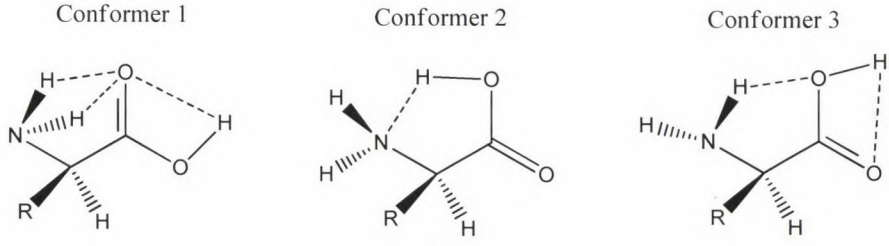

Figure 3.2: *The three general lowest energy conformers of amino acids, listed in order from lowest to highest as they occur in aliphatic amino acids.*

All calculations, unless specified otherwise, were performed using the Gaussian03 software package. All calculations were performed on a local cluster, or on NCSA machines (Mercury, Cobalt, Abe) using a Teragrid account. In general, the initial molecular geometry was taken from a model built in a 3D modeling package, such as Chem3D. The model was then minimized by MM2 molecular mechanics through a

GAMESS interface. This geometry was again minimized using UHF/6-311++G(d,p) to provide an initial geometry for the desired calculation.

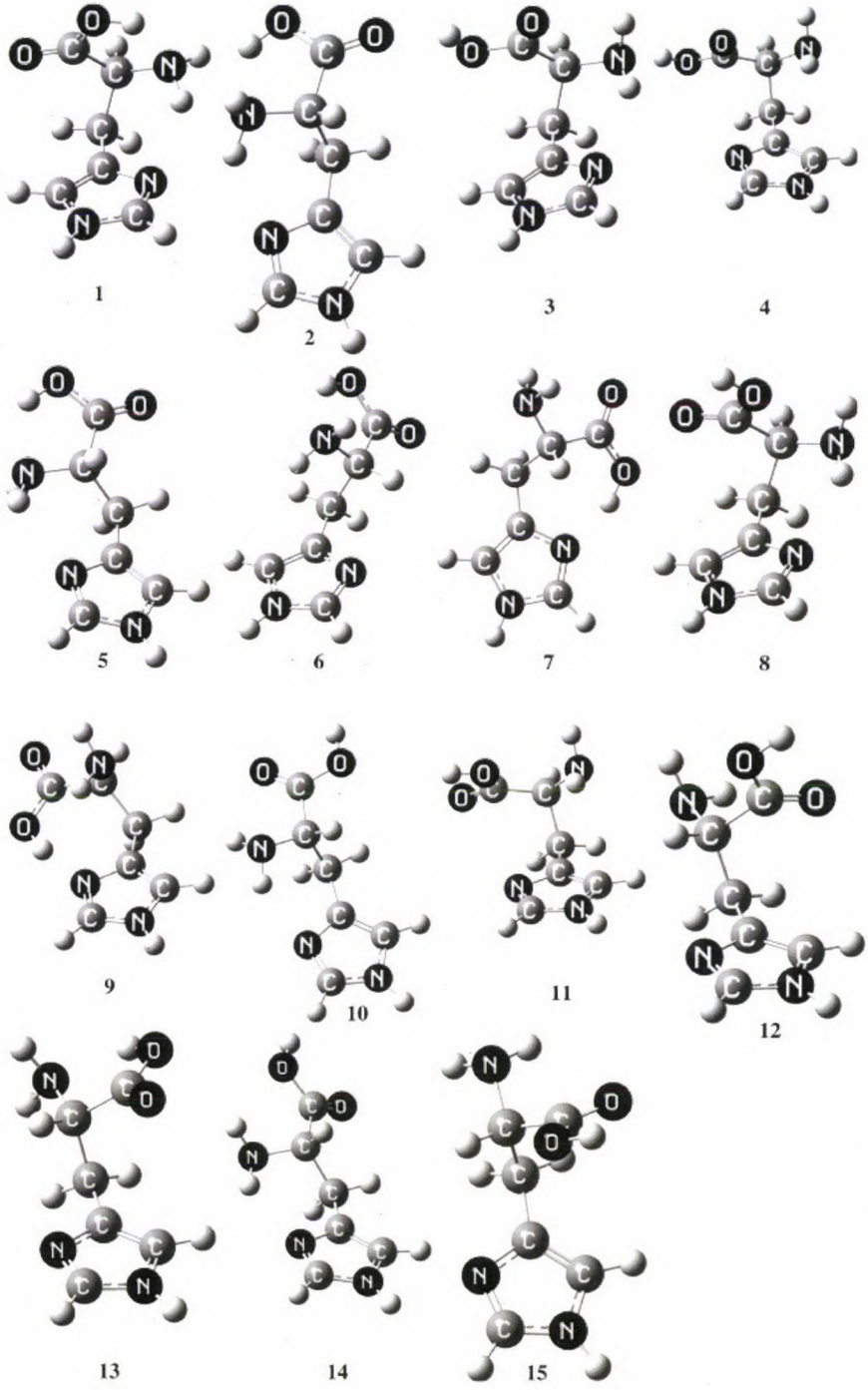

Figure 3.3: *The fifteen lowest energy conformers of histidine, as reported by Lin (2006). The orientation of the carboxylic acid and amine functional groups determine the general conformer type, although the side chain can provide a large amount of structural variety within each general type. Adapted from Lin (2006)*[17].

Two species were selected for study: histidine and phenylalanine. These represent the simplest, and thus easiest to study, aromatic species studied by means of IR-VUV ion dip spectroscopy. In earlier studies conducted by Lin[17] and Simons,[18] a number of molecular structures for these two species were studied and calculated. Out of these many structures, three specific conformations were selected. These particular conformations were intended to be used as a general representation of each of the three classes of conformers studied previously (Fig. 3.2.) All three were listed as the lowest energy structure within its class of conformer. (The lowest energy structure of a Conformer 1 type species was selected, the lowest energy structure of a Conformer 2 type species, etc.)

MP2 level optimizations were performed. Initial MP2 optimizations were performed at the MP2/6-311++G(d,p) level. The minimized geometry obtained through this 6-311++G(d,p) basis set optimization was then used as the initial geometry for a further optimization utilizing the aug-cc-pVDZ basis set.

The general method for CASSCF calculations is as described by Robb.[19-21] Structures obtained through MP2 optimizations were re-optimized at the RHF/STO-3G level in order to obtain the initial CAS orbitals. From there, the desired orbitals were chosen, and a single point CASSCF/STO-3G calculation was run. According to Robb, 6-31G* is usually a sufficiently large basis set to obtain acceptable results when performing CAS calculations. In order to project the basis set up to the desired level, a single point CASSCF/3-21G was run, followed by an optimization at CASSCF/4-31G, then a single point CASSCF/6-31G*, and finally an optimization at CASSCF/6-31G*.

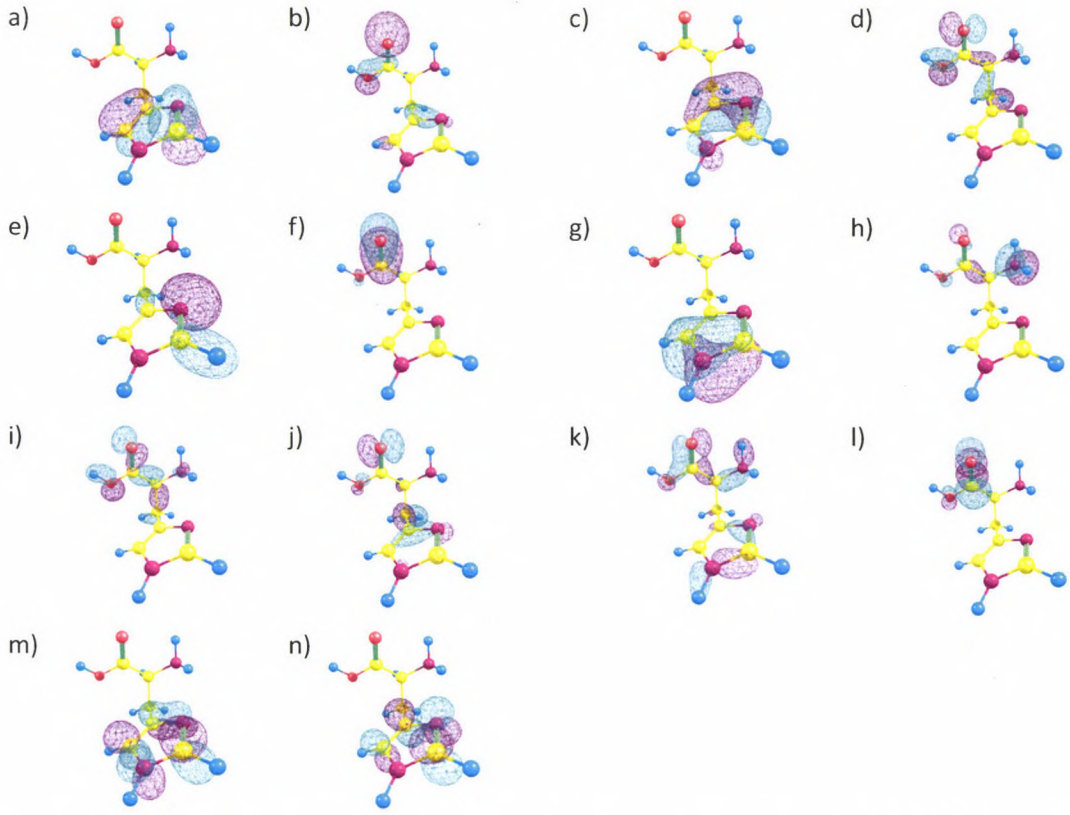

Figure 3.4: *Sample active space for histidine, consisting of: five aromatic π orbitals (a, c, g, m, n), three carboxylic acid π orbitals (f, k), four non-bonding orbitals on the carboxylic oxygens (b, d, i, j), and two non-bonding amine nitrogen orbitals (h, e).*

The largest active space available in the Gaussian03 software package is 14 orbitals, thus CASSCF(22,14) and CASSCF(21,14) calculations were performed for neutral and cation species, respectively. The active space selected for the CASSCF calculations consisted of fourteen orbitals, chosen to represent the various possible intra-molecular interactions within the molecule. In histidine, this consisted of five π orbitals located on the aromatic moiety, three carboxylic acid π orbitals, four non-bonding orbitals located on the carboxyilic oxygens, and a non-bonding orbital located on the amine nitroten and on one of the ring nitrogens. Representative orbital selections are shown in Figure 3.4.

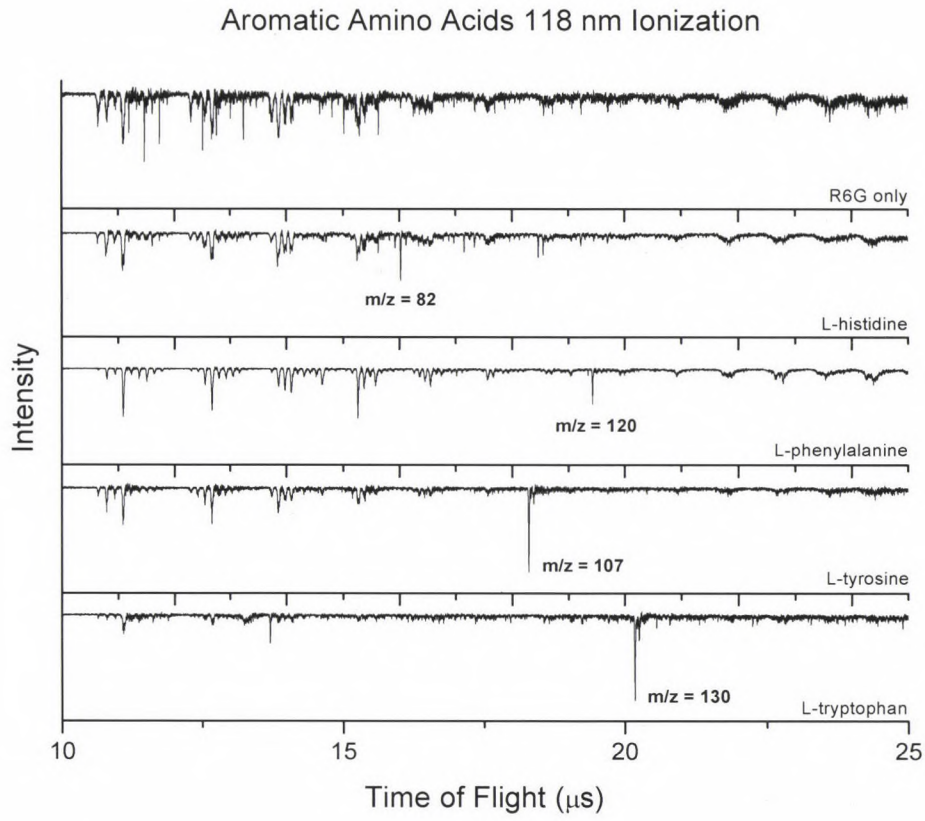

Figure 3.5: *Mass spectra of aromatic amino acids obtained using 118 nm single photon ionization. Mass to charge ratios are in amu.*

IR-VUV results

The mass spectra of histidine, pheylalanine, tyrosine, and tryptamine (see Figure 3.1 for masses in amu), obtained using 118 nm single photon ionization are shown in Figure 3.5, and the recoreded IR-VUV ion dip spectra can be seen in Figure 3.6. All ion dip spectra are the result of a summation of 13 individual scans. In each case, only one or two mass channels were available for observation. Almost all observed fragment channels involve a breaking of the secondary C–C bond, releasing the aromatic moiety containing side chain from the primary amino acid backbone. Additionally, in all

observed mass channels, the charge is located on the fragment containing the aromatic moiety.

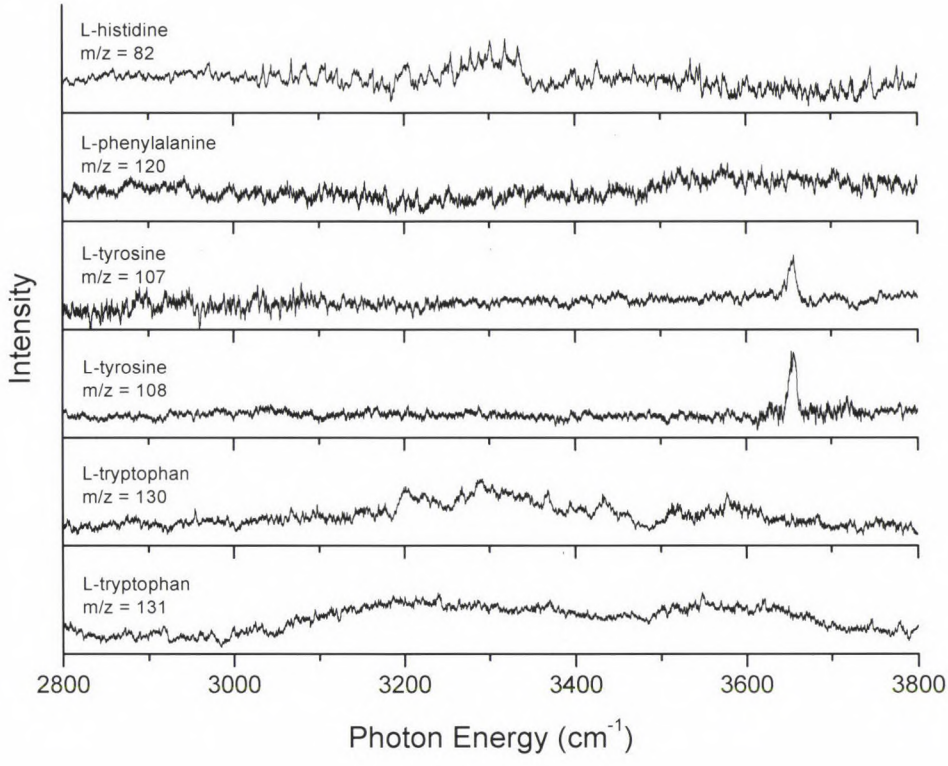

Figure 3.6: *IR-VUV ion dip spectra of aromatic amino acids. Species and mass channel monitored (in amu) are as labeled.*

Histidine

The only major mass channel available for observation from histidine is m/z=82. This likely corresponds to a fragment consisting of the CH_2–$C_3N_2H_3$ aromatic moiety containing side chain, with the inclusion of an additional hydrogen. (See Figure 3.7 for general proposed structure.) The extra hydrogen in this fragment is likely the result of a hydrogen atom transfer from the backbone amine group to an aromatic nitrogen atom (see Figure 3.1). While feature assignments are difficult, imidazole N–H stretching features around 3520 cm^{-1} and backbone N–H stretching around 3400 cm^{-1} can be

suggested. The broad feature between 3250 and 3350 cm^{-1} may be hydrogen bonded carboxylic O–H stretching.

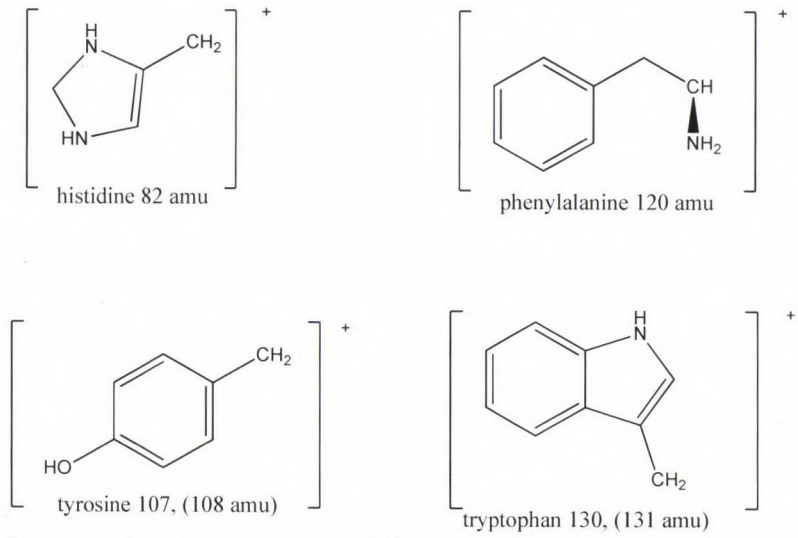

Figure 3.7: *Rudimentary fragment structures of the observed mass fragments resulting from 118 nm ionization of the aromatic amino acid species. Masses in parenthesis correlate to the shown structure, but with the a probable CH_3 in place of the shown CH_2 group.*

Phenylalanine

In the case of phenylalanine, only the 120 amu mass channel could be monitored to obtain an ion dip spectrum. This corresponds to the loss of a fragment of mass 45, which is likely the loss of COOH. (This fragmentation is observed for some conformers of aliphatic amino acids.) A possible feature around 3570 cm^{-1} may be attributed to a free carboxylic O–H stretching mode. The spectra are weak and thus hard to analyze, but are definitely reproducible from scan to scan. The signals for this molecule are weak and not readily assigned, implying that the IR absorption of the neutral phenylalanine does not change the mass signal significantly.

Tyrosine

In this molecule, two fragment ions were available for observation, one at 107 amu, and another at 108. These likely correspond to the aromatic side chain ion following the loss of the amino acid backbone due to a secondary C–C bond break, and the aromatic side chain with an additional hydrogen, respectively (Figure 3.7). A single peak around 3650 cm^{-1} appears in both mass channels and is almost certainly associated with the free phenol O–H stretch.

Tryptophan

Again, two fragment ions were available for observation, one at 130 and one at 131 amu. As in the case of tyrosine, these likely correspond to the remaining aromatic side chain after the loss of the amino acid backbone due to a secondary C–C bond break, and the aromatic side chain with an additional hydrogen, respectively. The spectrum obtained through motoring the 130 amu channel contains some very broad features likely associated with C–H overtones and/or hydrogen bonded O–H stretches. The peak located around 3510 cm^{-1} is possibly an indole N–H stretch. The feature at approximately 3570 cm^{-1} is likely due to the free carboxylic O–H stretch. The 130 amu channel largely provides the same broad C–H overtones and hydrogen bonded stretching features seen in the m/z=130 channel without any of the sharper, assignable peaks.

We note that in general R2PI and fluorescence dip produce IR spectra of tyrosine and tryptophan that are of much better signal to noise ratio and much better resolution. We are in the process of taking those spectra ourselves to try to understand the difference

between the two approaches, and why the aromatic system is a much better probe for the IR absorption than the amino acid backbone ion states.

Calculational Results

Geometries and relative energies for histidine and phenylalanine can be seen in Figures 3.8 and 3.9 The calculations clearly show Conformer 2 to be the lowest in energy in these aromatic species, a clear change from simple aliphatic amino acid behavior. As our own calculations and other, broader studies have shown,[17,18] the increased level of complexity for the structure in aromatic amino acids leads to a number of conformers, each exhibiting structural variation, which are very close in energy, and thus are present in some abundance in any sample. Thus, the observed spectra are clearly the result of many conformations contributing to the signal, resulting in a much broader, weaker spectrum.

Histidine

The calculated neutral species structures and relative energies of histidine are shown in Figure 3.8, and the calculated vertical ionization energies are shown in Table 3.1 (MP2/aug-cc-pVDZ) and in Table 3.2 (CASSCF(21,14)/6-31G*). As is predicted by Simons[9] and others,[10,11] the presence of an aromatic moiety on the amino acid side chain alters the potential energy landscape to such a degree that Conformer 2 is now the lowest energy conformer, followed by Conformer 1 and then Conformer 3. Their respective energies, however, are now much closer. This alone should be sufficient evidence that the presence of an aromatic moiety, especially when artificially placed into a system which

does not naturally contain one,[14] can alter the uni-molecular chemistry of the observed species.

Table 3.1: *Vertical ionization energies of histidine and phenylalanine as calculated at the MP2/aug-cc-pVDZ level. All energies are reported as eV above the neutral minimum of that particular conformer (S_0).*

	Conformer 1	*Conformer 2*	*Conformer 3*
Histidine	8.9	9.0	8.9
Phenylalanine	9.8	9.5	9.7

The vertical ionization energy of histidine is reported to be 8.5 eV.[22] As was observed in our earlier study on aliphatic amino acids (Chapter 1), MP2/aug-cc-pVDZ continues the trend of providing a high estimate of vertical ionization energies in general (likely due to the size of its basis set). In Chapter 1, however, it is observed that the relative energies between the adiabatic and vertical ions calculated at the MP2/aug-cc-pVDZ level are comparable to the relative energies calculated with the CASSCF method (a method which is considered to be more accurate, in general). It is therefore likely that the relative energies between the vertical and adiabatic ion energies calculated here at the MP2/aug-cc-pVDZ level are also reasonably accurate.

One of the hydrogens in the amine functional group is oriented toward, and possibly interacts with, the nitrogen atom on the aromatic ring (Figure 3.8). This interaction leads us to suggest that the extra hydrogen in the 82 amu fragment ion is a result of a hydrogen transfer from the backbone amine functional group to the aromatic nitrogen atom.

	MP2/aug-cc-pVDZ		CASSCF(22,14)/6-31G*	
	Structure	Rel. Energy (eV)	Structure	Rel. Energy (eV)
1	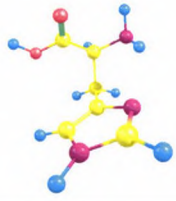	0.14	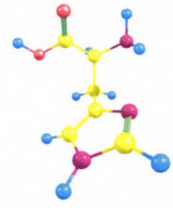	0.02
2	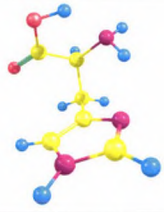	0	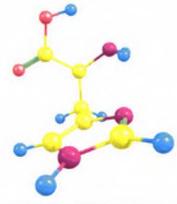	0
3	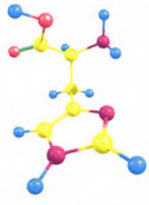	0.18	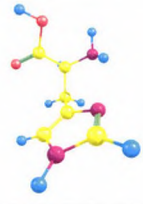	0.11

Figure 3.8: *The structures and relative energies of the three lowest-energy conformer types of neutral histidine, calculated at the MP2/aug-cc-pVDZ and CASSCF(22,14)/6-31G* levels.*

When we look at the CAS results, the difference between SPI IR-VUV ion dip spectroscopy and R2PI ion dip spectroscopy is further emphasized. A spectrum was obtained from histidine (Figure 3.6), which does not have an electronic transition that easily lends itself to R2PI spectroscopy. As can be seen in Table 3.2, the 10.5 eV ionization energy is, however, sufficient to access histidine in a number of electronically excited ion states. Thus, a previously unavailable species can now be explored.

Table 3.2: *Calculated vertical ionization energies of histidine, calculated at the CASSCF(21,14)/6-31G* level. Values are reported as eV above the neutral ground state (S_0) of the conformer.*

	D_0	D_1	D_2	D_3	D_4	D_5
Conf 1	7.6	8.7		9.7	10.2	
Conf 2	7.6	9.0	9.1		10.8	
Conf 3	7.5	8.7				

Because multiple ion states (up to six) can be accessed through the use of 10.5 eV radiation, even greater potential complexity within the observed spectra of the aromatic amino acids is possible. Again, this is different from R2PI spectroscopy, which by design accesses a single electronic ion state localized on the aromatic moiety. In larger, more complex systems such as aromatic amino acids, this potential for multiple electronic states and multiple resulting chemistries can result in even broader spectra than may be obtained through R2PI. The ion states D_n, n=0,1,…,5, can be associated with singly occupied molecular orbitals (SOMOs) that have localized ion character on various moieties of the molecule such as the aromatic moiety, carboxylic acid, amine group, etc. As we have shown in Chapter 2, localized charge upon ionization can lead to unique chemistry, depending on charge location and ion conformation. Future planned photoelectron spectroscopy studies may help clarify these chemistry issues.

Phenylalanine

The calculated neutral structures and relative energies for phenylalanine are shown in Figure 3.9, and calculated vertical ionization energies are reported in Table 3.1. The altered potential energy landscape with respect to aliphatic amino acid species can

also be observed for this amino acid. Again, the conformers are all very close to each other in energy, and thus likely to all be present, in many conformational and structural variations, along with other conformers in any cold sample. Again, this increase in conformational variety is reflected in a broad, weak spectrum.

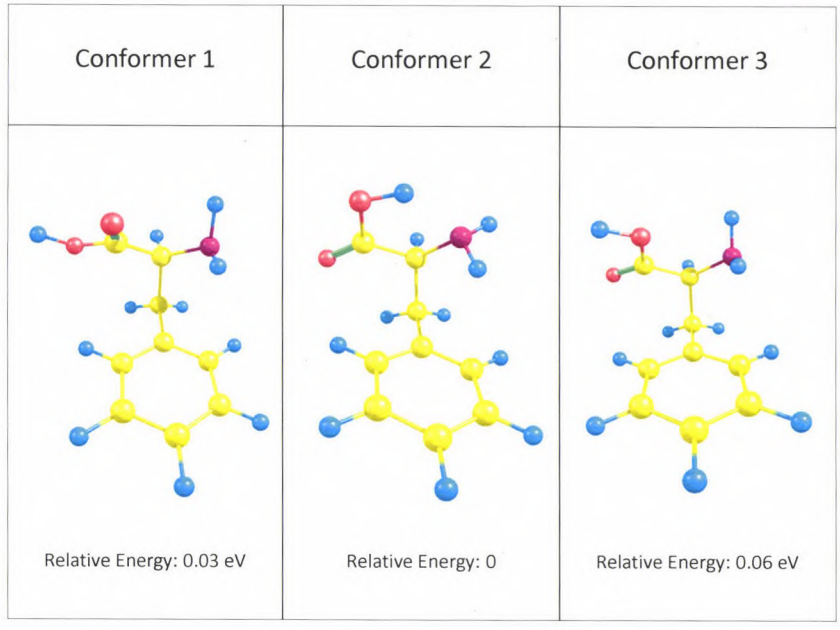

Figure 3.9: *The structures and relative energies of phenylalanine, calculated at the MP2/aug-cc-pVDZ level.*

To date, an experimental value for the vertical ionization energy of phenylalanine has not been reported. The calculated vertical ionization energies seem reasonable, however. Given that other MP2/aug-cc-pVDZ calculations of vertical ionization energies have been about 0.5 eV too high (Chaper 1), one can assume that these values are high by a similar amount. A vertical ionization energy of around 9 eV is certainly consistent with what has been experimentally reported for other amino acid species, and thus seems reasonable here as well.

3.4 Conclusions

The spectra obtained for aromatic amino acids demonstrate increased complexity for their conformational structures. This is likely due to a number of factors. A larger number of conformations can fragment to create the same ions, or ions of the same size. Within the main conformer types, a much greater variety of secondary structures and interactions can occur, each resulting in broadened vibrational features, or possibly slightly different features altogether.

Multiple ion states can be accessed by the 10.5 eV radiation employed for ionization. Thus, we are likely observing different chemistries when studying these species by means of single photon ionization IR-VUV ion dip spectroscopy. The single photon ionization does present a more general picture of photoionized amino acid behavior, which can lead to a better understanding of these species in a natural environment.

What should also be clear is that R2PI studies of species modified through the addition of an aromatic moiety are not the same as a study of the natural species through single-photon ionization. The R2PI method clearly represents a specific study on one type of chemistry within a species which may or may not correspond to its natural photoionization behavior. A more general approach may be useful in understanding these species in their natural environment, and a more general approach is what has been employed herein.

3.5 References

1. Page, R. H.; Shen, Y. R.; Lee, Y. T. *Journal of Chemical Physics*, **1988**, *88*, 4621.
2. Ebata, T.; Fujii, A. and Mikami, N. *International Reviews in Physical Chemistry*, **1998,** *17*, 331.
3. Nir, E.; Janzen, C.; Imhof, P.; Kleinermanns, K. and de Vries, M. S. *Journal of Chemical Physics,* **2001**, *115*, 4604.
4. Zwier, T. S. *Journal of Physical Chemistry A*, **2006**, *110*, 4133.
5. Abo-Riziq, B. C.; Grace, L. and de Vries, M. S. *Journal of the American Chemical Society,* **2005,** *127*, 2374.
6. Snoek, L. C.; Robertson, E. G.; Kroemer, R. T. and Simons, J. P. Chemical *Physics Letters*, **2000**, *321*, 49.
7. Simons, J. P.; Jockusch, R. A.; Çarçabal, P.; Hünig, R. A.; Kroemer, R. T.; Macleod, N. A. and Snoek, L. *International Reviews in Physical Chemistry*, **2005,** *24*, 489.
8. Simons, J. P.; Jockusch, R. A.; Çarçabal, P.; Huenig, I.; Kroemer, R. T.; Macleod, N. A. and Snoek, L. C. *International Reviews in Physical Chemistry*, **2005**, *24*, 489; Çarçabal, P.; Jockusch, R. A.; Huenig, I.; Snoek, L. C.; Kroemer, R. T.; Compagnon, I.; Oomens, J. and Simons, J. P. *Journal of the American Chemical Society*, **2005**, *127*, 11414.
9. Robertson, E. G.; Simons, J. P.; *Physical Chemistry Chemical Physics*, **2001**, *3*, 1.
10. de Vries, M. S. and Hobza, P. *Annual Reviews in Physical Chemistry*, **2007**. *58*, 585.
11. Černý, J. and Hobza, P. *Physical Chemistry Chemical Physics*, **2007**, *9*, 5291.
12. Ebata, T.; Hashimoto, T.; Ito, T.; Inokuchi, Y.; Altunsu, F.; Brutschy, B. and Tarakeshwar, P. *Physical Chemistry Chemical Physics*, **2006**, *8*, 4783.
13. Rizzo, T. R.; Park, Y. D.; Peteanu, L. A. and Levy, D. H. *Journal of Chemical Physics*, **1986**, *84*, 2534.
14. Lee, K. T.; Sung, J.; Lee, K. J.; Park, Y. D.; and Kim, S. K. *Angewandte Chemie International Edition,* **2002**, *41*, 4114.
15. Hu, Y. and Bernstein, E. R. *Journal of Chemical Physics* **2008**, *128*, 164311.
16. Hu, Y. and Bernstein, E. R. *Journal of Physical Chemistry A*, **2009**, *113*, 8454.
17. Huang, Z.; Yu, W.; Lin, Z. *Journal of Molecular Structure: THEOCHEM,* 2006, *801,* 7.
18. Lee, Y.; Jung, J.; Kim, B.; Butz, P.; Snoek, L. C.; Kroemer, R. T. and Simons J. P. *Journal of Physical Chemistry A*, **2004**, *108*, 69.
19. Robb, M. http://www.ch.ic.ac.uk/robb/casscf.php
20. Bearpark, M. J.; Ogliaro, F.; Vreven, T.; Boggio-Pasqua, M.; Frisch, M. J.; Larkin, S. M.; Morrison, M. and Robb, M. A. *Journal of Photochemistry and Photobiology A: Chemistry,* **2007**,*190* 207.
21. Smith, B. R.; Bearpark, M. J.; Robb, M. A.; Bernardi, F. and Olivucci, M. *Chemical Physics Letters,* **1995**, *242*, 27.
22. Wilson, K. R.; Belau, L.; Nicolas, C.; Jimenez-Cruz, M.; Leone, S. R. and Ahmed, M. *International Journal of Mass Spectrometry,* **2006,** *249–250,* 155.

Overall Conclusions

The simple aliphatic amino acids are of particular interest among biologically active molecules, in that they provide unique, identifiable fragmentation patterns based upon the ionization of their parent conformers. Larger amino acids—especially those containing an aromatic moiety—have a more complex fragmentation behavior depending on the ion states (local aromatic vs. extended backbone) accessed. The aromatic moiety in a biological molecule provides a set of localized neutral and ionic staes that are typically lower in energy than those associated with the fundamental structure of the species (e.g., $R(H)C(NH_2)COOH$, R=aromatic substituent such as indole, phenyl, etc.) These aromatic states tend to be localized in both the ion and the neutral species, and thus do not cause conformation specific ion fragmentation as found for the backbone ion states (e.g., $R(H)C(NH_2^+)COOH$, $R(H)C(NH_2)C(O^+)OH$, $R(H)C(NH_2)CO(OH)^+$, etc.)

Introduction of an aromatic moiety into the amino acid system certainly does change the system. In addition to the ring interacting with the amino acid functional groups—changing the relative and absolute energies of the conformers—the aromatic moiety introduces a number of accessible, low lying electronically excited states, both in the neutral and in the ion. Furthermore, an aromatic moiety can alter ionization energy, and localize the charge of an ion species.

The conformation specific and charge directed reactivity of the radical cation intermediates of aliphatic amino acids and analogue systems is clearly illustrated and an important chemistry mediating factor for ionic species. The conformation specificity and charge directed reactivity suggested for these systems can be generalized for radical

cation intermediate behavior for all bioactive carboxylic acids. Conformation specific fragmentation patterns of these nascent radical cationic intermediates are clearly demonstrated by recording different IR spectra (corresponding to different conformations) through the monitoring of different fragment TOFMS signals.

Aromatic amino acid IR spectra, detected through VUV backbone derived ionization, appear to be more difficult to analyze than IR spectra obtained for aliphatic species, again detected through VUV backbone ionization. The spectra for the aromatic species are both broader and less intense than are those of the aliphatic species. One possible explanation of this phenomenon is that the aromatic moiety intersects more strongly with these ion states than the aliphatic moiety and these less intense modes (e.g., combinations and overtones, and specific conformational details) can appear as features on the IR spectra of the neutral. Such effects would also render the IR-VUV spectra broader and less intense than the REMPI, which is also observed.

Ab initio calculations show that the electronic hole (positive charge) in the nascent radical cationic aliphatic amino acids and analogues directs the subsequent conformer specific decomposition reactions of these species. Generally, either a C_{α}-$C_{carboxylic}$ bond dissociation or a hydrogen transfer from the α-substituent to the carboxylic acid group is favored. The actual mechanism, however, depends on the relative orientation of the SOMO with respect to the C_{α}-$C_{carboxylic}$ σ-bond and the activation barrier associated with the reaction coordinate. Thus, different structural orientations of the molecule give rise to different fragmentation patterns in the simpler aliphatic bioactive systems: the reactivity of these systems is primarily governed by the local charge distribution.

Overall, single-photon ionization IR-VUV ion dip spectroscopy can present a means of studying conformer-specific chemistry. In simple systems for which only a few conformations can be present in any given sample, the IR-VUV spectroscopic technique is very effective. As the system being studied increases in size and complexity, however, the conformer specific behavior observed in the simpler systems becomes more difficult to identify. The IR-VUV ion dip spectroscopy method presented here clearly represents a general method of obtaining IR spectra of virtually any species, with few limitations, and thus has the potential to be a useful tool when studying the conformational behavior of many diverse species.